DEVELOPMENT OF ACTIVE INTEGRATED ANTENNAS AND OPTIMIZATION FOR HARMONIC SUPPRESSION ANTENNAS

Simulation and Measurement of Active Antennas for Amplifiers and Oscillators and Numerical Solution on Design and Optimization of Active Patch Antennas for Harmonic Suppression with Adaptive Meshing Using Genetic Algorithms

DAWEI ZHOU
B.Eng., M.Sc.

Submitted for the degree of
Doctor of Philosophy

School of Engineering, Design and Technology
University of Bradford

— 2007 —

Abstract

DEVELOPMENT OF ACTIVE INTEGRATED ANTENNAS AND OPTIMIZATION FOR HARMONIC SUPPRESSION ANTENNAS

Simulation and Measurement of Active Antennas for Amplifiers and Oscillators and Numerical Solution on Design and Optimization of Active Patch Antennas for Harmonic Suppression with Adaptive Meshing Using Genetic Algorithms

Dawei Zhou

Keywords
Active integrated antenna; Class F; Active oscillator antenna; AM Modulation; ASK Modulation; Sensor patch; Harmonic suppression; Genetic algorithms.

The objectives of this research work are to investigate, design and implement active integrated antennas comprising active devices connected directly to the patch radiators, for various applications in high efficiency RF front-ends, integrated oscillator antennas, design and optimization of harmonic suppression antennas using a genetic algorithm (GA).

A computer-aided design approach to obtain a class F operation to optimizing the optimal fundamental load impedance and designing the input matching circuits for an active integrated antenna of the transmitting type is proposed and a case study of a design for 1.6 GHz is used to confirm the design principle. A study of active integrated oscillator antennas with a series feed back using a pseudomorphic high electronmobility transistor (PHEMT) confirms the design procedure in simulation and measurement for the oscillator circuit connected directly to the active antenna. Subsequently, another design of active oscillator antenna using bipolar junction transistor (BJT) improves the phase noise of the oscillation and in addition to achieve amplitude shift keying (ASK) and amplitude modulation (AM) modulation using the proposed design circuit. Moreover, the possibility of using a sensor patch technique to find the power accepted by the antenna at harmonic frequencies is studied.

A novel numerical solution, for designing and optimizing active patch antennas for harmonic suppression using GA in collaboration with numerical electromagnetic computation (NEC), is presented. A new FORTRAN program is developed and used for adaptively meshing any planar antenna structure in terms of wire grid surface structures. The program is subsequently implemented in harmonic suppression antenna design and optimization using GA. The simulation and measurement results for several surface structures show a good agreement.

Acknowledgements

I would like to thank the following persons who accompanied me during the time that I was working for this degree.

I wish to express my gratitude to my supervisors**,** ***Dr. Raed A. Abd-Alhameed*** and ***Prof. Peter S. Excell.*** I am most grateful to them for advice, assistance, support and their continuous encouragement during the difficult starting times, sharing with me the exciting times and for being consistently supportive throughout this work. I will never forget the many opportunities that they gave me in facilities, publications, teaching and travel during the years of my PhD study.

My thanks are also extended to all the other people in the research laboratories, ***Mr. C.H. See***, ***Mr. S.W.J. Chung*** and ***Mr. A. Mistry*** whose co-operation in connection with the practical aspect of this work cannot be underestimated.

My greatest acknowledgements are to ***my parents*** who are away in P. R. China but with me all the time with their support and deep love. I would like to express my debt of gratitude and love to my girl friend ***Chenchen Zou*** for her continuous support in many of the critical times and thousands of little ways, and for being there to remind me to follow our dreams together.

Table of Contents

List of Figures

List of Tables

List of Abbreviations

ADS	Advanced design system
AIA	Active integrated antenna
AM	Amplitude modulation
AMP	Antenna modelling program
AR	Axial ratio
ASK	Amplitude shift keying
BJT	Bipolar junction transistor
CAD	Computer aided design
CPW	Coplanar wave
CW	Continuous wave
CP	Circular polarization
EM	Electromagnetic
EMI	Electromagnetic interference
FEM	Finite element method
FET	Field effect transistor
FFT	Fast Fourier transform
FIT	Finite integration technique
FM	Frequency modulation
FLA	Folded loop antenna
FSK	Frequency shift keying
GA	Genetic algorithms
GSM	Global System for Mobile Communications

HB	Harmonic balance
HBT	Heterojunction bipolar transistor
HEMT	High electronmobility transistor
HFSS	High frequency structure simulator
HSA	Harmonic suppression antenna
IMPATT	Impact ionization avalanche transit-time
LAN	Local area network
LFCP	Left-hand circular polarization
LO	Local oscillator
MESFET	Metal-epitaxial semiconductor FET
MOSFET	Metal-oxide semiconductor FET
MOM	Method of Moments
MIMO	Multiple input multiple output
MWS	Microwave studio
NEC	Numerical electromagnetic computation
PA	Power amplifier
PAE	Power added efficiency
PBG	Photonic bandgap
PHEMT	Pseudomorphic high electronmobility transistor
PIFA	Planar inverted F antenna
PSK	Phase shift keying
QHA	Quadrifilar helix antenna
RF	Radio frequency
RFID	Radio frequency identification

RFCP	Right-hand circular polarization
RL	Return loss
SAR	Specific absorption rate
UWB	Ultra wideband
VHF	Very high frequency
VSWR	Voltage wave standing ratio
3G	The third generation

CHAPTER 1

INTRODUCTION

1.1 BACKGROUND AND OBJECTIVES

The active integrated antenna (AIA) has been growing area of research over the recent years. An AIA can generally be considered as an active microwave circuit in which the output or input port is free space instead of a conventional design methodology of the conventional 50 Ω interface. In all cases, the antenna is fully (or closely) integrated with the active device to form a subsystem on the same board and can provide certain circuit functions such as resonating, duplexing, filtering as well as its original role as a radiator. Since there is no cable required between them then there is no need to attempt and transform to an intermediate standard impedance (e.g. 50 Ω), or alternatively any matching circuit that can transform the antenna input impedance directly to an impedance that is optimized for the active device. Numerous innovative designs based on AIA technology has been proposed and successively implemented in a number of related fields for use in the microwave and millimetre-wave systems because they provide an effective solution to several fundamental problems at these frequencies, including higher transmission-line loss, reduced antenna efficiency and limited source power.

Next generation wireless communication systems require a compact and low-cost

transmitter front-end with long operating time. To achieve this, a small - size transmitter with high efficiency is therefore desired. Since the output power amplifier (PA) consumes most of the power in a small wireless transmitter, much attention has to be paid to maximize the efficiency (i.e. power added efficiency) of this crucial component. It turns out that the efficiency of radio frequency PA is strongly affected by the load impedance presented at harmonic frequencies so that the efforts to improve the efficiency of a PA in a traditionally 50 Ω system can be done by optimizing the load impedance at the fundamental and by optimally loading the harmonics using designated tuning circuits.

When applied in the context of active integrated antennas, the antenna acts as both radiating element and harmonic tuning for achieving the high efficiency using AIA. This approach allowing the traditionally separated sub-circuits, are now integrated into a single compact and efficient unit. However, this high efficiency approach presents new problems. The major one is to design an antenna which presents the desired impedance to the amplifier at harmonics of the operating frequency as well as at the fundamental. This can be realized by modifying the shape of the integrated antenna to control the impedance function. A major part of this thesis considered this problem.

The principal objectives of this thesis are therefore defined as investigation, design and implementation of this emerging technique and its application in high efficiency RF front-end. This thesis will describe this application on modelling aspect at how to obtain the optimal load impedance at desired fundamental and harmonic frequencies for an active integrated antenna of the transmitting type, and then introduce a novel numerical solution technique on designing and optimizing such multi-functional patch

antennas in use for active integrated antennas as a high efficiency and compact transmitter.

In addition, another objective of this thesis is to develop some novel designs for active integrated antennas comprising active devices connected directly to the patch radiators, for the applications in integrated oscillator antennas. Active antennas as oscillators can be considered as inexpensive microwave sources. Given a dc power supply and a modulating circuit, such an inexpensive source may become a compact transmitter for communication applications. In the course of this investigation, it became clear that it is necessary to evaluate existing measurement technique to find the power accepted by active integrated antennas at the harmonics of the operating frequency. This thesis will also describe development of the measurement technique in application of finding the accepted power by the input of the antenna at harmonic frequencies.

1.2 REVIEW OF EXISTING WORK ON ACTIVE INTEGRATED ANTENNAS

1.2.1 Definition and classification of active integrated antennas

Active integrated antennas can be defined as a system in which an active device is coupled directly to the antenna without an intervening match (or mismatch) to any sort of transmission line. The whole system is treated together with the antenna simultaneously serving the function of load as well as radiator. This is in contrast to a conventional antenna subsystem design in which each component is designed separately and then connected via transmission lines. Such antennas have the potential of reducing

the size, weight, and cost of conventional transmitter, receiver, and transceiver designs by incorporating the circuit component functions at the antenna terminals [1, 2].

The present work is concerned with active integrated antennas that will be implemented using three terminal devices and microstrip patch radiators. It is interesting to see how active integrated antennas can be classified. Generally, the basic functions of active devices in active integrated antennas are RF signal amplification, RF signal generation, or frequency conversion. Depending on the function of the active device, the active integrated antennas can be classified into three types [1, 3-5]:

a. The amplifier type is classified as a passive microstrip antenna integrated with a two-port active device at the input or the output for the purpose of signal amplification.
b. The oscillator type is classified as a microstrip antenna integrated with an active device for the purpose of generating a steady state oscillation.
c. The frequency conversion type is defined as a microstrip antenna integrated with an active device for the purpose of frequency conversion either up or down.

For the amplifier-type active integrated antennas, when the antenna is placed at the input port, it acts as source impedance for the active device. In this case, the active integrated antenna functions as a receiver. The low noise amplifier design technique is generally applied in order to attain the required noise performance [6-12]. On the contrary, when the antenna is connected at the output port, it is regarded as load impedance to the active device. The active integrated antenna acts as a transmitter. The design techniques for achieving gain bandwidth performance for a power amplifier are

usually employed [13, 14]. Interest in this type of active integrated microstrip antennas is growing due to its potential applications in compact high efficiency RF front-end transmitters [15-25], in large quasi-optical arrays [26-28] and in spatial power combining amplifier [29-32].

Oscillator type AIA is applied for converting dc power to RF power using the negative resistance characteristics of active devices [33-47]. An integrated version of such an active antenna has been developed for sensor applications [48, 49]. The oscillator consists of an active device in conjunction with a microstrip antenna that simultaneously serves both as a load determining the frequency of oscillation and as an element radiating the generated RF power into space. Proper selection of an operating point of the active device is important for the operational performance.

Frequency conversion type of active integrated antennas can be used as oscillator/modulator in a compact transmitter application or as an oscillator/mixer in a receiver application. The former can be identified as two forms: one is a self-oscillating one-port antenna using two or three terminal devices in negative resistance circuit itself, and the other is a self-oscillating two-port antenna in which the antenna is placed in feedback loop of three terminal device [50, 51]. The latter can be subdivided into two kinds, including integrated mixer with separate local oscillator (LO) and self-oscillating mixer [52, 53].

The present work discusses all of these three types of active integrated antennas with some novel development for various applications in high efficiency RF front-ends, integrated oscillator antennas.

Active solid state devices were first integrated into antenna in the early - and mid - 1960s. Copeland and Robertson demonstrated a mixer integrated antenna [54]. Meinke and Landstorfer described the integration of a FET transistor with dipole terminal serving as a very high frequency (VHF) amplifier for reception at 700 MHz [55]. Following their work, in 1971 Ramsdale and Maclean combined the BJT device and dipole to form a transmission application [56]. In February 1985, Gunn integrated rectangular microstrip patch antenna operating at X-band frequencies was developed by Thomas et al. [57], which is generally accepted as the first modern active antenna.

1.2.2 Advantages, disadvantages and applications of active integrated microstrip antennas

In active integrated antennas the active circuits and antenna configuration require to fabricate on dielectric substrates. Low loss substrate can be used to minimise dielectric losses and optimise antenna efficiencies [1]. Generally the active circuits are placed either directly within the physical structure of the antenna or in its very close proximity. When the active device is connected in the immediate vicinity of the antenna, the antenna itself works as a match network.

Active integrated microstrip antennas, in which an amplifier or oscillator is integrated with a patch antenna, and is used to convert dc energy to RF power [1], has recently drawn a great deal of attention. The present work deals with active microstrip integrated antenna, particularly with planar microstrip antennas. Many other types of antennas employed for the integrated antenna operations have been reported, including dipoles [58], cavity-backed slot antennas [59], notch antennas [60], leaky-wave antennas [61], inverted-F antennas [62], log periodic antennas [63] and yagi-like antennas [64].

Besides compact size, low production cost and the avoidance of impedance matching networks with attendant losses, there are possibilities for improved bandwidth, monolithic integrated at millimetre and subillimetre wavelengths [3, 4].

For active integrated microstrip antennas, the following advantages have therefore been identified:

1. Easy integration with a transceiver's RF circuitry.
2. The circuit offers the advantages of low cost, simplicity of design and compact size.
3. They are amenable to monolithic implementation due to their planar nature [2].
4. Avoidance of losses in interconnecting transmission lines between amplifiers and antennas. The antenna also reduces spurious radiation from connecting cables because only frequency signals are transmitted to or from the antenna.
5. The active device can be used to compensate for the frequency dependence of the realised gain of the passive microstrip antenna.
6. An array antenna can be produced in which a large power splitting feed network is not necessary and a high power microwave tube can be replaced by a large number of low power solid-state devices placed on each antenna.
7. The active device and the antenna are mounted on the same side of the circuit, thereby preserving the conformal nature of the structure, and in array applications the inter-patch mutual coupling can also be reduced.
8. Detection and mixing have been performed on the patch and arrays incorporating harmonic frequency conversion have allowed operation at high frequencies.
9. Large power can be achieved by combining the outputs of a number of devices which are integrated directly into an antenna array. By synchronising the

oscillations of a large number of such oscillators, a high power source may be achieved and radiated directly into free space, where propagation losses are low.

However, active integrated microstrip antennas also have some disadvantages such as the following:

1. Efforts to integrate a number of devices directly into a signal patch have been unsuccessfully because low dc to RF efficiencies of Gunn diodes led to overheating problems.
2. The active devices are integrated or located next to patch antennas, which in practice might increase their inherently high cross polarisation field.

The potential for applications of AIAs is broad. Functions, which would normally occur in a circuit away from the antenna such as detection, modulation, mixing, and amplifying, occur within the AIA. Comparing to the conventional approach, size, weight, and costs can be reduced. Applications for active antennas in radar and communications are listed in Table 1.1.

A full review of the large literature on active integrated antennas and their applications is outside the scope of the present chapter. Excellent reviews of active integrated antenna developments can be found in [1-5].

Table 1.1 Applications of active integrated antennas.

Communications and sensor applications	
RFID Tagging [65, 66]	Cars radio antenna [67, 68]
Wireless Satellite communications [69, 70]	Burglar alarm [71]
Indoor communications systems [72-75]	Television receiver [76]
Wireless mobile communications [77-78]	
Automotive applications	
Doppler radar [79]	Velocity over ground detection [80]
FM-CW or pulsed radar [81-83]	Direction detection [84]
Blind area surveillance Side-crash prediction [85]	

1.3 SCOPE OF THE WORK

Chapter 2 presents a simple CAD-oriented approach to optimise load impedance at the fundamental frequency for the application of the active antenna concept. The design method and procedure are demonstrated through a case study of a design for 1.6 GHz to confirm the design principle. Chapter 3 describes the first phase of the investigation in designing the oscillator-type active integrated antenna. Characteristics of the active devices for various applications are briefly reviewed. In this instance, a common source PHEMT transistor is used, with positive feedback to enhance the instability of the active device. Microstrip-fed circular and rectangular patch antennas are employed as output terminating element for the unstable device. Design procedure of the active integrated oscillator antenna with the aid of ADS simulator is investigated in detail and performance of the prototype oscillator circuits is evaluated and justified with

predictions. A measurement technique for obtaining the free running oscillating frequency and the accepted power at the fundamental frequency by the active oscillator integrated antenna using a calibrated sensor patch in this chapter is demonstrated.

In chapter 4 an integrated antenna oscillator, operated simultaneously as a source generator and function as amplitude modulator, to generate the amplitude modulation (AM) and amplitude shift keying (ASK), is developed. The design theory of the active oscillator antenna and the generation of AM and ASK modulations are described and demonstrated. An HP AT-41411 silicon bipolar transistor is used as the active device for a hardware realisation. Prototype circuits showed about 15 dBm of output power and a free running oscillation at 2.367 GHz. A modulating signal source is injected at the emitter of the transistor to mix with the obtained oscillating signal to produce AM and ASK modulation. It is observed in the case study that the modulated signal has little effect on the self-oscillating generated signal.

Chapter 5 describes the possibility of using this technique to find the power accepted by the antenna at harmonic frequencies. Performance of the sensing patch technique for measuring the accepted power at the antenna feed port of active patch antennas at harmonic frequencies is evaluated using an electromagnetic (EM) simulator in terms of the current distribution. A prototype antenna, including two sensors at appropriate locations around the patch, is fabricated and tested at three designated frequencies to estimate the accepted power by the antenna, including determination of the sensor calibration factor. The original technique is confirmed that can also be employed to measure the second harmonic power based on experimental results; measurement of the

third harmonic power is also possible if another sensing patch is added in an appropriate position.

Chapter 6 introduces a novel numerical solution technique for the development and implementation of designing harmonic suppression antennas for active integrated antennas. The need to develop such antennas for harmonic suppression and a summary on the existing techniques for achieving harmonic suppression antennas are reviewed. A FORTRAN program to adaptively generate equivalent wire-grid structures for electromagnetic simulation of 2D/3D structures is developed with the primary objective of simulating planar microstrip patch antenna designs, using the NEC-2 in collaboration with a genetic algorithm. Two case studies are used to demonstrate the viability of applying the method in designing circularly-polarized microstrip patch antennas. In addition four novel microstrip patch antennas designs were proposed for suppression of the first two harmonics.

The conclusions of this work are brought together and reviewed in Chapter 7 and suggestions for further work are made.

1.4 REFERENCES

[1] J.A. Navarro and K. Chang, "Integrated active antennas and spatial power combining", Wiley Series in microwave and optical engineering, John Wiley & Sons, Inc., New York, 1996.

[2] R. Garg, P. Bhartia, I. Bahl and A. Ittipiboon, "Microstrip antenna design handbook", Artech House, Inc., Chapter 11, 2001.

[3] R.A. York and Z.B. Popovic, “Active and quasi-optical arrays for solid-state power combining”, John Wiley & Sons, New York, 1997.

[4] A. Mortazawi, T. Itoh and J. Harvey, “Active antennas and quasi-optical arrays”, IEEE Press, New York, 1998.

[5] J. Lin and T. Itoh, “Active integrated antennas”, IEEE Trans. Microwave theory and techniques, vol. MTT-42, pp. 2186-2194, 1994.

[6] R. Gillard, H. Legary, J.M. Flowch and J. Citerne, “Rigorous modelling of receiving active microstrip antenna”, Electronics Letters, vol. 27, no. 25, pp. 2357-2359, 1991.

[7] H. An, B. Nauwelaers and A. Van de Capelle, “Noise figure measurement of receiving active microstrip antennas”, Electronics Letters, vol. 29, no. 29, pp. 1594-1596, 1993.

[8] L. Roy, “30 GHz GaAs monolithic low noise amplifier-antennas”, IEEE MTT-S Digest, pp. 967-970, 1997.

[9] A.S. Andrenko, Y. Ikeda, M. Nakayama and O. Ishida, “Impedance matching in active integrated antenna receiver fount end design”, IEEE microwave and guided wave letters, vol. 10, no. 1, pp.16-18, January 2000.

[10] B.N. Biswas, A. Bhattacharya, P. Lahiri and D. Mondal, “A novel scheme for reception using an active microstrip antenna”, IEEE Transactions on microwave theory and techniques, vol. 48, no. 10, pp.1765-1768, October 2000.

[11] R.K. Raj, S.O. Kundukulam, C.K. Aanandan, K. Vasudevan, P. Mohanan and P. Kumar, “Compact amplifier integrated microstrip antenna”, Microwave and optical technology letters, vol. 40, no. 4, pp. 296-298, February 2004..

[12] B. Al-Khateeb, V. Rabinovich and B. Oakley, “An active receiving antenna for short-range wireless automotive communication”, Microwave and optical technology letters, vol. 43, no. 4, pp. 293-297, November 2004.

[13] B. Robert, T. Razban and A. Papiernik, “Compact amplifier integration in square patch antenna”, Electronics Letters, vol. 28, no. 19, pp. 1808-1810, Sep. 1992.

[14] X.-D. Wu and K. Chang, “Compact wideband integrated active slot antenna amplifier”, Electronics Letters, vol. 29, no. 5, pp. 496-497, March 1993.

[15] V. Radisic, S.T. Chew, Y. Qian and T. Itoh, “High-efficiency power amplifier integrated with antenna”, IEEE microwave and guided wave letters, vol. 7, no. 2, pp. 39-41, February 1997.

[16] V. Radisic, Y. Qian, and T. Itoh, “Class F power amplifier integrated with circular sector microstrip antenna,” IEEE MTT-S Digest, pp. 687-690, 1997.

[17] F.J.O. Gonzalez, A.A. Lopez, V.G. Posadas, J.L.J. Martin and C.M. Pascual, "High efficiency mode "E" amplifier power high efficiency active transmitting patch antenna", IEEE MTT-S Digest, pp. 455-458, 1998.

[18] V. Radisic, Y. Qian and T. Itoh, "Novel architectures for high-efficiency amplifiers for wireless applications", IEEE Transactions on microwave theory and techniques, vol. 46, no. 11, pp. 1901-1909, November 1998.

[19] W.R. Deal, V. Radisic, Y. Qian and T. Itoh, "Integrated-antenna push-pull power amplifiers", IEEE Transactions on microwave theory and techniques, vol. 47, no. 8, pp. 1418-1425, August 1999.

[20] C.Y. Hang, W.R. Deal, Y. Qian and T. Itoh, "Push-pull power amplifier integrated microstrip leaky-wave antenna", Electronics Letters, vol. 35, no. 22, pp. 1891-1893, October 1999.

[21] C.Y. Hang, W.R. Deal, Y. Qian and T. Itoh, "High-efficiency push-pull power amplifier integrated with quasi-yagi antenna", IEEE Transactions on microwave theory and techniques, vol. 49, no. 6, pp. 1155-1161, June 2001.

[22] Y. Chung, C.Y. Hang, S. Cai, Y. Qian, C.P. Wen, K.L. Wang and T. Itoh, "AlGaN/GaN HFET power amplifier integrated with microstrip antenna for RF front-end applications", IEEE Transactions on microwave theory and techniques, vol. 51, no. 2, pp. 653-659, February 2003.

[23] H. Kim, I.-J Yoon and Y.J. Yoon, "A novel fully integrated transmitter front-end with high power-added efficiency", IEEE Transactions on microwave theory and techniques, vol. 53, no. 10, pp. 3206-3214, October 2005.

[24] E. Lee, K.M. Chan, P. Gardner and T.E. Dodgson, "Active integrated antenna design using a contact-less, proximity coupled, differentially fed technique", IEEE Transactions on antennas and propagation, vol. 55, no. 2, pp. 267-276, Feb. 2007.

[25] H. Kim and Y.J. Yoon, "Wideband design of the fully integrated transmitter front-end with high power-added efficiency", IEEE Transactions on microwave theory and techniques, vol. 55, no. 5, pp. 916-924, May 2007.

[26] S. Ortiz, T. Ivanov and A. Mortazawi, "A cpw fed microstrip patch quasi-optical amplifier array", IEEE MTT-S Digest, pp.1465-1468, 1998.

[27] J.A. Mazotta, K.S. Ching and W.A. Shiroma, "A three-dimensional quasi-optical source", IEEE MTT-S Digest, pp.547-550, 1999.

[28] S.B. Yeap, M.R. Rayner and C.G. Parini, "Global quasi-optical simulations of millimetre-wave receivers", IEEE microwave and wireless components letters, vol. 14, no. 10, pp. 478-480, October 2004.

[29] J.A. Navarro, Y.-H. Shu and K. Chang, "Broadband electronically tunable planar active radiating elements and spatial power combiners using notch antenna",

IEEE Transactions on microwave theory and techniques, vol. 40, no. 2, pp. 323-328, February 1992.

[30] W.K. Leverich, X.-D. Wu and K. Chang. “FET active slotline notch antennas for quasi-optical power combining”, IEEE Transactions on microwave theory and techniques, vol. 41, no. 9, pp. 1515-1518, September 1993.

[31] O.-P. Lunden, “Power combining of Ku-band active dipoles in cylindrical resonant cavity”, IEEE MTT-S Digest, pp. 701-704, 1995.

[32] A.R. Perkons, Y. Qian and T. Itoh, “TM surface-wave power combining by a planar active-lens amplifier”, IEEE Transactions on microwave theory and techniques, vol. 46, no. 6, pp. 775-783, June 1998.

[33] J. Birkeland and T. Itoh, “Planar FET oscillators using periodic microstrip patch antennas”, IEEE Transactions on microwave theory and techniques, vol. 37, no. 8, pp. 1232-1236, August 1989.

[34] V.F. Fusco, “Series feedback integrated active microstrip antenna synthesis and characterisation”, Electronics Letters, vol. 28, no. 1, pp. 89-91, January 1992.

[35] Y. Shen, R. Fralich, C. Wu and J. Litva, “Active radiating oscillator using a reflection amplifier module”, Electronics Letters, vol. 28, no. 11, pp. 991-992, May 1992.

[36] N.J. Rohrer, M.A. Richard, G.J. Valco and K.B. Bhasin, “A 10 GHz Y-Ba-Cu-O/GaAs hybrid oscillator proximity coupled to a circular microstrip patch antenna”, IEEE Transactions on applied superconductivity, vol. 3, no. 1, pp. 23-27, March 1993.

[37] B.K. Kormanyos, W. Harokopus, L.P.B. Katehi and G.M. Rebeiz, “CPW-fed active slot antennas”, IEEE Transactions on microwave theory and techniques, vol. 42, no. 4, pp. 541-545, April 1994.

[38] P. Liao and R.A. York, “A varactor-tuned patch oscillator for active arrays”, IEEE microwave and guided wave letters, vol. 4, no. 10, pp. 335-337, October 1994.

[39] C.-C. Huang and T.-H. Chu, “Radiating and scattering analysers of a slot-coupled patch antenna loaded with a MESFET oscillator”, IEEE Transactions on antennas and propagation, vol. 43, no. 3, pp. 291-298, March 1995.

[40] G. Forma and J.M. Laheurte, “CPW-fed oscillating microstrip antennas”, Electronic Letters, vol. 32, no. 2, pp. 85-86, January 1996.

[41] G.-J. Chou and C.-K. C. Tzuang, “Oscillator-type active-integrated antenna: the leaky-mode approach”, IEEE Transactions on microwave theory and techniques, vol. 44, no. 12, pp. 2265-2272, December 1996.

[42] G. Ma, P.S. Hall, P. Gardner and M. Hajian, “Local oscillator radiation from active integrated antennas”, Electronics Letters, vol. 35, no. 25, pp. 2163-2164, December 1999.

[43] A.A. Melcon, V. Campos, J.-F. Zurcher and J.R. Mosig, “A simple low-cost coplanar twin-slot active antenna oscillator for wireless applications”, Microwave and optical technology letters, vol. 23, no. 1, pp. 18-25, October 1999.

[44] K.H.Y. Ip, T.M.Y. Kan and G.V. Eleftheriades, “A single-layer CWP-fed active patch antenna”, IEEE microwave and guided wave letters, vol. 10, no. 2, pp. 64-66, February 2000.

[45] D. Bonefacic and J. Bartolic, “Compact active integrated antenna with transistor oscillator and line impedance transformer”, Electronic Letters, vol. 36, no. 18. pp. 1519-1521, August 2000.

[46] D.-H. Choi and S.-O. Park, “A varactor-tuned active-integrated antenna using slot antenna”, IEEE antennas and wireless prop. letters, vol. 4, pp. 191-193, 2005.

[47] D.-H. Choi and S.-O. Park, “Active integrated antenna using T-shaped microstrip-line-fed slot antenna”, Microwave and optical technology letters, vol. 46, no. 6, pp. 538-540, September 2005.

[48] S.P. Kwok and K.P. Weller, “Low cost X-band MIC BARITT Doppler sensor”, IEEE Transactions on microwave theory and techniques, vol. 27, no. 10, PP. 844-847, 1979.

[49] B.M. Armstrong, R. Brown, F. Rix and J.A.C. Stewart, “Use of microstrip impedance-measurement technique in the design of a BARITT diplex Doppler sensor”, IEEE Transactions on microwave theory and techniques, vol. 28, no. 12, PP. 1437-1442, 1980.

[50] R.D. Martinez and R.C. Compton, “A quasi-optical oscillator/modulator for wireless transmission”, IEEE MTT-S Digest, pp. 839-842, 1994.

[51] I. Angelov, H. Zirath and J. Sevdin, “A new mixer for sensor applications”, IEEE MTT-S Digest, pp.1051-1054, 1998.

[52] C.M. Montiel, L. Fan and K. Chang, “A novel active antenna with self-mixing and wideband varactor-tuning capabilities for communication and vehicle identification applications”, IEEE Transactions on microwave theory and techniques, vol. 44, no. 12, part 2, pp. 2421-2430, 1996.

[53] J. Zhang, Y. Wang and Z. Chen, “Integration of a self-oscillating mixer and an active antenna”, IEEE microwave and guided wave letters, vol. 9, no. 3, pp. 117-119, March 1999.

[54] J. Copeland and W. Robertson, “Antenna-verters and antennafiers,” Electronics, pp. 68-71, Oct. 1961.

[55] H. Meinke and F. Landstorfer, "Noise and Bandwidth Limitations with Transistorized Antennas," IEEE Antennas and Propagation Symposium, vol. 6, pp. 245-246, Boston, September 1968.

[56] P. Ramsdale and T. Maclean, "Active Loop-Dipole Aerials," Proc. IEE, vol. 118, no.12, pp. 1698-1710, December 1971.

[57] H. Thomas, D. Fudge, and G. Morris, "Gunn source integrated with a microstrip patch," Microwaves and RF, vol. 24, no. 2, pp. 87-89, February 1985.

[58] O.P. Lunden, "Ku-band active dipole antenna", Electronic Letters, vol. 30, no. 19, pp. 1560-1561, September 1994.

[59] H.P. Moyer and R.A. York, "Active cavity-backed slot antenna", IEEE microwave and guided wave letters, vol. 3, no. 4, pp. 95-97, April 1993.

[60] W.K. Leverich, X.-D. Wu and K. Chang, "New FET active notch antenna", Electronics Letters, vol. 28, no. 24, pp. 2239-2240, November 1992.

[61] C.-J. Wang, C.F. Jou and J.-J. Wu, "A novel two-beam scanning active leaky-wave antenna", IEEE Transactions on antennas and propagation, vol. 47, no. 8, pp. 1314-1317, August 1999.

[62] G.A. Ellis and S. Liw, "Active planar inverted-F antennas for wireless applications", IEEE Transactions on antennas and propagation, vol. 51, no. 10, pp. 2899-2906, October 2003.

[63] M.K. Rahim and P. Gardner, "Active microstrip log periodic antenna", IEEE RF and microwave conference, pp. 136-139, Malaysia 2004.

[64] M. Murata, K. Li and T. Matsui, "Planar active yagi-like antenna", Electronics Letters, vol. 36, no. 23, pp. 1913-1913, November 2000.

[65] M. Kaleja, A. Herb, R. Rasshofer, G. Friedsam, and E. Biebl, "Imaging RFID System at 24 GHz for Object Localization," IEEE MTT-S Int. Microwave Symp. Dig., pp. 1497-1500, 1999.

[66] M. Kossel, R. Kung, H. Benedickter, and W. Bachthold, "An Active Tagging System using Circular-Polarization Modulation," IEEE Trans. Microwave Theory and Tech., vol. MTT-47, pp. 2242-2248, Dec. 1999.

[67] E. H. Nordholt and B.C. Van Eerden, "An integrated amplifier for an active car-radio antenna", IEEE Journal of solid-state circuits, vol. 17, no. 3, pp. 591-593, June 1982.

[68] K.-I. Konno, H. Wada, and K. Matsukawa, "A 2.45 GHz Wireless IC Card System for Automatic Gates," IEEE MTT-S Int. Microwave Symp. Dig., pp. 797-

800, 1993.

[69] D. Roques, H.C.K. Sheung, F. Dubos, D. Cogo and J.-L. Cazaux, "Ku-band quadric-SSPA for stentor satellite transmit active antenna", IEEE MTT-S Digest, pp. 657-660, 2001.

[70] C.-J. Wang, C.F. Jou, J.-J. Wu and S.-T. Peng, "An active microstrip antenna for satellite communication", Vehicular technology conf., vol. 2, pp. 1386-1389, 2000.

[71] S. Battiboia, A. Caliumi, S. Catena, E. Marazzi, and L. Masini, "Low-Power X-Band Radar for Indoor Burglar Alarms," IEEE Trans. Microwave Theory and Tech., vol. MTT-43, pp. 1710-1714, July 1995.

[72] T. Seki, K. Uehara and K. Kagoshima, "A three-dimensional active antenna for a high-speed wireless communication application", IEEE MTT-S Digest, pp. 975-978, 1997.

[73] C. M. Montiel, L. Fan and K. Chang, "Active-norch antennas stablized with a slotline-ring resonator for wireless applications", IEEE Transactions on antennas and propagation, vol. 46, no. 6, pp. 945-946, June 1998.

[74] F. Bilotti, "Design of an active integrated antenna for a PCMICA card", Progress in electromagnetics research, PIER 61, pp.253-270, 2006.

[75] B.D. Mulder, H. Rogier, J. Vandewege and D.D. Zutter, "Highly sensitive, co-optimised active receiver antenna: its use in Doppler radar in 2.4 GHz ISM band", Electronics letters, vol. 39, no. 18, pp. 1299-1301, September 2003.

[76] M. Taguchi, T. Fujimoto and K. Tanaka, "CPW fed active dipole antenna for television receivers", Electronics Letters, vol. 30, no. 22, pp. 1815-1816, Oct. 1994.

[77] D. Sanchez-Hernandez and I. Robertson, "60 GHz-band active microstrip patch antenna for future mobile systems applications", Electronics Letters, vol. 30, no. 9, pp. 677-678, April 2004.

[78] D. Segovia-Vargas, V. Gonzalez-Posadas, D. Castro-Galan, J.L. Vazquez and E. Rajo, "Broad band active receive microstrip antenna for DCS-UMTS", IEEE AP-S symposium, vol. 4, pp. 3935-3938, 2004.

[79] R.H. Rasshofer and E.M. Biebl, "Surface-wave coupling of active antennas for homodyne sensor systems", IEEE Transactions on microwave theory and techniques, vol. 46, no. 12, pp. 2457-2462, December 1998.

[80] M.J. Kelly, V.F. Fusco, J.A.C. Stewart, S. Sancheti and S. Drew, "HBT active antenna as a self-oscillating Doppler sensor", IEE Proc.-Microwave Antennas Propagation, vol. 147, no. 1, pp. 43-47, February 2000.

[81] G. Seehausen, "24-GHz-FM-CW Radar for Detection of Information for Traffic

Purposes", IEEE MTT-S Int. Microwave Symp. Dig., pp. 251-253, 1984.

[82] M. Nalezinski, M. Vossiek, and P. Heide, "Novel 24 GHz FMCW Front-End with 2.45 GHz SAW Reference Path for high-precision Distance Measurements," IEEE MTT-S Int. Microwave Symp. Dig., pp. 185-188, 1997.

[83] W. Menzel, D. Pilz, and R. Leberer, "A 77- GHz FM/CW radar front-end with a lowprofile low-loss printed antenna," IEEE Trans. Microwave Theory and Tech., vol. MTT-47, pp. 2237-2241, Dec. 1999.

[84] R. Rasshofer and E. Biebl, "A Direction Sensitive, Integrated, Low Cost Doppler Radar Sensor for Automotive Applications." IEEE MTT-S Int. Microwave Symp. Dig., pp.1055-1058, 1998.

[85] M. Kaleja, J. Büchler, R. Rasshofer, J.-F. Luy, and E. Biebl, "Low-cost automobile crash-sensor using a 61 GHz active integrated SIMMWIC Antenna," IEEE MTT-S Int. Microwave Symp. Dig., pp. 1969-1972, 2000.

CHAPTER 2

CAD-ORIENTED ACTIVE CLASS F ANTENNA DESIGN

2.1 INTRODUCTION

This chapter presents a general computer-aided design (CAD) approach to obtaining optimal fundamental load impedance, and designing input matching circuits, in an active integrated antenna of transmitting type. A case study of a design for 1.6 GHz is used to confirm the design principle, and uses a previously reported patch antenna shape to achieve Class F operation with an alternative type of power transistor.

The work discusses a CAD-oriented approach to optimising fundamental load impedance in the design of a class-F power amplifier AIA for transmitters. Also a 2 x 2 coupler at the input stage is used in designing the input matching circuit, by showing the effect of various load impedances on the input reflection coefficients. To demonstrate the principle, we present a case study of a class-F power amplifier AIA design for 1.6 GHz wireless communications. In fact, the active antenna design can be applied at any operated frequency band; however, 1.6 GHz was selected for the present work since there is some measurements data were available from earlier work [1, 2]. A published

design [3, 4] for the antenna structure has been chosen, but has been integrated with a different transistor.

2.2 THEORY OF ACTIVE CLASS F ANTENNA DESIGN

Class-F operation is a well-known technique for improving PAE of RF power amplifiers [5-10]. It uses a multi-resonator to control harmonic waveforms so that the drain voltage waveform of a FET (ideally) becomes rectangular and the drain current waveform becomes half sinusoidal, thereby reducing dc power dissipation and increasing efficiency. This requires optimised impedance at the fundamental, low impedance at even harmonics, and very high impedance at odd harmonics. A simple method is to interpose a quarter-wave line between the drain and the final load, and to design the latter to have the lowest possible impedance at all harmonics above the fundamental.

In the AIA harmonic tuning technique, it is convenient to use the same technique. This has been done in [3, 4], where, to obtain class-F operation, the second and third harmonics are shaped through the input resistance of the antenna, which would allow these harmonic resistances to be almost zero at twice and three times the design frequency so that harmonic power is efficiently suppressed from radiation by the antenna. In addition, the input impedance of the antenna at the fundamental frequency (f_o) should be equal to the optimum load impedance (Z_{opt}) at f_o of the amplifier for maximum PAE and P_{out}. In this design approach, an output matching circuit is eliminated because the antenna impedance is directly transformed to the Z_{opt} for maximum efficiency, thus decreasing the circuit complexity and power losses.

In this CAD oriented approach, due to the intrinsic active device nonlinear behaviour, the PA design is based on large-signal simulation. The class-F power amplifier was designed and optimised at 1.6 GHz using Agilent Technologies' Advanced Design System (ADS). Following selection of a suitable output power and operating frequency range, the active device selected was the TriQuint CLY5 power GaAs field effect transistor (FET). For a simple design, it is desirable to use a device like the CLY5 which does not include built-in matching circuits, other than unavoidable parasitics, within the package. Even with CAD tools, it is a very difficult problem to optimise all aspects of the design in one pass. No exact synthesis technique is known for shaping a patch antenna to achieve prescribed impedances at a set of harmonically related frequencies. However it is feasible to use the method of [4, 11] whereby the fundamental impedance can be kept reasonably close to optimum, while higher resonances of the patch can be separated as much as possible from harmonics of the operating frequency, so that the input resistance of the patch remains low at the harmonics. This may of course be a realistic target only for the first few harmonics, which fortunately dominate the efficiency optimisation. Feedback effects on input impedance at harmonic frequencies will be a complex issue. In this case study we proceed by initially optimising the fundamental load impedance only, and this value is used in optimising the input match, again initially neglecting harmonic frequency feedback.

2.3 AIA PA DESIGN AND HARMONIC LOADING CONSIDERATIONS

The non-linear model of this device (which was provided by the device manufacturer), and harmonic balance simulation including the first five harmonics, were used in the simulation. The drain bias voltage V_{ds} was 5 V, while the gate bias voltage V_{gs} was set to be –2.25 V so that dc drain current is 155 mA. Fig. 2.1 shows the dc characteristics of the device and the selected quiescent bias point.

For matching network design in PAs, a set of large-signal S parameters is usually required. However, the measurement of these S parameters is not well defined. An alternative method is to derive reflection coefficients of the active device from measurements of the voltage of the incident wave and reflected wave. In this AIA scenario, only the input reflection coefficient (Γ_{in}) needs obtaining because of the elimination of output matching. A 2 x 2 simple coupler was inserted at the input stage of a class-F harmonic load-pull measurements [12, 13] design circuit (which was in ADS's amplifier design guide) in order to measure Γ_{in} of large signal S-parameters of the nonlinear model. The simulation circuit with a coupler for the input matching design is shown in Fig. 2.2. In this circuit, the coupler is connected between a signal generator and the active device in order to make a measurement of incident voltage (V_{in}) incoming from the source and reflected voltage (V_{ref}) reflected back from the active device. It should be noted that the coupler is not intended to be a realizable hardware component, but is defined in software as the operation of converting actual current and voltage into equivalent forward and reverse wave components. Then the Γ_{in} of the transistor is calculated according to the defining equation of Γ:

$$\Gamma = V_{ref} / V_{in} \qquad 2.1$$

The principle of this CAD load-pull measurement circuit design is to obtain the Z_{opt} at the fundamental design frequency of the PA with a class-F biasing operation at f_o for maximum PAE and P_{out} (the accepted power to the load or antenna), using an algorithm to vary the fundamental load impedances which are contained in an one-port device as S_{11} data. In fact, the algorithm is provided by the ADS package, arbitrarily setting a center point and radius for a circle on Smith Chart and also setting the number of points on the circle (making sure the generated circle is fully inside the Smith Chart). Each point of the circle gives an individual value of the load impedance. The optimum load impedance can be obtained by changing the location of the circle on the chart. In addition, the source and load impedances at harmonic frequencies were defined arbitrarily as 50 Ω. These assigned values are somehow sub-optimal. Thus, the obtained PAE and P_{out} from this simulation design are not finalised and the design can be used as a starting point when the one-port block is replaced by the antenna which hopefully should provide the correct harmonics load impedances. The input reflection coefficients were also simulated as a function of the output load impedances for the maximum power and efficiency. Due to dependence between input reflection coefficient Γ_{in} and load reflection coefficient Γ_{load} of the two-port device, therefore, the advantage of this proposed design approach is that it simplifies the considerations of designing the output matching circuit and the simulation only aims to obtaining Z_{opt}. Once the Z_{opt} with the satisfied output power and efficiency was obtained, the corresponding Γ_{in} with this Z_{opt} value was also calculated so that the input matching circuit could be designed accordingly with the aid of the Smith Chart.

Under the biasing condition mentioned above, the Γ_{in} value was found in the form of magnitude and angle when the Z_{opt} was optimised to be (16.049-j*10.096) Ω. With the help of the Smith Chart tool, an input matching circuit with two lumped elements was plotted and the coupler at the input stage was replaced with it. Discrete components could be used for the matching network because these components have been well enough characterised at the lower microwave communication frequencies. A modified measurement circuit with optimal components' value is shown in Fig. 2.3.

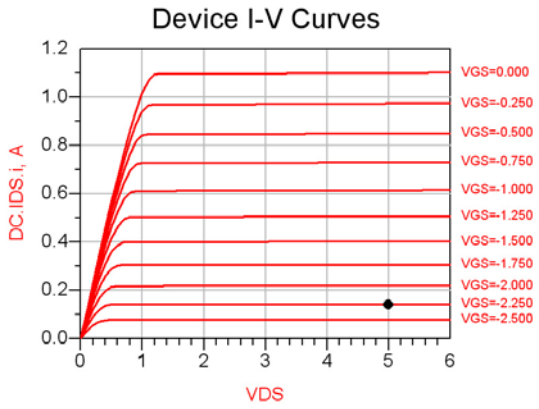

Figure 2.1 dc characteristics of the device and the selected quiescent bias point.

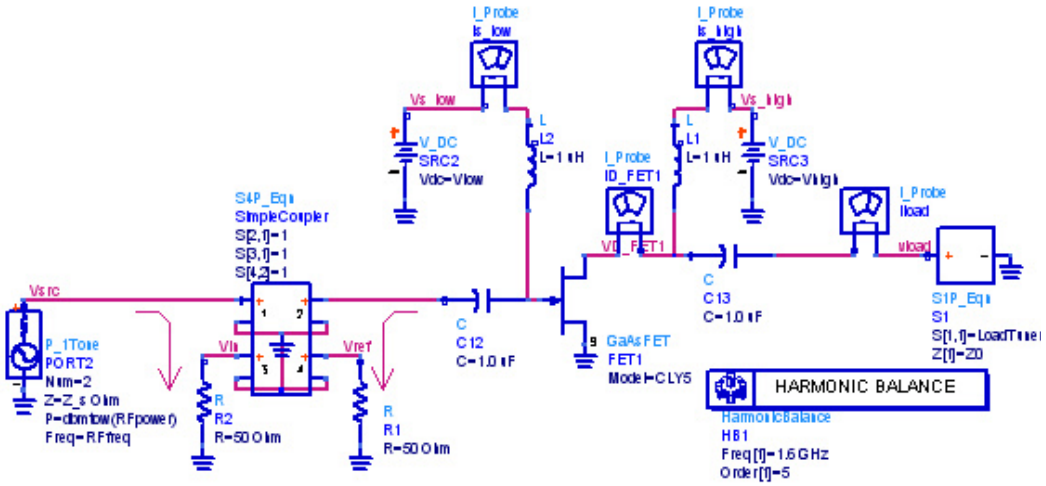

Figure 2.2 Harmonic loadpull simulation circuit with a coupler.

After introduction of the input matching, the PAE and P_{out} of the PA were dramatically improved while the Z_{opt} was still found to be (16.049-j*10.096) Ω with the same input power level. Once the Z_{opt} value was set, microstrip lines were required to connect these components together. An Ultralam 2000 substrate of ε_r = 2.55, thickness T = 1.524 mm, metal thickness T_m = 0.035 mm and tan δ = 0.0019 was assumed. Fig. 2.4 shows the design circuit connected using microstrip line with optimal lengths and widths. One-tune swept Harmonic Balance analysis, with load impedances at harmonic frequencies set at 50 Ω and the optimum load impedance at the fundamental frequency set as (16.049 –j*10.096) Ω, was employed. The output power P_{out} and the power-added efficiency characteristics from the active device versus input driving power at 1.6 GHz are shown in Fig. 2.5. The PAE of the transistor reaches 69.7% with an input power level of 18 dBm. The corresponding performances are the following: 27.81 dBm output power and 9.85 dB gain. Table 2.2 shows the power amplifier's performances with the same input power level versus various load impedances at harmonic frequencies.

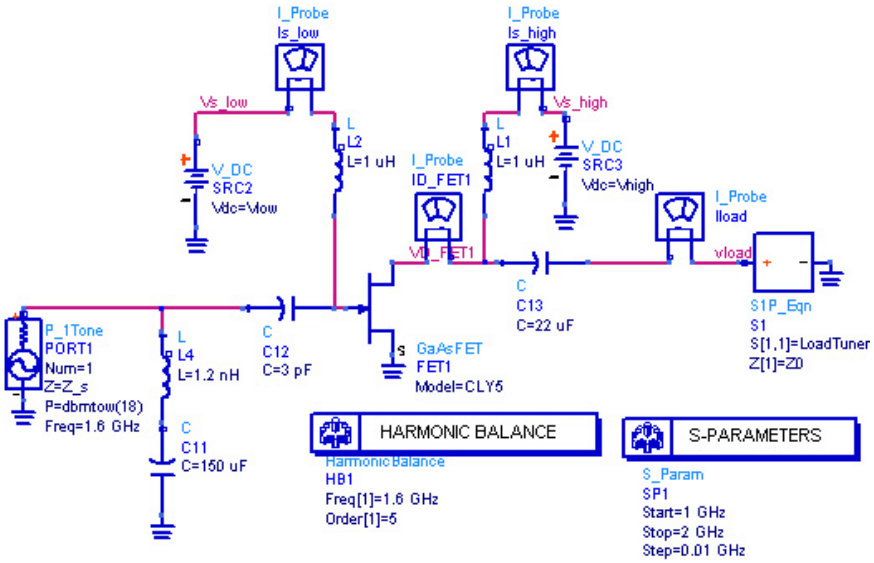

Figure 2.3 Harmonic loadpull simulation circuit with input matching.

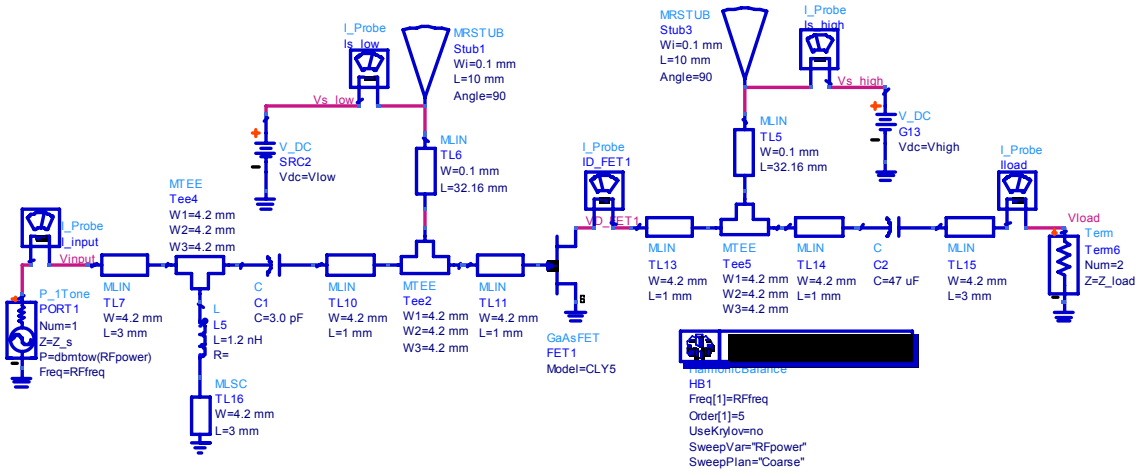

Figure 2.4 Simulated circuit model with optimal load.

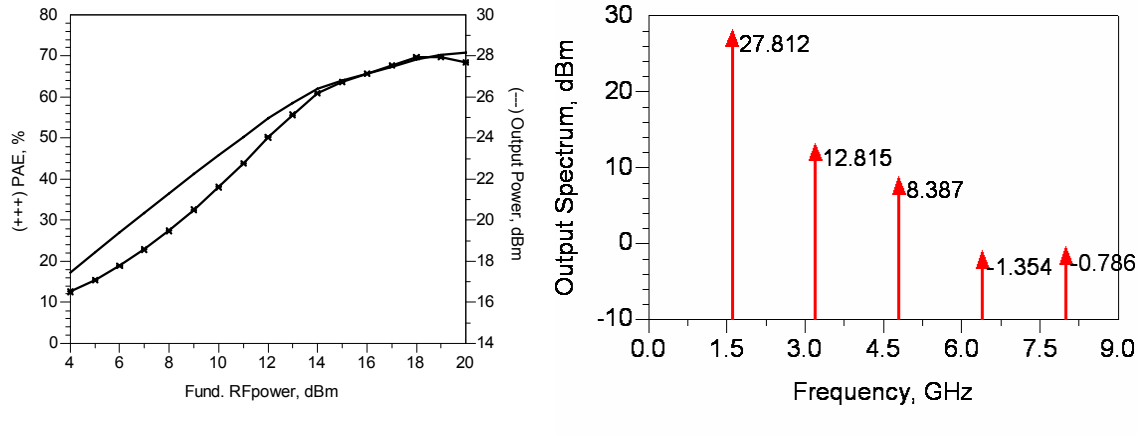

Figure 2.5 Simulated results of the PA: P_{out} and PAE (left) and higher order harmonic level (right).

2.4 ACTIVE ANTENNA DESIGN AND THE INPUT IMPEDANCE CONSIDERATIONS

Various antenna types could be chosen for the radiating element of the AIA, such as patch antennas [11] and planar inverted F antennas (PIFA) [14]. To realise class-F

operation with the AIA concept, this study followed the approach of [3, 4] and adopted the same antenna geometry as in [3], which used a circular-sector microstrip patch antenna, as shown in Fig. 2.6.

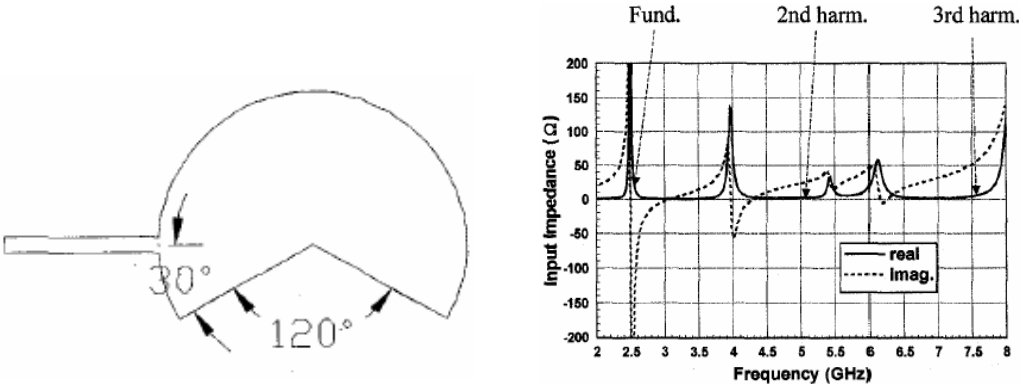

Figure 2.6 Layout of the circular-sector microstrip antenna (left) and input impedance of the adopted antenna (right) [15].

In [3], the authors did not mention where the feeding point of the antenna is. Thus, it might be either at the edge of the antenna or at the edge of feeding line of the antenna. The radius of the antenna was given in the paper [15] is 740 mil, which is equivalent to 18.80 mm, and the design frequency was chosen off resonance at 2.55 GHz where input impedance is (19.8 –j*114) Ω. Antenna simulation using Momentum was carried on in order to find out exact position of the feeding point. As can be seen in Fig. 2.7, it turned out from the simulation result of the antenna's input impedance that the proposed antenna in [3] was fed actually at the edge of the antenna rather than the edge of the feeding line.

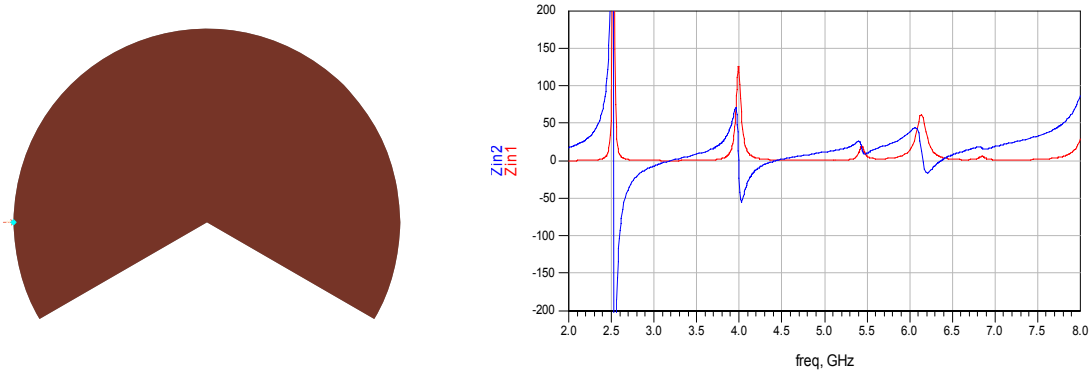

(a)

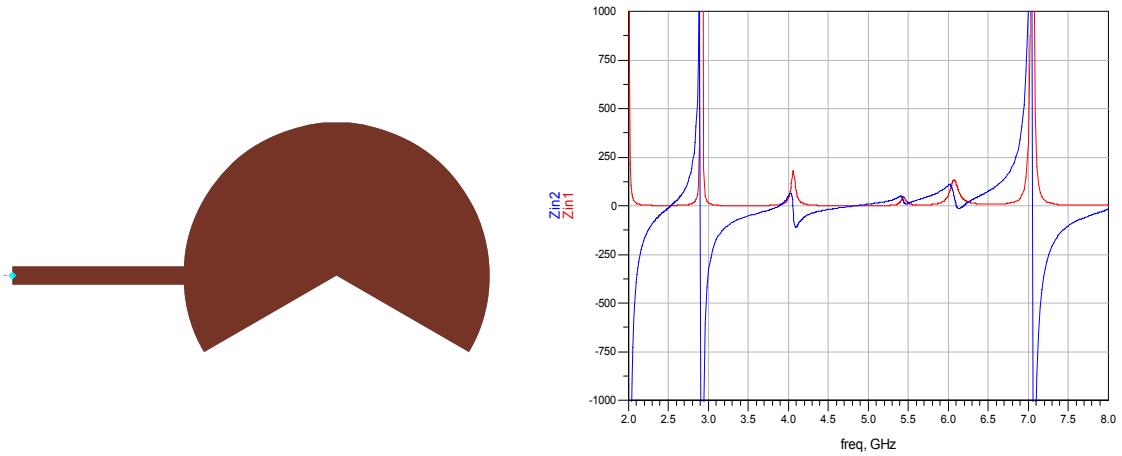

(b)

Figure 2.7 Feeding point clarifications in terms of input impedance of the antenna: (a) edge of the antenna; (b) edge of the quarter wavelength line.

Since the optimum load at the fundamental frequency from the software (ADS) shows (16.049-j*10.096) Ω, input impedance at the edge of the antenna after a quarter wavelength transmission feeding line is required to be (120.61+ j*80.48) Ω. Following the results of the edge load impedances for the 2nd and 3rd harmonics are expected to show reactive load only. Varying radius of the antenna may be able to make a shift of resonance frequencies of the antenna. Several attempts by varying antenna size had been tried to obtain the expected fundamental load impedance at the edge of the antenna

at the design frequency, which is slight off at the first resonance of the antenna. As can be seen in the Fig. 2.8, input impedance of the antenna is not likely to achieve the required load impedance near the first resonance when the antenna radius was chosen to be 27.8 mm.

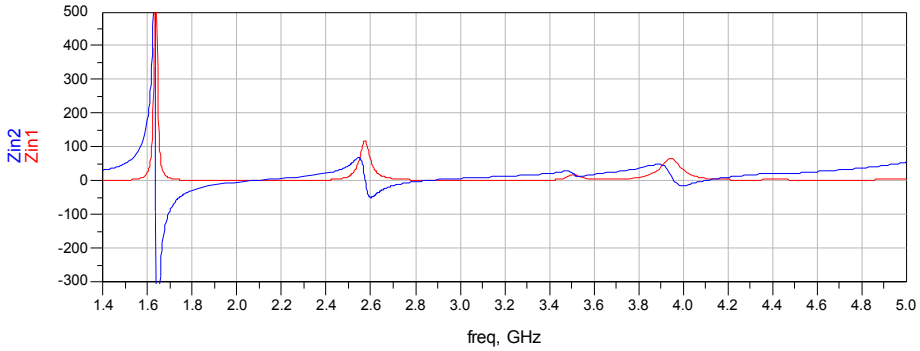

Figure 2.8 Input impedance of the antenna with radius of 27.8 mm.

It was found that a simple output matching network would have to be included [11] between the drain and antenna input port. In order to avoid this network, we had to increase the antenna size in order to be able to make a matching near the patch antenna's second resonance. The following Fig. 2.9 shows the simulated input impedance for an antenna radius of 45 mm, the intended operating frequency being 1.6 GHz. The antenna's impedance at the first three harmonic frequencies is also shown in Table 2.1.

The antenna was incorporated in the class-F PA simulation as a one-port device containing the S parameters data from 0.2 to 9 GHz. The final simulated model including the antenna data is shown in Fig. 2.10. The amplifier performance with the integrated antenna as harmonic loading is shown in Fig. 2.11 and Table 2.2 (note Fig.

2.5 was used without the antenna data). It is obvious from Table 2.2 that an increase in PAE, output power, and power gain at 18 dBm input power have been obtained. These results demonstrate an approach to showing how the harmonic loading of the actual antenna can contribute to the PA performance as compared to the simple harmonic loading (i.e., without the actual antenna data) introduced by the ADS package. Fig. 2.12 shows the simulated drain voltage and drain current waveforms. They show deviations from the ideal case waveforms, but a performance improvement has nevertheless been obtained. These deviations are believed to be due to the parasitic reactive elements of the non-linear model of the active device, and particularly packaging parasitics at the drain and in the common (source) lead. A check was made that including more harmonics would have little effect on this result. Similar waveform deviations observed in Ref. [3] with four harmonics were used for the simulation work.

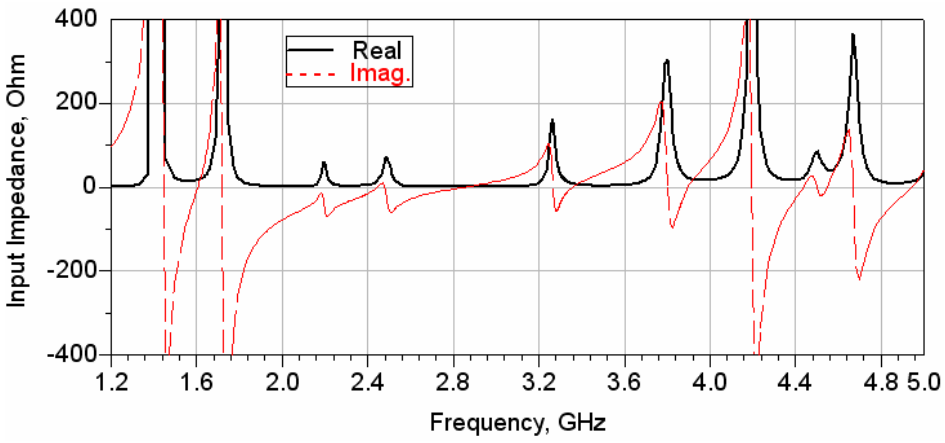

Figure 2.9 Simulated input impedance of the circular-sector microstrip antenna with radius of 45 mm.

Table2.1 Input impedances of the antenna at fundamental and harmonics.

Feeding point	Z_{opt}/Ω	f_1/GHz	F_2/GHz	F_3/GHz
At the edge of the patch	-	99.231+j59.96	13.849+j65.92	5.067+j24.870
At the edge of the λ/4 line	16.049-j10.09	16.684-j9.895	10.912+j59.25	12.706-j73.388

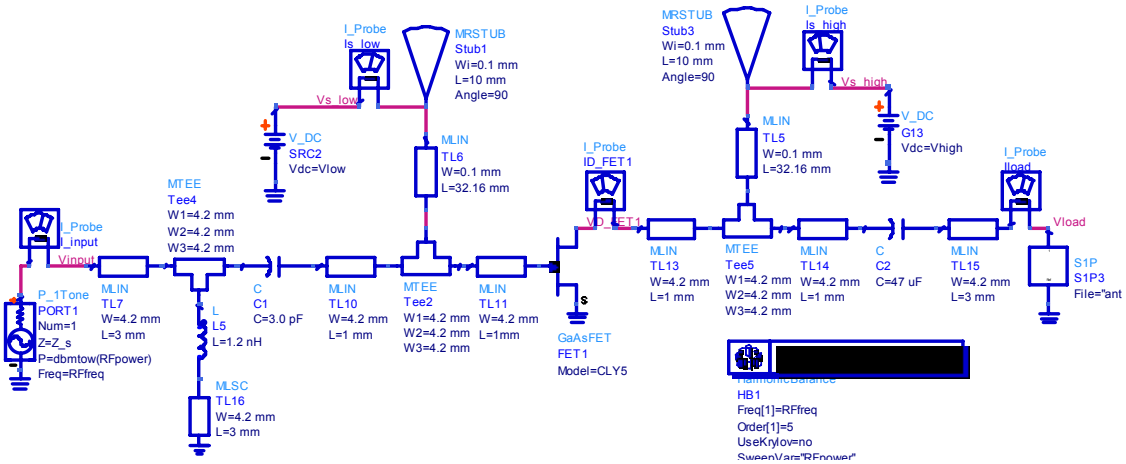

Figure 2.10 Final simulated model integrated with the antenna data.

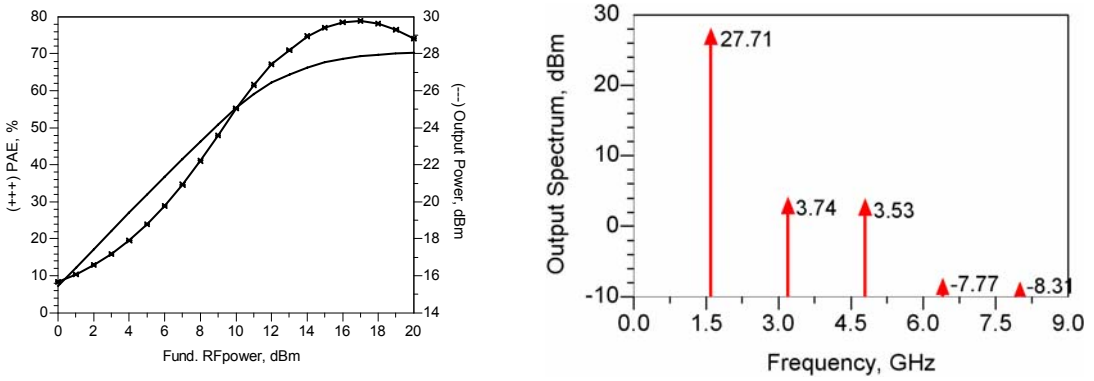

Figure 2.11 Improved Simulated results of the PA: P_{out} and PAE (left), higher order harmonic level (right).

Table 2.2 PA performance with and without the integrated antenna.

P_{in} = 16 dBm	PA Performance with various load impedances at harmonics						PA Integrated with antenna data
Harmonic load impedances (Ω)	0	10	20	30	40	50	
P_{out} (dBm)	27.52	27.73	27.57	27.47	27.41	27.36	27.71
PAE (%)	72.47	75.42	73.62	72.53	71.92	71.59	78.45
Gain (dB)	11.52	11.73	11.57	11.47	11.41	11.36	11.71

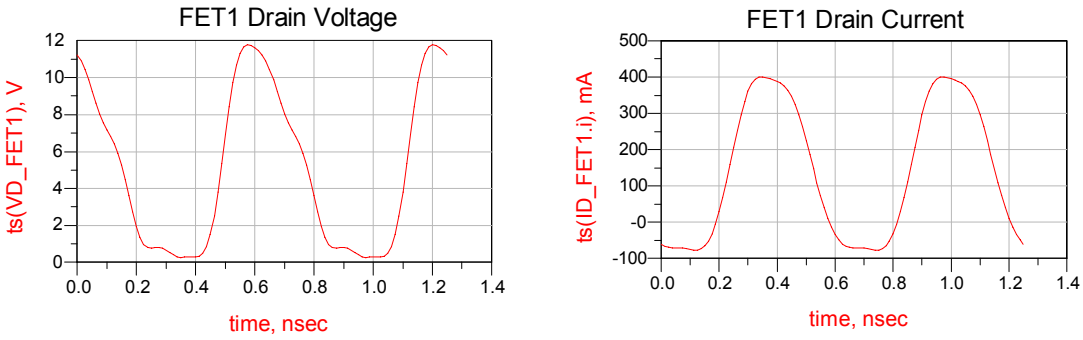

Figure 2.12 Simulated drain voltage and drain current waveforms.

2.5 CONCLUSION

A simple CAD-oriented approach to optimise load impedance at the fundamental frequency for the application of the active antenna concept was described. The design method and procedure were presented. In addition, one design example at an operating frequency of 1.6 GHz was demonstrated as well to verify the design principle. It was confirmed that performance could be substantially enhanced in an active integrated

antenna by shaping a patch radiator to control the harmonic load impedances. One intention is to try to design a novel harmonic suppression antenna, which then will be applied to this AIA design approach.

2.6 REFERENCES

[1] E.A. Elkhazmi, 'Measurement and optimisation of efficiency and harmonic rejection in transmitting active patch antenna, PhD thesis, University of Bradford, 2001.

[2] E.A. Elkhazmi, N.J. McEwan, and N.T. Ali, "A power and efficiency measurement technique for active patch antennas", IEEE Transactions on microwave theory and techniques, pp. 868-870, vol. 48, no. 5, May 2000.

[3] V. Radisic, Y. Qian, and T. Itoh, "Class F power amplifier integrated with circular sector microstrip antenna", IEEE MTT-S Digest, pp. 687-690, 1997.

[4] Y. Chung, C.Y. Hang, S. Cai, Y. Qian, C.P. Wen, K.L. Wang, and T. Itoh, "AlGaN/GaN HFET power amplifier integrated with microstrip antenna for RF front-end applications", IEEE Transactions on microwave theory and techniques, vol. 51, no.2, pp. 653-659, February 2003.

[5] F.H. Raab, "Class-E, Class-C, and Class-F power amplifiers based upon a finite number of harmonics", IEEE Transactions on microwave theory and techniques, vol. 49, no, 8, pp. 1462-1468, August 2001.

[6] F.H. Raab, "Class-F power amplifiers with reduced conduction angles", IEEE Transactions on broadcasting, vol. 44, no. 4, pp. 455-459, December 1998.

[7] F.H. Raab, "Class-F power amplifiers with maximally flat waveforms", IEEE Transactions on microwave theory and techniques, vol. 45, no. 11, pp. 2007-2012, November 1997.

[8] F.H. Raab, "An introduction to Class-F power amplifiers", RF Design, pp. 79-84, May 1996.

[9] C. Duvanaud, S. Dietsche, and J. Obregon, "High-efficienct class-F GaAs FET amplifiers operating with very low bias voltage for use in mobile telephones at 1.75 GHz", IEEE microwave and guided wave letters, vol. 3, no. 8, pp. 268-270, August 1993.

[10] M. Wren and T.J. Brazil, "Experimental Class-F power amplifier design using computationally efficient and accurate large-signal pHEMT model", IEEE

Transactions on microwave theory and techniques, vol. 53, no. 5, PP. 1723-1731, May 2005.

[11] V. Radisic, Y. Qian, and T. Itoh, "Novel architectures for high-efficiency amplifiers for wireless applications", IEEE Transactions on microwave theory and techniques, vol. 46, no. 11, pp. 1901-1909, November 1998.

[12] D. Barataud, M. Campovecchio, and J.-M. Nebus, "Optimum design of very high-efficiency microwave power amplifiers based on time-domain harmonic load-pull measurements", IEEE Transactions on microwave theory and techniques, pp. 1107-1112, vol. 49, no. 6, June 2001.

[13] P. Colantonio, F. Giannini, E. Limiti, and V. Teppati, "An approach to harmonic load- and source-pull measurements for high-efficiency PA design", IEEE Transactions on microwave theory and techniques, pp. 191-198, vol. 52, no. 1, January 2004.

[14] S. Liw and G.A. Ellis, "Planar inverted-F antennas as an inverse class-F termination for wireless applications", IEEE antennas and wireless propagation letters, vol.2, pp. 250-253, 2003.

[15] V. Radisic, Y. Qian, and T. Itoh, "Active antenna approach to high efficiency power amplifiers with EMI distortion", Proceedings of IEEE military communications conference, vol. 3, pp. 699-703, 1998.

CHAPTER 3

SIMULATION AND MEASUREMENT OF ACTIVE INTEGRATED OSCILLATOR ANTENNA FOR WLAN APPLICATIONS

3.1 INTRODUCTION

In this chapter, the AIA concept was also applied to oscillator designs at microwave frequencies [1-10]. When an active device is integrated with a microstrip antenna for the purpose of generating a steady-state oscillation, it is classified as an oscillator-type active microstrip antenna. A microwave oscillator converts dc power to RF power, and is one of the most essential components in a microwave system. The oscillator consists of an active device in conjunction with a microstrip antenna that simultaneously serves both as a load and as an element radiating the generated RF power into space. The design process requires the linear and nonlinear models of the active device. In addition, a planar microstrip patch antenna is considered as the load of the oscillator. Due to active nonlinear element and the integrated antenna, the complete analysis of oscillator design is very difficult.

The design of an oscillator integrated with an active antenna, working at 2.4 GHz for wireless local area networks (LANs) was investigated. A common source PHEMT transistor was used, with positive feedback to enhance the instability of the active device. A microstrip-fed rectangular patch antenna was employed as output terminating element for the unstable device. The antenna was directly connected with the active device for reducing the power loss and circuit complexity and input impedance of the antenna was optimised in terms of output power and harmonic levels. A calibrated sensor placed next to the antenna edge having maximum voltage was used to measure the performance of the active oscillator antenna.

We will first compare the uses and characteristics of various types of active devices and decide the suited ones in terms of phase noise, which will be selected for the design of active oscillator antenna. Then a case study using FET, on the design of an oscillator integrated with an active antenna will present and analysis in detail. Finally, we introduce and discuss the sensor patch technique for measuring the output power of the active oscillator antenna at its fundamental frequency.

3.2 CHARACTERISTICS OF THE ACTIVE DEVICES

The active devices can be either two-terminal devices [11-13], for instance, impact ionization avalanche transit-time (IMPATT) devices and Gunn diodes, or then can be three-terminal devices such as MESFET, HEMT, and HBT. In general, both advantages and disadvantages are associated with each type of solid-state source.

Properly biased IMPATT and Gunn diodes exhibit negative resistance characteristics than can be utilized in conjunction with an external resonant circuit to design a solid-state microwave oscillator, but have low dc-to-RF conversion efficiency, thus requiring special consideration of heat dissipation in the circuit design.

Three-terminal devices have high dc-to-RF efficiency and lower 1/f noise, making them preferable for oscillator designs, where other constrains permits this. The uses and characteristics of a few kinds of active devices are summarised in the following Table 3.1.

Table 3.1 Summary of uses characterises of typical active devices [14].

Bipolar junction transistor (BJT)	Small-signal amplifiers; not low noise. Fast digital circuits. *Low 1/f noise makes them ideal for low-noise oscillators.*
Heterojunction bipolar transistor (HBT)	Power amplifiers. Fast analog circuits. *MESFETs and HEMTs have much better noise figures, but HBTs have lower 1/f noise, making them preferable for oscillators.*
Metal-epitaxial semiconductor FET (MESFET)	Amplifiers, oscillators, mixers, modulators, frequency multipliers, control components, in short, everything.
High electronmobility transistor (HEMT)	Much then same as MESFETs; best suited for small-signal, low-noise uses, but power devices are possible.
Metal-oxide semiconductor FET (MOSFET)	Analog, digital, and RF Si IC applications.

3.3 MICROWAVE TRANSISTOR OSCILLATORS

3.3.1 Basic concepts of two port negative-resistance oscillators

The general block diagram for two-port negative resistance oscillators is shown in Fig. 3.1. The transistor network is characterized by its S parameters, Z_T is the generator tuning network impedance, and Z_L is the load matching network impedance. It should be noted that in an oscillator either port of the transistor can be used as the load

matching port. Once the load matching port is selected, the other port is referred to as the input port.

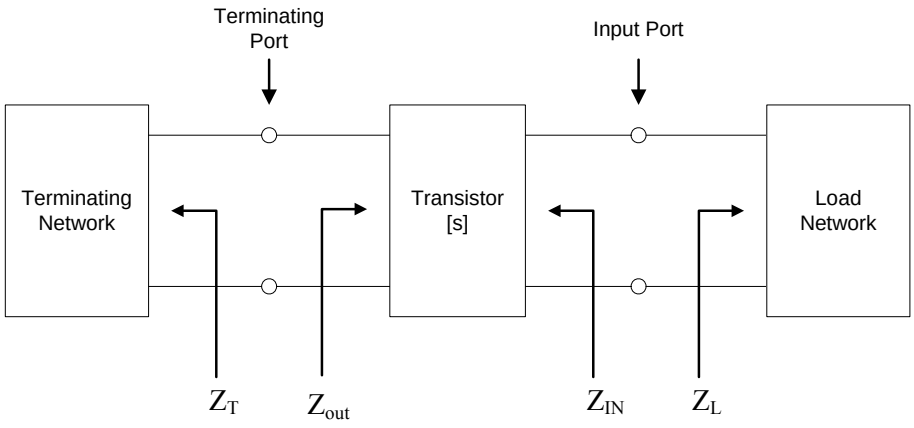

Figure 3.1 Microwave transistor oscillator circuit diagram.

As the oscillator power builds up, it is necessary to choose R_T so that $R_T + R_{out} < 0$. Otherwise, oscillation will stop when the increasing power increases R_{out} to the point, where $R_T + R_{out} > 0$. In practice, value of R_T typically is chosen to be $-R_{out}/3$ and the reactive part of Z_T is chosen to resonant the circuit,

$$X_T = -X_{out} \tag{3.1}$$

When the input port is made to oscillate, the output port also oscillates. The conditions for oscillation can be summarized as follows [15]:

$$K = \left(1 - |S_{11}|^2 - |S_{22}|^2 + |\Delta|^2\right) \Big/ 2|S_{12}||S_{21}| < 1 \tag{3.2}$$

$$\Gamma_T \Gamma_{out} = 1 \tag{3.3}$$

$$\Gamma_L \Gamma_{in} = 1 \qquad 3.4$$

Where, K is the stability factor. Since the stability factor is dependent on the S parameters of the active device we have to make sure that condition is satisfied first and foremost. Typically, a common emitter or common base bipolar configurations are used (common source or common gate for FET devices). If the S parameters at the design frequency do not ensure this requirement, a (series or shunt) positive feedback can be added to enhance the instability of the active device.

3.3.2 Phase noise

One important factor that determined the performance of an oscillator is phase noise. Phase noise will have a negative effect on the oscillator frequency stability. Low phase noise is required for many receiver and transmitting system. This is especially true when dealing with the wireless communication traffic system. For a given receiver, if the phase noise of the local oscillator is high, it will distort the signal frequency and this will limit the receiver ability to recover the modulated signal. When the receiver is used to receive PSK or FSK signals, the phase noise may limit the maximum bit error rate which the system can achieve. All active devices exhibit noise. The two main types of active devices noise are flicker (1/f) noise, and shot noise. Since the oscillator design is based on active device, therefore these noises will dominant the phase noise. Phase noise can be described as short-term random frequency fluctuations of a signal. Phase noise is measured in frequency domain. Phase noise is defined as the ratio of signal power to noise power measured in a 1Hz bandwidth at a given offset from the desired signal as shown in Fig. 3.2 [16].

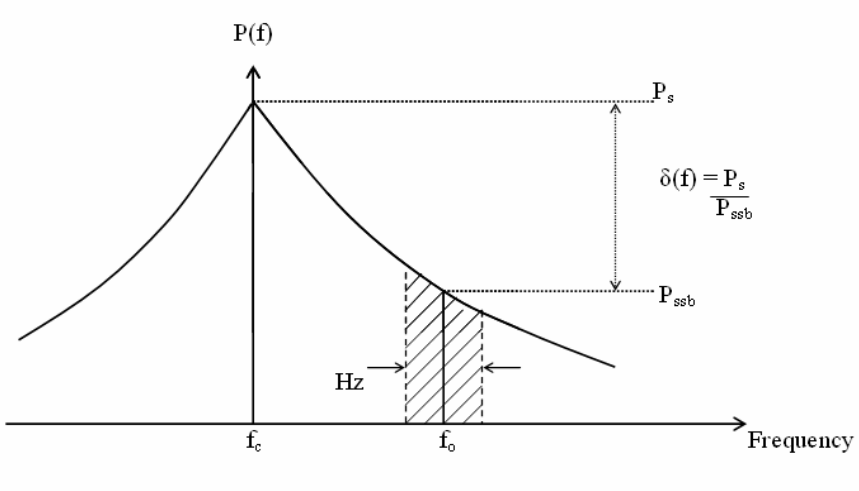

Figure 3.2 Phase Noise output spectrum.

3.3.3 Microwave oscillator characteristics

There are several characteristics are used to specify and describe an oscillator. These are listed below [17].

1. *Power output*: a) Is the continuous power generated by an oscillator in watts or milliwatts for continuous wave (CW) operation, or b) the peak or average power generated for pulse operation.
2. *Operating frequency and tuning range*: A fixed output frequency or a tunable output frequency range for a mechanically or electronically tunable oscillator.
3. *Efficiency*: dc-to-RF conversion efficiency in percent.
4. *Stability*: The ability of an oscillator to return to the original operating point after having a small electrical or mechanical disturbance.
5. *Noise*: a) AM noise (amplitude variation of output signal), b) Frequency modulation (FM) noise (unwanted frequency variations) and c) Phase noise (phase variations).

6. *Quality (Q) factor*: a) Unloaded (for resonator losses only), b) External (for the load resistor only and assumes resonator losses=0) and c) Loaded (for both).
7. *Frequency*: a) Jumping (discontinuous change in oscillator frequency), b) Pulling (change in oscillator frequency against a specified load mismatch over 360° of phase variation) and c) Pushing (change in oscillator frequency against dc bias point variation).
8. *Spurious signals*: output signals at frequencies other than the desired oscillation carrier.

3.4 DESIGN PROCEDURE FOR INTEGRATED-OSCILLATOR MICROSTRIP ANTENNA

The aim of this study is to design an integrated-oscillator active patch antenna to operate at 2.4 GHz for wireless LAN application. A common source PHEMT transistor was used, with positive feedback to enhance the instability of the active device. A microstrip-fed patch antenna was employed as output terminating element for the unstable device. The antenna was directly connected with the active device for reducing the power loss and circuit complexity and input impedance of the antenna was optimised in terms of output power and harmonic levels. The design configuration of active integrated oscillator antenna is illustrated in Fig. 3.3. To meet the target a number of tasks need to be carried out:

1. Choose an active device and make it unstable by applying positive feedback.
2. Design the antenna and run the simulation to get the value of S_{11} (using ADS). The input impedance of the antenna from its feeding point at oscillating frequency should have exactly desired value, which was obtained from the optimisation of load impedance in the oscillator design.

3. Store antenna S_{11} data (in magnitude and phase format) as a one-port device.
4. Design the input matching network for the active device to matching it to 50 Ω and optimize oscillator load impedance for the purpose of maximizing the input and output reflection coefficients at the active device two sides.
5. Use one-port device (antenna) replace optimal oscillator load so that the microwave oscillator circuit can be directly integrated with the antenna; optimize oscillator load impedance for the purpose of maximizing the output power at the fundamental and its harmonic contents.
6. Fabricate a prototype integrated active oscillator antenna circuit and test it.

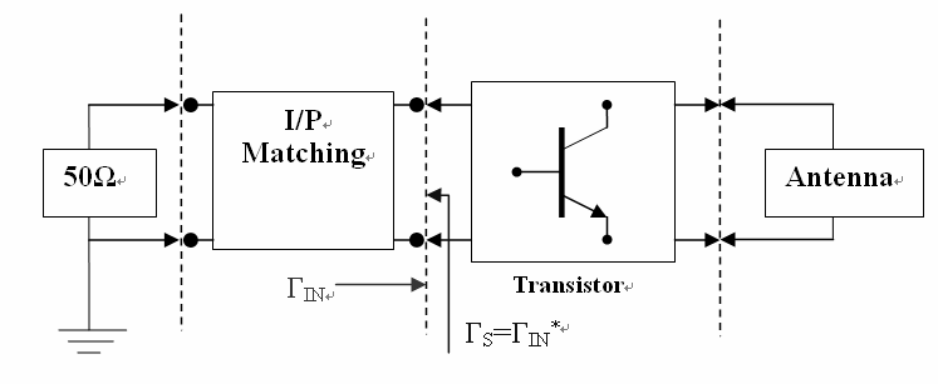

Figure 3.3 AIA integrated oscillator circuit diagram.

3.5 SIMULATION OF INTEGRATED ACTIVE OSCILLATOR ANTENNA

3.5.1 Oscillation generation of active device

In any RF/Microwave system the oscillator is the main and very important component. Designing an oscillator system, we would prefer to bring into play an oscillator with high gain, low noise and good stability conditions. A transistor of ATF-35143

Pseudomorphic HEMT with feature of low noise figure and high gain was selected as the active device for the presented design. According to the S parameters of the device in the datasheet provided from device manufacturer, the drain bias voltage is 2 V, while gate bias voltage is set for having dc drain current of 30 mA. The S parameters of the device under the stated biasing condition at design frequency of 2.4 GHz are shown in Table 3.2 and the stability factor K was calculated using obtained S parameters and found to be less than 1 (K = 0.458). It means that the active device at desired frequency is conditionally stable.

Table 3.2 Simulated S parameters of the transistor at 2.4 GHz.

freq	S			
	S(1,1)	S(1,2)	S(2,1)	S(2,2)
2.400GHz	0.772 / -91.800	0.078 / 38.800	6.274 / 105.600	0.366 / -64.600

An open microstrip transmission line, connected to the source of the PHEMT, was applied the voltage series feedback in order to improve the instability of the device by adding reactance to the source. Fig. 3.4 shows the simulated schematic circuit diagram and corresponding results for S_{11} and S_{22} of the transistor from 0.1 GHz to 5 GHz. As can be seen, the magnitude (in dB) of the S_{11} and S_{22} of the transistor is greater than 1 (K= -0.73), which indicates that the active device is able to produce negative resistance from its input and output ports.

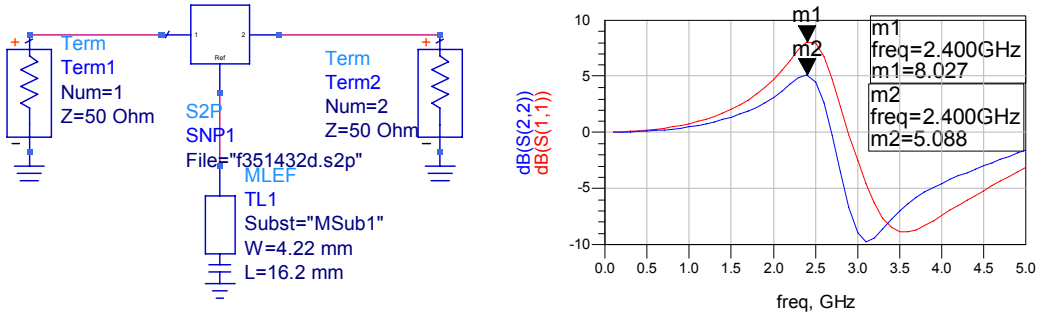

Figure 3.4 Simulated circuit and results for enhancing instability of the transistor.

3.5.2 Biasing circuit design

When designing the dc bias for an oscillator circuit at microwave frequencies we have to be very careful, as it is a very important part of the circuit. Poor oscillator performance in a final design measurement, often leads to improper dc biasing. The main principle is to generate a constant quiescent point (Q) in order to be able to maintain transistor's characteristics even with temperature fluctuations or any changes may occur in the active element.

The biasing circuit (see Fig. 3.5) consists of two parts, one connected to the drain with a series large value inductor providing high impedance RF path, followed by a large value shunt capacitor, which offers low path to ground (dc blocking). And the passive bias circuit where a self-biased resistor is used to set Ids current and so to allow operation without negative voltage for the gate of the transistor. The appropriate calculations required for the dc bias of the transistor are shown below

.

From technical data sheet we get:

V_{DS}=2 V, I_{DS}=30 mA, V_P= -0.5 V, I_{DSS} = 65 mA.

$$V_{GS} = V_P\left(1-\sqrt{\frac{I_D}{I_{DSS}}}\right) = -0.5\left(1-\sqrt{\frac{30E-3}{65E-3}}\right) = -0.1605\,V \tag{3.5}$$

$$R_S = \frac{|V_{GS}|}{I_D} = \frac{0.1605}{0.030} = 5.35\,\Omega \tag{3.6}$$

$$R_D = \frac{V_{DD} - |V_{GS}| - V_{DS}}{I_D} = \frac{5 - 0.1605 - 2}{0.030} = 94.65\,\Omega \tag{3.7}$$

$$V_D = V_{DS} - |V_{GS}| = 2 - 0.1605 = 1.8395\,V \tag{3.8}$$

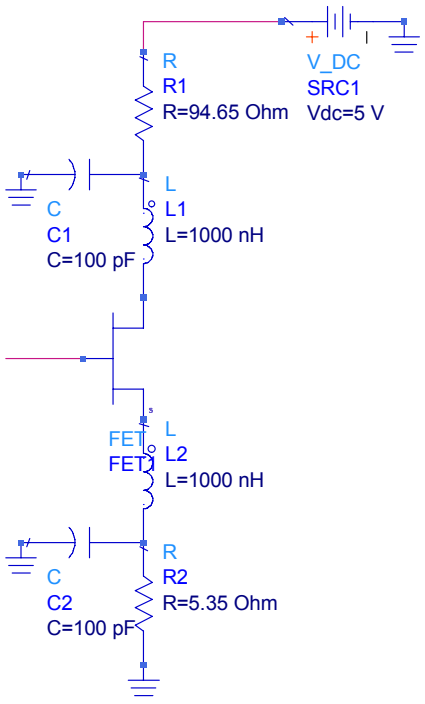

Figure 3.5 Biasing circuit of PHEMT active device.

3.5.3 Design of microstrip patch antenna with a circular-sector

The design procedure for a practical design of a circular microstrip antenna for the dominant TM_{11} mode is outlined below, which is based on the cavity model formulation.

The procedure includes that the specified information needed are the dielectric constant of substrate (ε_r), the resonant frequency (f_r) and the height of the substrate (h).

- ε_r=2.55
- f_r=2.4 GHz
- h=1.524 mm

The actual radius 'a' of the patch needs to be determined using the following formulas [18, 19]

$$\alpha = \frac{F}{\left\{1 + \frac{2h}{\pi \varepsilon_r F}\left[\ln\left(\frac{\pi F}{2h}\right) + 1.7726\right]\right\}^{1/2}} \quad 3.9$$

Where,

$$F = \frac{8.791 \times 10^9}{f_r \sqrt{\varepsilon_r}} \quad 3.10$$

Using (Eqn. 3.10)

$$F = \frac{8.791 \times 10^9}{2.4 \times 10^9 \sqrt{2.55}} = 2.294 \approx 2.3 \quad 3.11$$

Therefore using (Eqn. 3.9)

$$\alpha = \frac{2.294}{\left\{1 + \frac{2 \times 0.1524}{\pi 2.55 \times 2.294}\left[\ln\left(\frac{\pi 2.294}{2 \times 0.1524}\right) + 1.7726\right]\right\}^{1/2}} = 2.21cm \quad \Rightarrow \underline{\underline{\alpha = 22.1mm}} \quad 3.12$$

Thus, the calculations shown that the circular patch has to be designed having a radius of 22.1 mm. A feeding line had to be connected to the patch, which placed at the middle of the circle. Also had to be calculated as follows:

$$\lambda = \frac{c}{f} = \frac{3\times10^{8}}{2.4\times10^{9}} = 0.125m \qquad 3.13$$

$$\lambda/4 = 0.03125m \Rightarrow \underline{\underline{\lambda/4 = 31.25mm}} \qquad 3.14$$

The feeding line length found to be 31.25 mm. To gain the desired minimum return loss the radius of the circle and the dimensions of the feeding line had to take many optimizations. Changing the radius of the patch tends to vary the frequency response of the antenna, while changing the feeding line length we get variation of the return loss value. Mismatching the radius and the dimensions of the microstrip line, results in appearance of side harmonics near to the operating frequency, which will affect the stability of the two port device. Therefore, after optimization of the calculated values the radius was set to 30 mm, the length of the feeding line 20.4 mm and the width 2 mm.

The simulation analysis of the patch was done on ADS software using a layout window. With the aid of trigonometric equations we calculated the values that used in order to cut off the exact 120° arc-sector of the circular patch. The circular-sector patch is illustrated below (see Fig. 3.6).

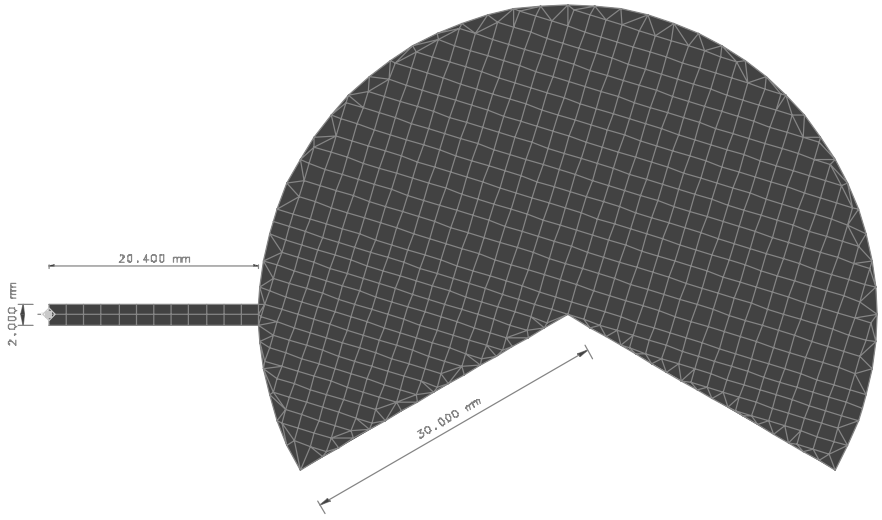

Figure 3.6 Layout of proposed patch antenna with meshing.

As can be clearly seen in Fig. 3.6, the feeding point was positioned at the middle of feeding line for best return loss results. The substrate specifications and simulation frequency range was set up at momentum palette window, and we run the simulation. In Fig. 3.7, the minimum return loss of the patch at operating frequency is presented.

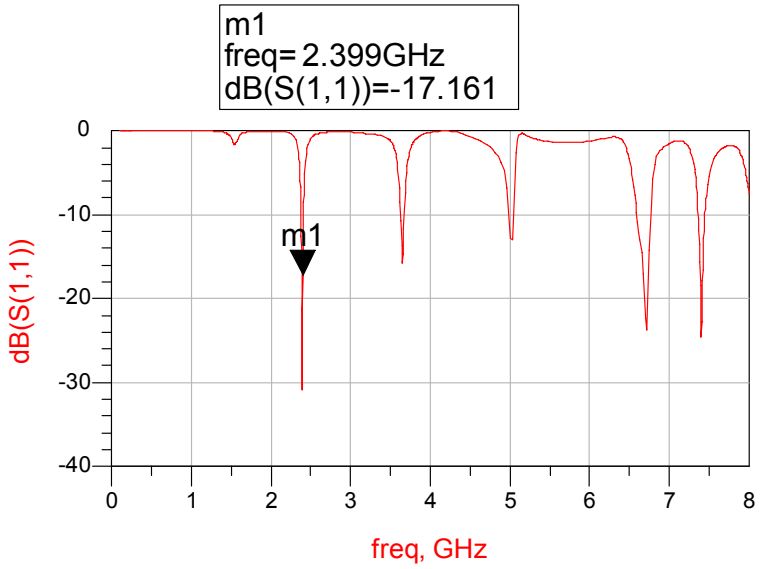

Figure 3.7 Simulated antenna return loss.

With the values of S_{11}, provided in Table 3.3, we were able to calculate the input impedance of the antenna using the Eqn. 3.15.

$$Z_{in} = \frac{(1 + S_{11})}{(1 - S_{11})} \qquad 3.15$$

Antenna load impedance (Z_{in}) was calculated to be (80.057-j*22.58) Ω. The equivalent circuit will be an R-C circuit which consists of a resistor R=80.057 Ohm and a capacitor C=2.93 pF connected in series. Thus, the R-C equivalent circuit in schematic diagram is illustrated in Fig. 3.8.

Table 3.3 Antenna S_{11} in different format at design frequency.

freq	S(1,1)	S(1,1)	S(1,1)
2.399GHz	-17.161 / 88.512	0.004 + j0.139	0.139 / 88.512

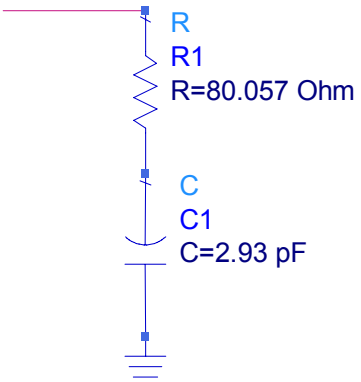

Figure 3.8 Schematic diagram of the antenna equivalent circuit.

3.5.4 Optimisation load impedance and input matching network design

After we have proved transistor's instability, by providing series feedback, the next step was to introduce the antenna load impedance to the transistor. The "R-C" circuit was connected in series to transistor's drain with resistor and inductor values of R=80.057 Ω and L=2.93 nH, respectively, as illustrated in Fig. 3.9.

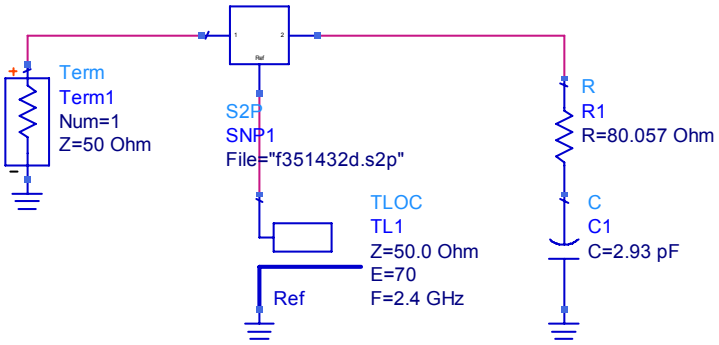

Figure 3.9 Unstable transistor integrated antenna load impedance.

After running the simulation, the S parameters values were not promising, and we realized that the load was not capable to drive the transistor to instability. Our aim became to vary the load in order to get a high value of S_{11} parameter, which would drive the transistor with the load in the unstable region. Therefore using "Optimization" and "Tuning" tools in ADS package we obtained the appropriate values of an "R-L" configuration. The load of the unstable two port device was optimized to be of 52.1 Ω in series with 4.37 nH. The circuit with series feedback and load is shown in Fig. 3.10 and the reflection coefficient S_{11} is plotted against frequency and presented in Fig. 3.11.

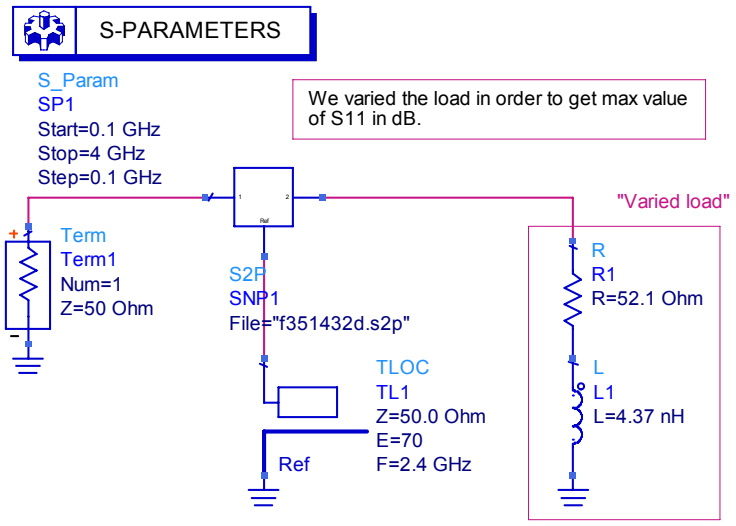

Figure 3.10 Transistor with a load in the unstable region.

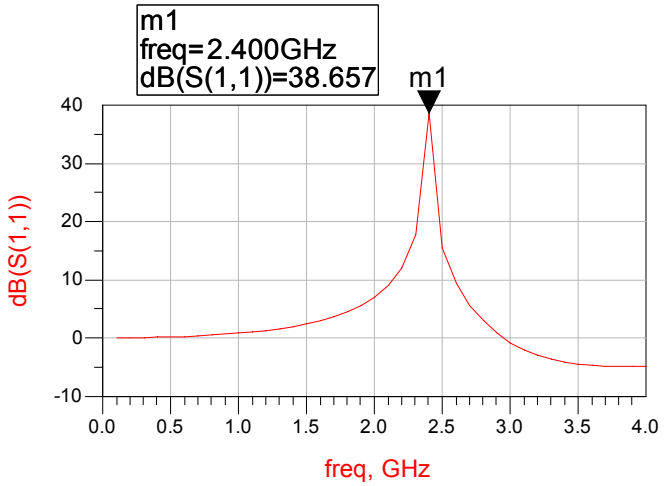

Figure 3.11 Maximum S_{11} value for PHEMT with load.

In addition, using the equations in the Data Display window of ADS, the impedance Z_{11} was calculated. Then, with Z_{11}= (-70.049-j*49.325) Ω we were able to calculate the input impedance Z_{in} as follows:

$$\left.\begin{array}{l} Z_{11} = (-70.049 - j*49.325)\Omega \\ \text{Using } Z_{IN} = -\dfrac{G}{3} \end{array}\right\}$$

$$\Rightarrow \quad Z_{IN} = -\left(-\frac{70.049}{3} - j*49.325\right) = (23.35 + j*49.33)\Omega \qquad 3.16$$

Thus, with the value of Z_{in} we calculated the input reflection coefficient, Γ_{in}, which will be used for the design of the input matching network.

$$\Gamma_{IN} = \frac{Z_{IN} - Z_0}{Z_{IN} + Z_0} = \frac{23.35 + j*49.33 - 50}{23.35 + j*49.33 + 50} = (0.061 + j*0.631)\Omega \qquad 3.17$$

Thus, input matching network for the active device can therefore be established.

3.5.5 Simulation of integrated active oscillator with circular patch

A linear simulation using the small signal S parameters [20] of the active device was employed to determine the oscillating frequency and optimise for maximum reflections at 2.4 GHz for input and output ports. Fig. 3.12 shows the linear circuit model of the oscillator. This linear model of the oscillator is based on two oscillation conditions at the desired frequency of oscillation: one is that there is excess negative resistance and the other is the total reactance goes to zero.

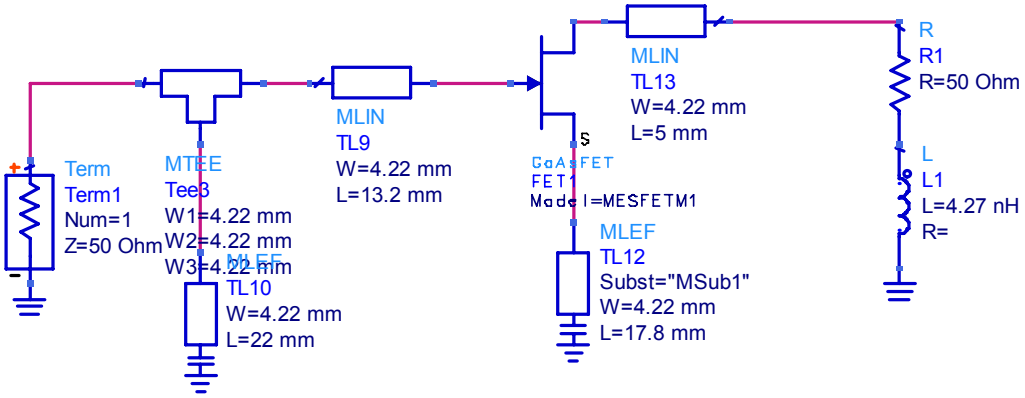

Figure 3.12 Linear circuit model of the oscillator.

With proper selection of values for the resistor components in the dc biasing circuit, a non-linear model of the device and harmonic balance simulation including first 3 harmonics are used in the design to predict the characteristics of the active oscillator design in terms of output power, harmonic level, frequency pushing and phase noise. The load impedance at the fundamental frequency of the oscillator was optimized for producing maximum output power and reasonable harmonic level. The simulator used was ADS. The antenna was directly incorporated in the simulation as a one-port device containing the S parameters data from 0.1 GHz to 8 GHz. The non-linear model of the simulated active oscillator circuit including the antenna data and the corresponding simulated results are shown in Figs. 3.13 and 3.14, respectively.

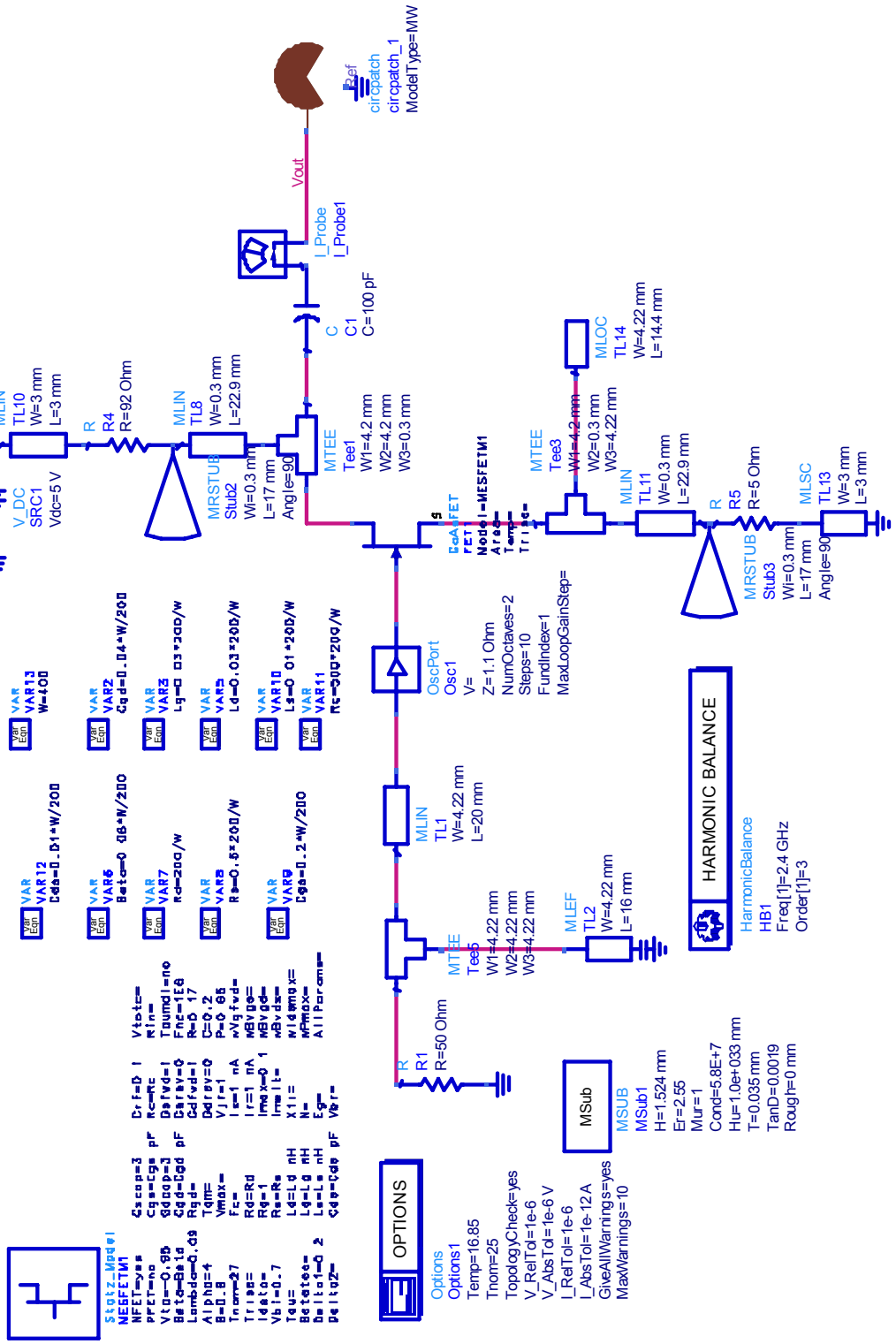

Figure 3.13 Final non-linear model circuit for the oscillator of the reactive load.

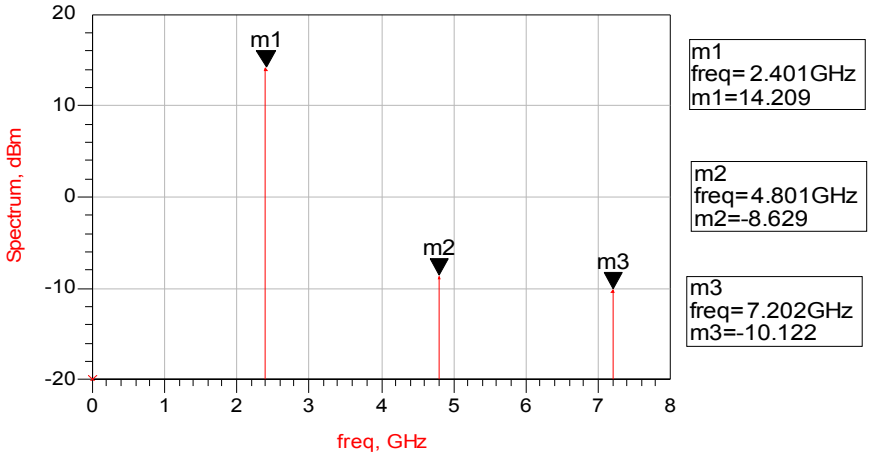

Figure 3.14 The simulated spectrum of the designed oscillator without containing the antenna data.

Moreover, the simulated output current and voltage waveforms generated from the drain of the transistor were also investigated, which are presented in Fig. 3.15. As can be seen, the sinusoidal wave with little distortion was observed due to the non-linear characteristics of the active device.

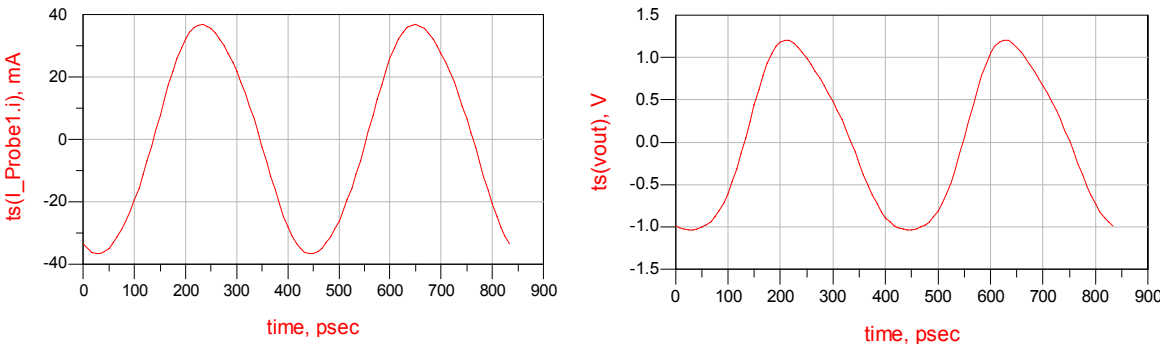

Figure 3.15 The drain output waveforms, current (left) and voltage (right).

Fig. 3.16 presents the final layout of the proposed microwave oscillator directly integrated with circular sector microstrip patch. The prototype of oscillator integrated with antenna, including the sensor, was fabricated on Duroid material (ε_r = 2.55, thickness h = 1.524 mm, and tanδ = 0.0018). The sensor here is applied to measure the power accepted at the input of the integrated antenna and more details about it will be discussed in the next section.

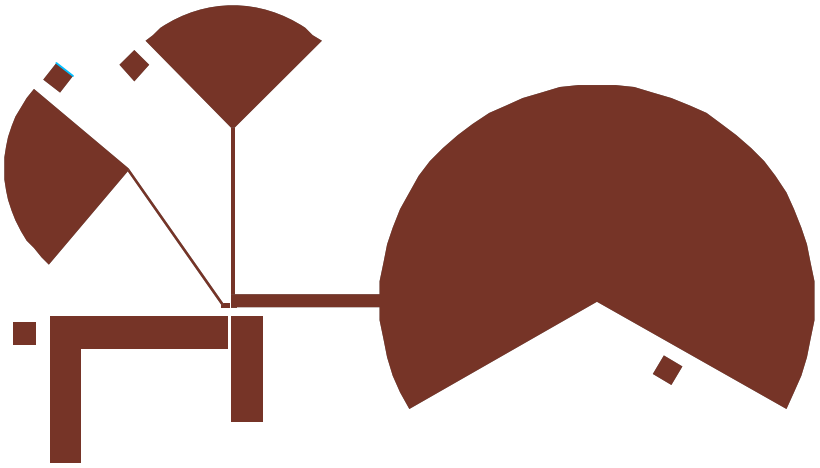

Figure 3.16 Layout for the integrated active oscillator circular antenna.

3.5.5 Simulation of integrated active oscillator with rectangular patch

In this section, a microstrip rectangular patch antenna, operating at 2.4 GHz, was designed and used to replace the circular sector patch antenna for the active integrated oscillator design, in order to verify performance of the active integrated oscillator antenna at the harmonic level. As we studied earlier, the circular sector patch antenna is a harmonic suppression antenna; but the rectangular patch antenna does not provide a

freedom to control its input impedance at harmonics, unless otherwise, shorting pins are applied at the centre of the patch to terminate the 2nd harmonic frequency.

The antenna was considered as microstrip line fed rectangular patch. The dimensions of the patch and the feed line are (height 52 mm x width 38 mm) and (height 2 mm x width 16 mm), respectively. Fig. 3.17 shows the layout the proposed antenna. With this dimension, the input impedance of the antenna from its feeding point at oscillating frequency should have exactly desired value, which was obtained from the optimisation of load impedance in the oscillator design. The input impedance of the antenna at fundamental was found to be (29.246 + j*4.917) Ω using Momentum and Fig. 3.18 shows the simulated antenna return loss from 0.1 GHz to 8 GHz which well covers the fundamental frequency and second and third harmonics. The antenna works here as resonant component as well as radiating element.

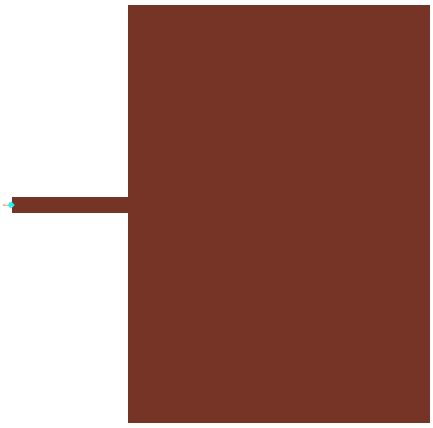

Figure 3.17 Layout of the microstrip rectangular patch antenna.

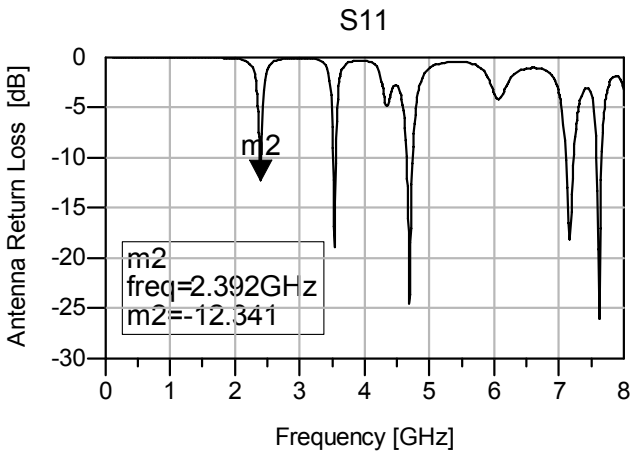

Figure 3.18 Simulated antenna return loss up to 8 GHz.

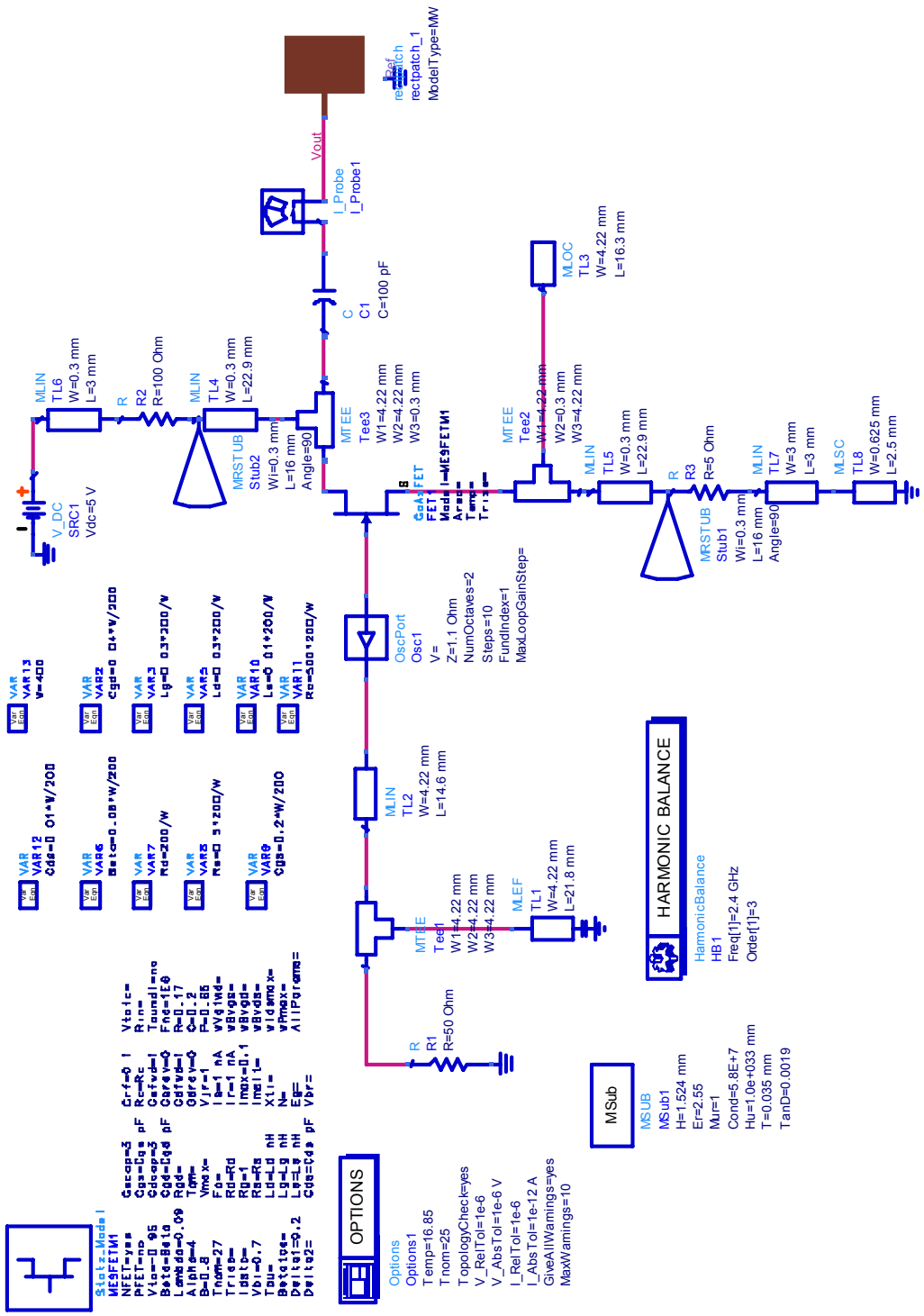

Figure 3.19 Final non-linear model circuit for the active oscillator antenna.

Subsequently, the one-port device, containing antenna simulated data, was directly integrated with the same microwave oscillator circuit to replace the existing circular patch in the forgoing section. The performance of this new integrated active oscillator antenna with rectangular patch (see Fig. 3.19) was optimized in terms of oscillating frequency, output power at fundamental and harmonics.

Fig. 3.20 presents the simulated results of the active oscillator antenna circuit at the targeted design frequency and accepted output power and harmonic performance. A layout of the integrated antenna circuit is illustrated in Fig. 3.21.

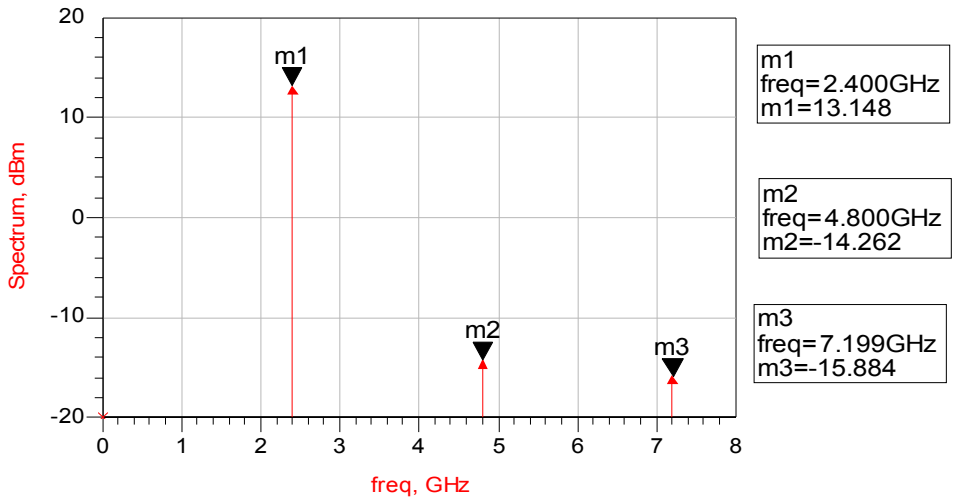

Figure 3.20 The simulated spectrum of the active oscillator rectangular antenna.

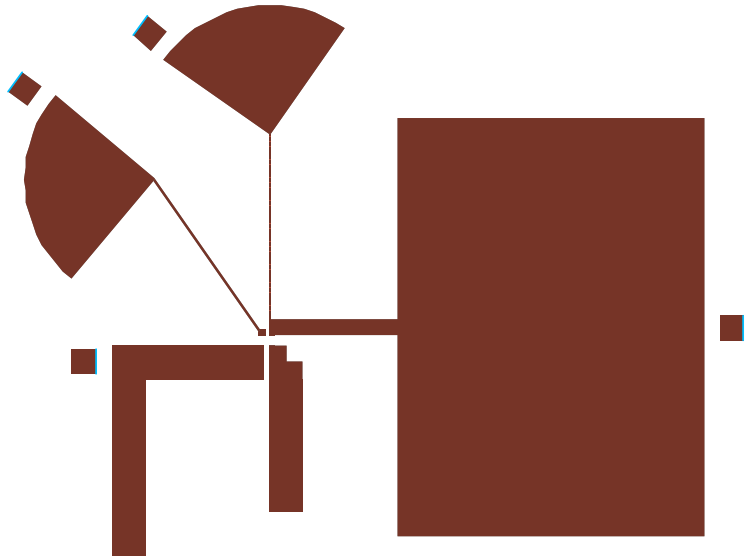

Figure 3.21 Layout for the integrated active oscillator rectangular antenna.

3.5.6 Sensor Element Design and Calibration

The sensor, which is shown in Fig. 3.22, was created by a small patch with dimension of 3 mm x 5 mm, placed at the edge of the antenna in which the maximum voltage exists. It was found that a 2 mm space distance between the sensor and the antenna edge was adopted for the measurements and the presence of the sensing patch has very little effect on the return loss of the main patch. The sensor patch was connected to ground via a 50 Ω chip resistor, improving the output matching of the sensor circuit. A 50 Ω coaxial probe was mounted at the rear of the circuit board and connected to the resistor load. This fed the sensor output to a well-calibrated network analyser, avoiding room reflections as far as possible. The inclusion of the 50 Ω resistor for such a sensor insures that the output connector of the sensor appears as a relatively well-matched source.

$$S_{21}^{'} = \sqrt{\left|S_{21}\right|^2 \Big/ \left(1-\left|S_{11}\right|^2\right)} \qquad 3.18$$

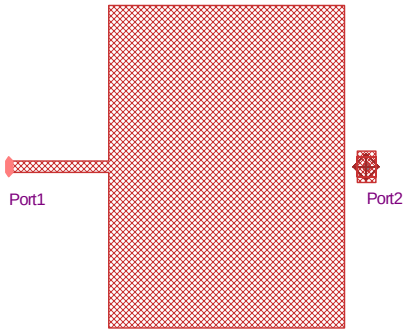

Figure 3.22 The configuration of sensor patch element.

The S-parameter attained from the design shown in Fig. 3.23 was exported as Touchstone file and then the data was imported to ADS circuit simulator as a two-port device. In addition, the shunt 50 Ω resistor was added to work as matched source. Fig. 3.23 illustrates the circuit diagram for measuring the S parameters between the patch antenna and the sensor patch element where as the simulated S parameters are presented in Fig. 3.24. Using the foregoing Eqn. 3.18, the predicted calibration factor between the antenna and the sensor patch was found to be about -26 dB.

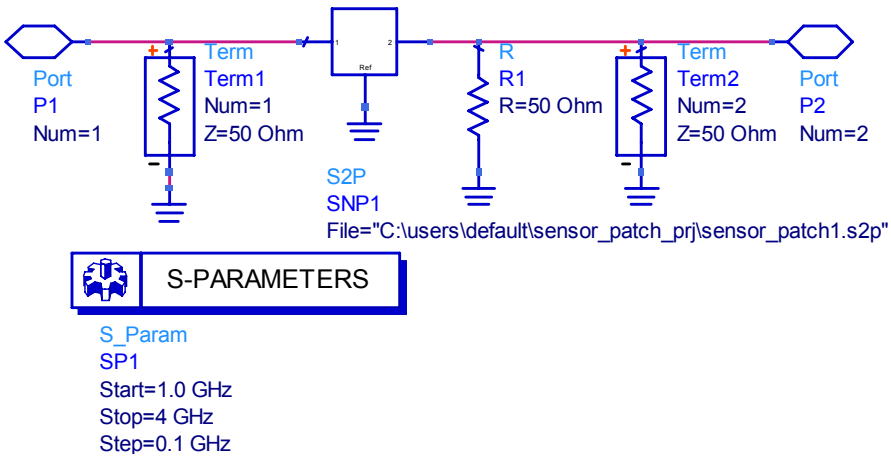

Figure 3.23 The circuit diagram for measuring the coupling between the antenna and the sensor patch element.

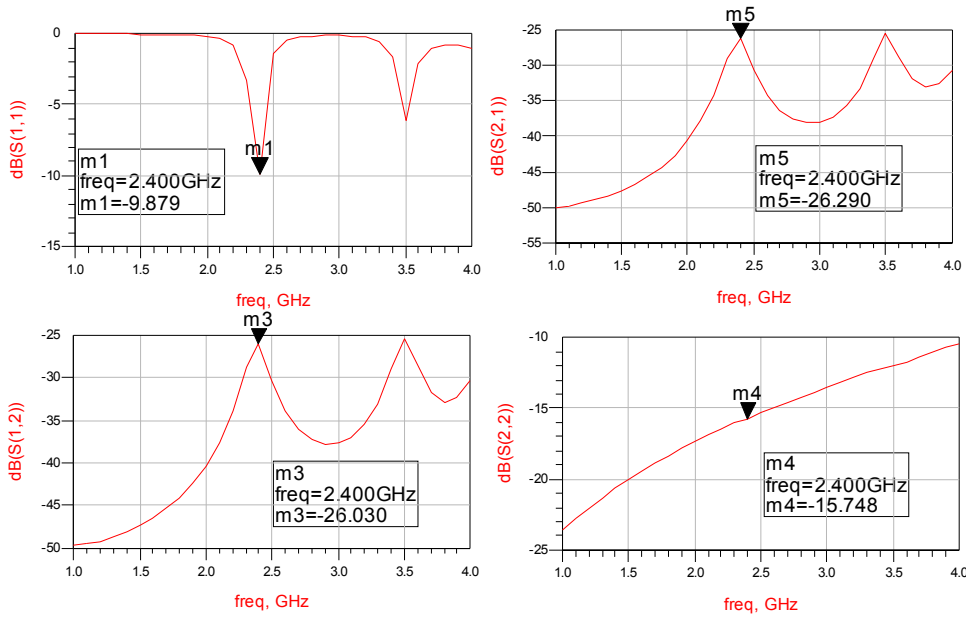

Figure 3.24 The simulated S-parameter between the antenna patch and the sensor element.

3.6 MEASUREMENT OF THE INTEGRATED ACTIVE OSCILLATOR ANTENNA

3.6.1 Sensor patch Calibration in measurement

The measured frequency and the accepted power at the antenna input port was measured using a sensor element and determined by a sensor calibration factor $S_{21}^{'}$, shown in Eqn. 3.18 that had been evaluated when the antenna was disconnected from the oscillator circuit [21, 22]. The prototypes of oscillator integrated with antenna, including the sensor, were fabricated on Duroid material ($\varepsilon_r = 2.55$, thickness h = 1.524 mm, and $\tan\delta = 0.0018$) and are shown in Figs. 3.25 and 3.26 for circular patch and rectangular patch, respectively. The calibration factor was measured first when the antenna was

disconnected from the RF oscillator circuit. The two-port S parameters from 1.4 GHz to 4 GHz between the antenna input feed line and the sensor output are shown in Figs. 3.27 and 3.28 for circular patch and rectangular patch, respectively. The corresponding calibration factor from the measured antenna data was computed using the Eqn. 3.18 and the response of the calibration factor over the band between 2 GHz to 2.8 GHz is shown in Figs. 3.29 and 3.30 for two different antennas. As can be seen in Fig. 3.30, a peak coupling of about -26.5 dB between the sensor and the rectangular patch at the oscillating frequency was observed, which is well agreed with the prediction.

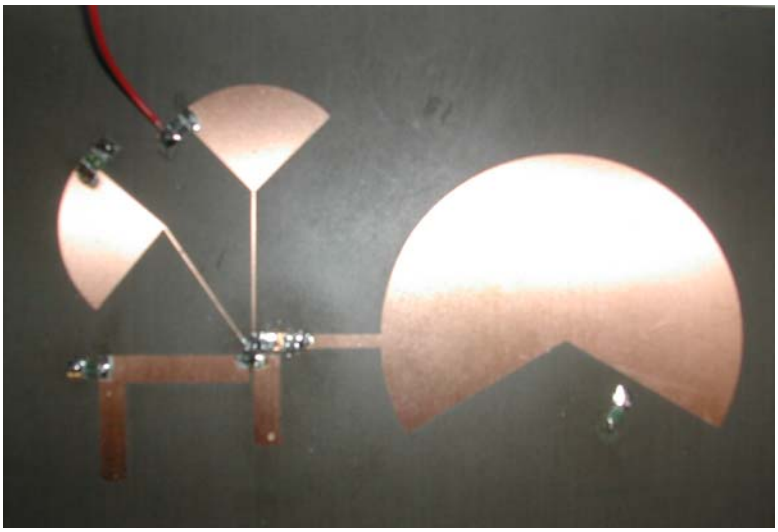

Figure 3.25 Photograph of the oscillator circuit integrated with circular antenna.

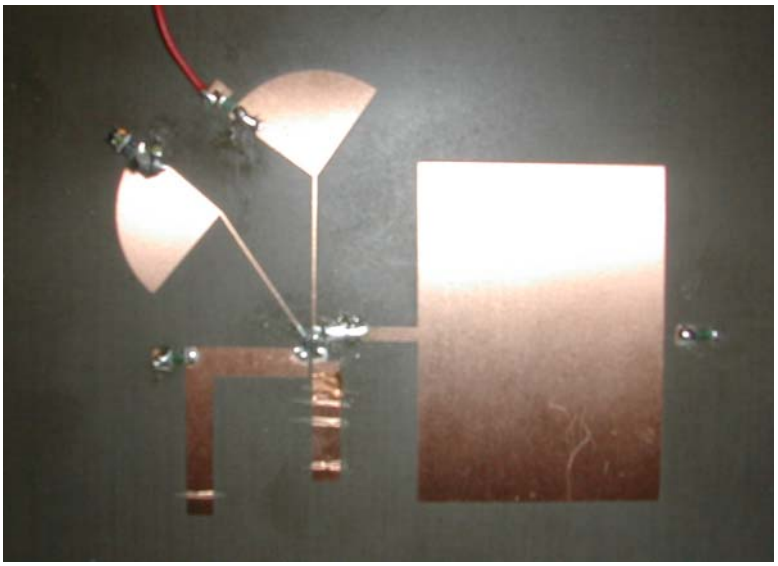

Figure 3.26 Photograph of the oscillator circuit integrated with circular antenna.

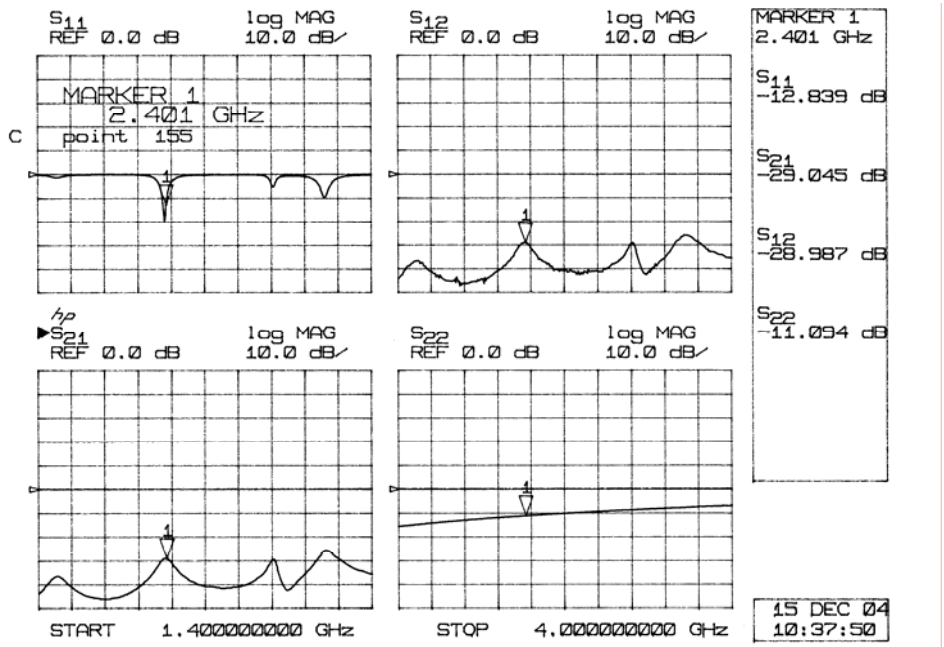

Figure 3.27 The measured two-port S parameters between the antenna input port and sensor output for circular patch.

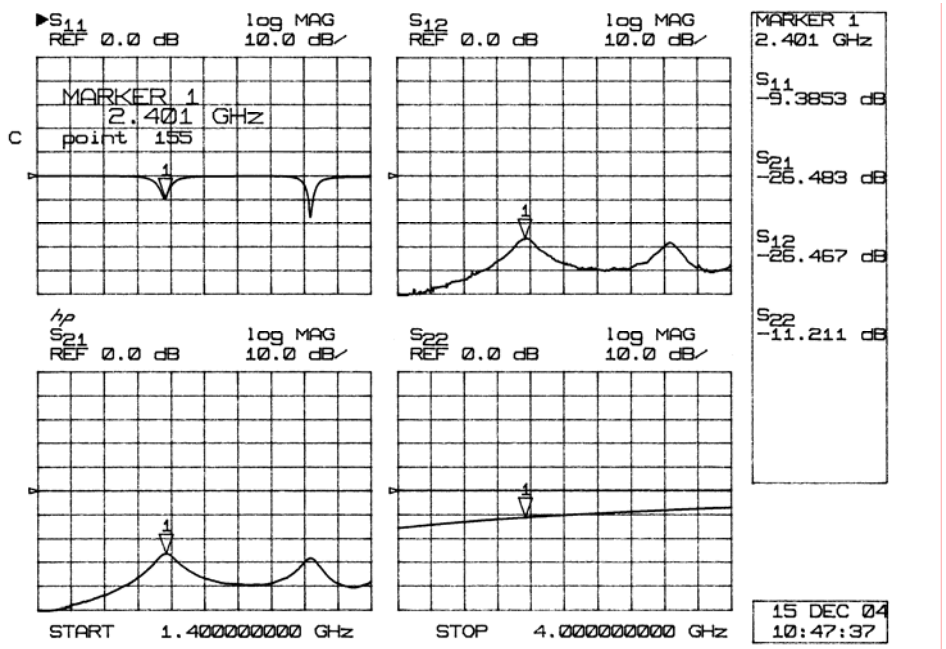

Figure 3.28 The measured two-port S parameters between the antenna input port and sensor output for rectangular patch.

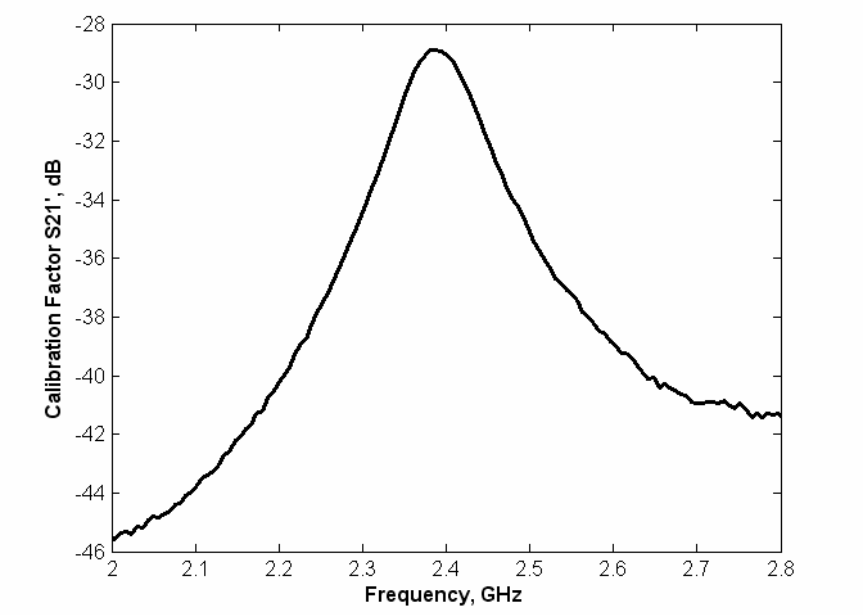

Figure 3.29 Response of calibration factor $S_{21}^{'}$ for circular patch.

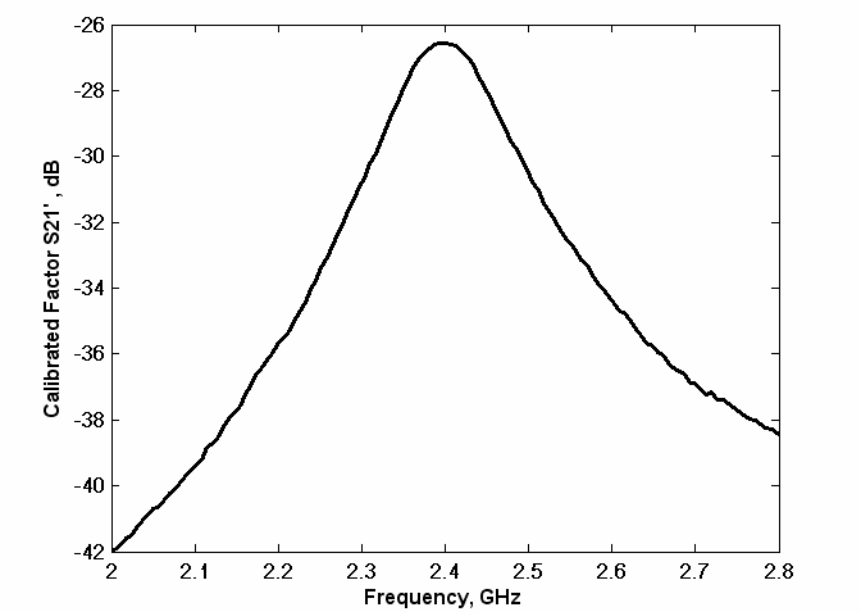

Figure 3.30 Response of calibration factor $S_{21}^{'}$ for rectangular patch.

3.6.2 Results and Discussion

To the oscillator circuit integrated with circular patch, after some adjusting the input matching shut stub and positive series feedback (see Fig. 3.31), the free running oscillation was observed at 2.43540 GHz with 16.17 (-13.83-(-30)) dBm output power. The phase noise at 100 kHz offset was found to be around -40 dBc/Hz, which is quite high compared to the oscillator design specification. This is mostly caused by involving a sensing patch in the measurement that may generate noise and degrade the phase noise performance of the active oscillator. Fig. 3.32 shows the measured free-running oscillation, output power (i.e. the accepted power by the antenna at its input), and phase noise performance that were achieved. The measured efficiency was about 27.6%. Fig. 3.33 shows the output spectrum harmonic contents of the oscillator. The oscillator characteristics on harmonics can not be judged since sensor patch only works for the fundamental frequency. In order to evaluate performance of the oscillator active antenna

at harmonic frequencies, a development on the improvement of measurement techniques for active antennas to find the power accepted by the antenna at harmonic frequencies is studied in Chapter 5, using a sensor patch technique [23].

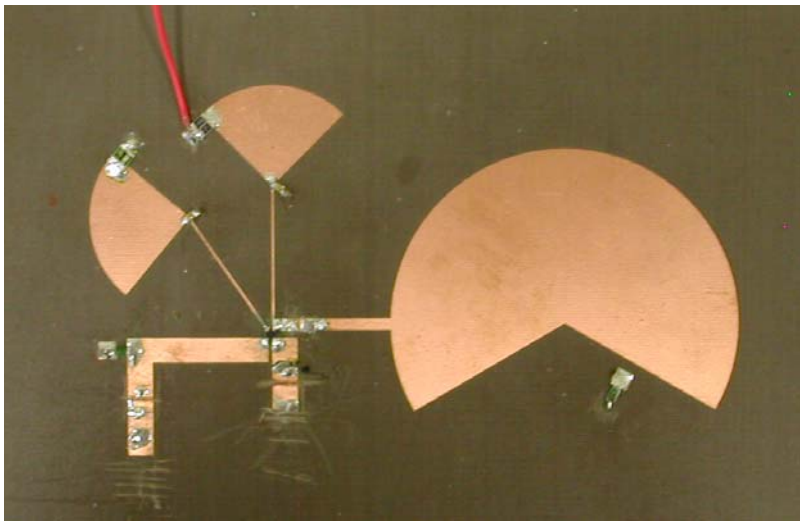

Figure 3.31 Oscillator circuit integrated with circular patch after adjustment.

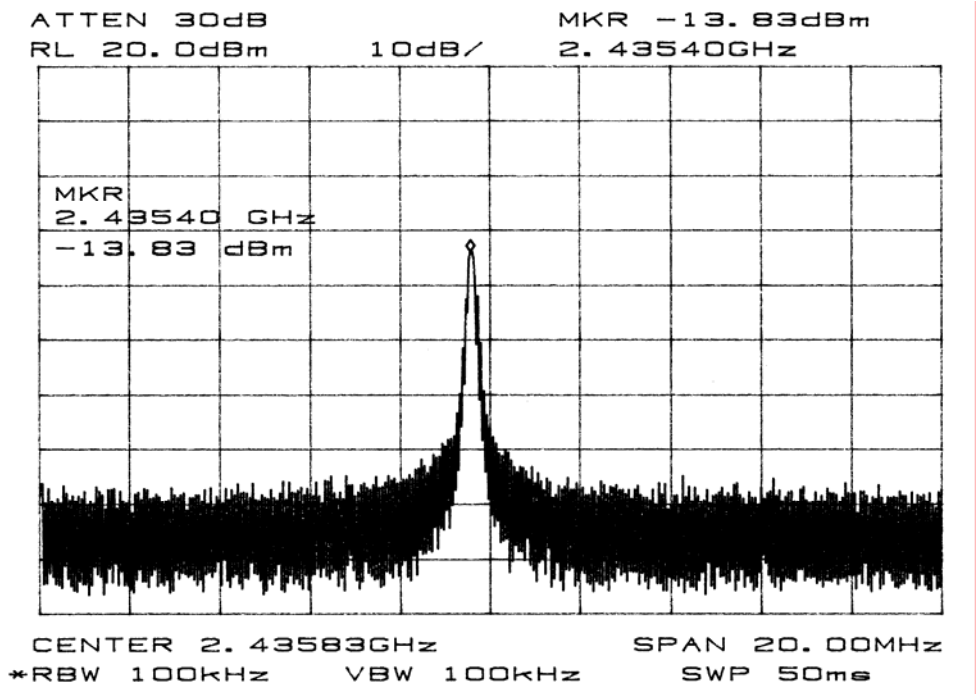

Figure 3.32 Free running oscillation around 2.43 GHz for circular active antenna.

In addition, to the oscillator circuit integrated with rectangular patch, after some adjusting the input matching shut stub and positive series feedback (Fig. 3.34), the free running oscillation was observed at 2.39950 GHz with 11.5 (-15- (-26.5)) dBm output power. The phase noise at 100 kHz offset was found to be around -40 dBc/Hz, which is quite high compared to the oscillator design specification. This is mostly caused by involving a sensing patch in the measurement that may generate noise and degrade the phase noise performance of the active oscillator. Fig. 3.35 shows the measured free-running oscillation and output power performance that were achieved. The measured efficiency was about 9.42%. Fig. 3.36 shows the output spectrum harmonic contents of the oscillator.

Two main problems had drawn our attention from the forgoing measurements. Firstly, the two active oscillator antenna circuits initially did not generate oscillation straight way. Some adjustment had to be carried out on either the oscillator input matching or the positive feedback line (see Figs. 3.31 and 3.34). This is mainly because the nonlinear model of the active device used in the two designs is inaccurate in the modelling so that modification to the circuit had to be applied in order to overcome the problem. The other one is the performance of the phase noise in the active oscillator antenna. The phase noise characteristic observed in the measurement using spectrum analyser, was presented poorly (see Figs. 3.32 and 3.35), even increasing the span of the spectrum or improving the measurement environment with some absorber material around the circuit. This is maybe because of the phase noise of the active device (PHEMT) we used in the design. One suggestion is to use bipolar transistor instead of FET as active device due to its low 1/f noise characteristics, as illustrated in Table 3.1 at the beginning of this chapter.

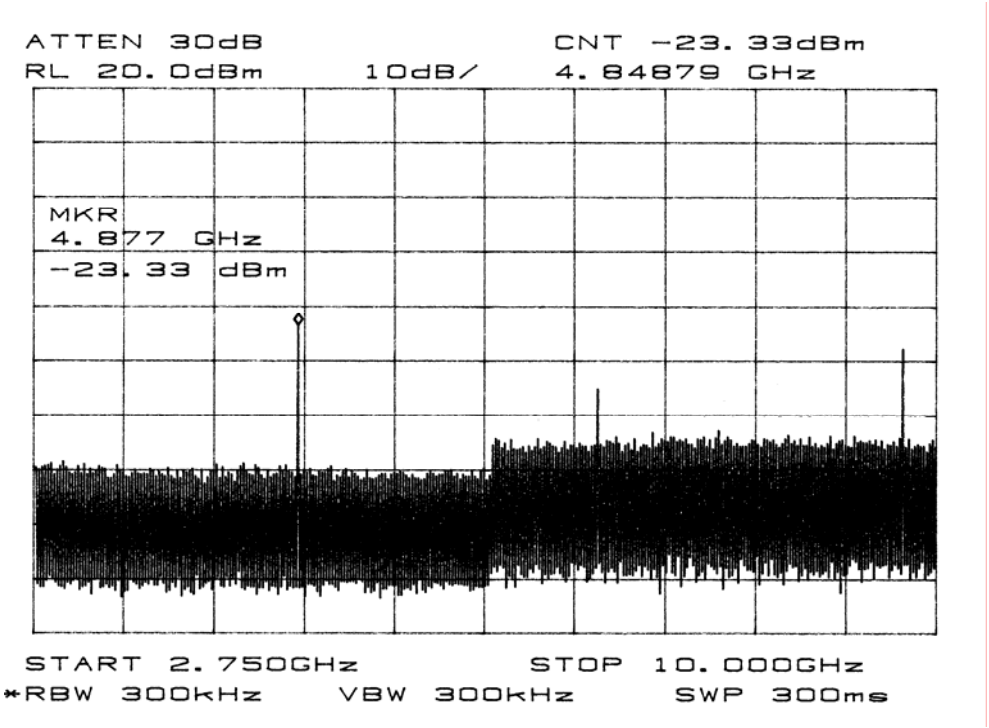

Figure 3.33 The measured harmonic contents for the circular active antenna.

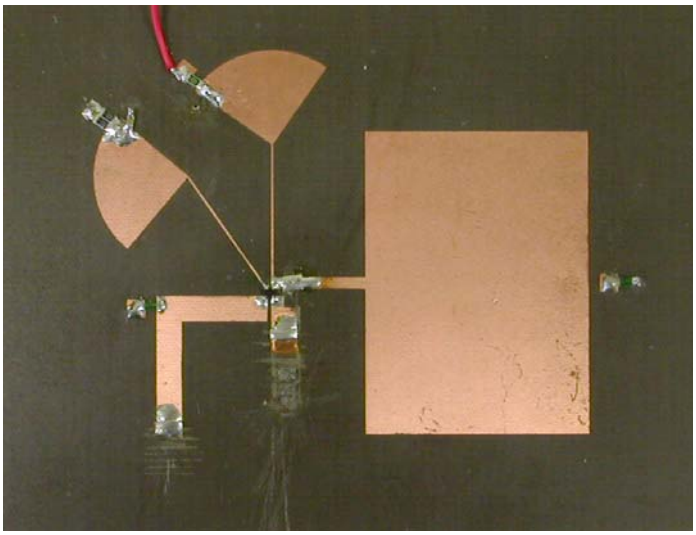

Figure 3.34 Oscillator circuit integrated with rectangular patch after adjustment.

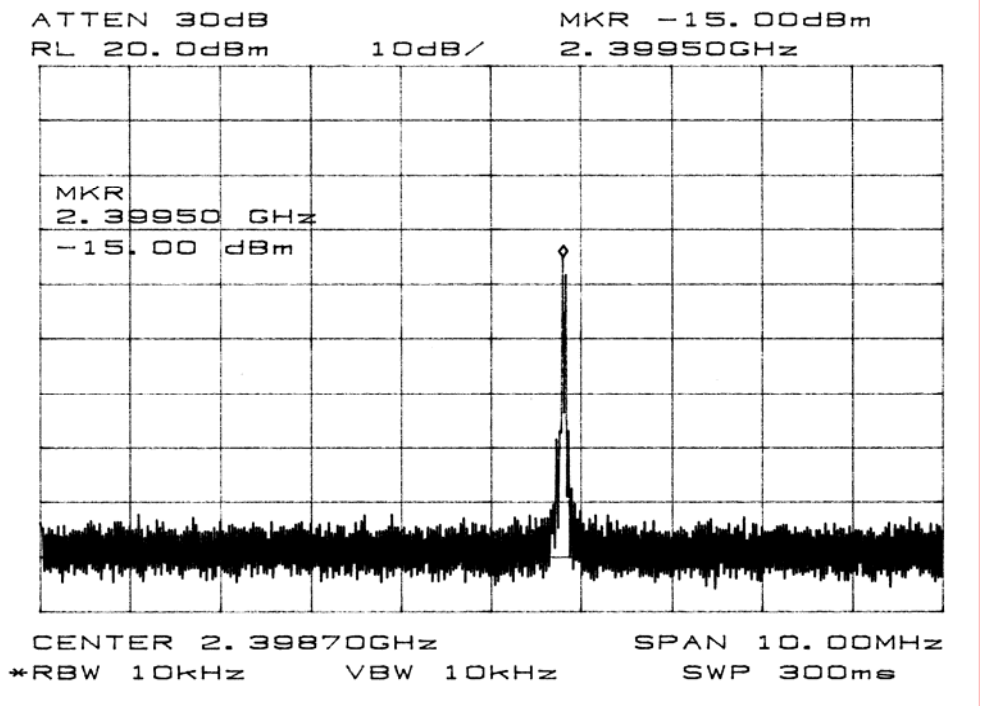

Figure 3.35 Free running oscillation around 2.43 GHz for rectangular active antenna.

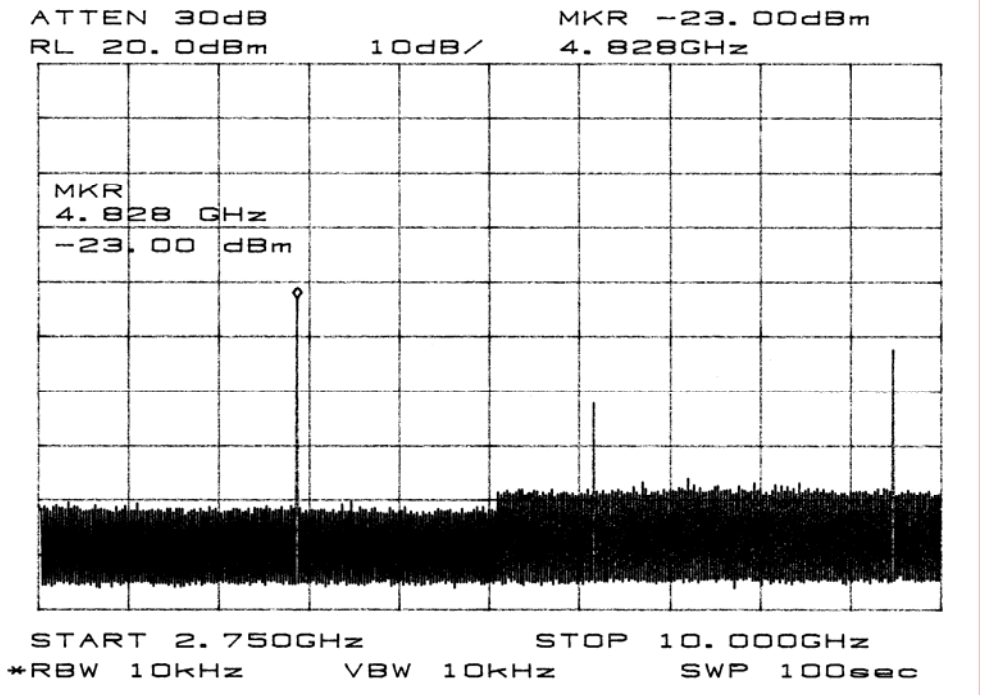

Figure 3.36 The measured harmonic contents for the rectangular active antenna.

3.7 CONCLUSION

The design of an oscillator integrated with an active antenna, working at 2.4 GHz for wireless LANs was designed and investigated. A common source HEMT transistor was used, with positive feedback to enhance the instability of the active device. A microstrip-fed patch antenna (circular and rectangular) was employed as output terminating element for the unstable device. The antenna was directly connected with the active device for reducing the power loss and circuit complexity and input impedance of the antenna was optimised in terms of output power and harmonic levels. A simple design procedure was described and measured results were then discussed. A calibrated sensor placed next to the antenna edge having maximum voltage was used to measure the performance of the active oscillator antenna. The results were encouraging in terms of the free running oscillating frequency and output power. The design goal was well met.

3.8 REFERENCES

[1] J.-Y. Park, S.-M. Han, and T. Itoh, "A rectenna design with harmonic-rejecting circular-sector antenna", IEEE antenna and wireless propagation letter, vol. 3, pp. 52-54, 2004.

[2] J.A. Navarro, K.A. Hummer, and K. Chang, "Active integrated antenna elements", Microwave Journal, pp. 115-126, January 1991.

[3] G. Forma and J.M. Laheurte, "CPW-fed oscillating microstrip antennas", Electronics Letters, vol. 32, no. 2, pp.85-86, 18th January 1996.

[4] A. A. Melcon, V. Campos, J.-F. Zurcher, and J.R. Mosig, "A simple low-cost coplanar twin-slot active antenna oscillator for wireless applications", Microwave and optical technology letters, vol. 23, no.1, pp. 18-25, October 5 1999.

[5] D.-H. Choi and S.-O. Park, "Active integrated antenna using a T-shaped microstrip coupled-patch antenna", Microwave and optical technology letters, vol. 44, no. 5, pp. 434-436, March 5 2005.

[6] C.M. Montiel, L. Fan, and K. Chang, "An FET active notch antenna stabilized with a slot-line ring resonator", Microwave and optical technology letters, pp. 288-291, vol. 21, no. 4, May 20 1999.

[7] M.J. Cryan, G.R. Buesnel, and P.S. Hall, "Analysis and control of harmonic radiation from active integrated oscillator antennas", IEEE Transactions on microwave theory and techniques, vol. 50, no. 11, pp.2639-2646, November 2002.

[8] D. Zhou, R.A. Abd-Alhameed and P.S. Excell, "Design of Active Oscillator Microstrip Patch Antenna for 2.4 GHz", proceedings of the sixth informatics workshop for research students, pp. 216-219, University of Bradford, Bradford, UK, 23rd March 2005.

[9] T. Razban, M. Nannini, and A. Papiernik, "Integration of oscillators with patch antennas", Microwave Journal, pp. 104-110, January 1993.

[10] T. Razban, H. Frances, B. Robert, and A. Papiernik, "A compact oscillator integrated in a microstrip patch antenna", Microwave Journal, 37, pp. 110-5, February 1994.

[11] S.P. Kwok and K.P. Weller, "Low cost X-band MIC BARITT Doppler sensor", IEEE Transactions on microwave theory and techniques, vol. 27, no. 10, pp. 844-847, October 1979.

[12] B.M. Armstrong, "Use of microstrip impedance-measurement technique in the design of a BARRTT diplex Doppler sensor", IEEE Transactions on microwave theory and techniques, vol. 28, no. 12, pp.1437-1442, December 1980.

[13] J.A. Navaro, K.A. Hummer and K. Chang, "Active integrated antenna elements" Microwave Journal, 35, pp.115-121, 1991.

[14] S.A. Mass, "Nonlinear Microwave and RF circuits", Norword, MA: Artech House, 1998.

[15] D.M. Pozar, "Microwave Engineering", Second edition, John Wiley & Sons, INC., pp. 641-647, 1998.

[16] G.R. Buesnel, M.J. Cryan and P.S. Hall, "Harmonic control in active integrated patch oscillator", Electronics Letters, vol.34, no.3, pp. 228-229, 5th February 1998.

[17] K. Chang, I. Bahl and V. Nair, "RF and Microwave circuit and component design for Wireless systems", John Wiley & Sons, New York, 2002.

[18] L.C. Shen, M. Allerding and M. Walton, “Resonant frequency of a circular disc, printed-circuit antenna”, IEEE Transactions on antennas and propagation, vol. 25, no. 4, pp. 595-596, 1977.

[19] W.F. Richards, J.D. On and S.A. long, “A theoretical and experimental investigation of annular, annular sector, and circular sector microstrip antennas”, IEEE Transactions on antennas and propagation, vol. 32, no. 8, pp. 864-867, 1984.

[20] G.D. Vedelin, A.M. Pavio and U.L. Pohde, “Microwave circuit design using linear and nonlinear techniques”, Wiley-Interscience, 1990.

[21] E. Elkhazmi, “Measurement and optimization of efficiency and harmonic rejection in transmitting active patch antenna”, PhD thesis, University of Bradford, UK, 2001.

[22] E.A. Elkhazmi, N.J. McEwan, and N.T. Ali, “A Power and Efficiency Measurement Technique for Active Patch Antennas”, IEEE Transactions on microwave theory and techniques, vol. 48, no. 5, pp. 868-870, May 2000.

[23] D. Zhou, R.A. Abd-Alhameed, N.J. McEwan and P.S. Excell, “Investigations on Second Harmonic Measurements Using a Sensor Patch for Active Patch Antennas”, In proceeding of the seventh informatics workshop for research students, pp. 200-201, Bradford, UK, 29th March 2006.

CHAPTER 4

AM AND ASK MODULATION USING INTEGRATED OSCILLATOR ANTENNAS

4.1 INTRODUCTION

Active oscillator antennas are antennas in which active devices are integrated directly with the antenna structure. The basic function of the active device is the RF signal generation where as the antenna acts as a resonant load as well as a radiating element. This type of active antenna has received much attention due to its compact size, low weight, low cost and multi-functionality. They have been developed for low cost and compact sensor and transceiver applications and also have strong potential for applications in commercial wireless communications [1, 2].

Much of the research on integrated oscillator antennas has concentrated on several designs to generate a steady-state oscillation using either two-port active devices (IMPATT diodes and Gunn diodes) or three-port active devices (MESFET, HEMT, and HBT) with different antenna configurations. Advantages and disadvantages associated with each type of solid state device are addressed in a well known text book [3]. Surprisingly, however, little research in the open literature can be found for the integrated oscillator antenna to be used as a modulator. With this scenario, the type of

active antenna can be classified as a frequency conversion type and employed to design compact transmitters. Some examples of this frequency conversion-type antenna have been reported in the literature for FM, PM, BPSK and QPSK modulation for transponding applications [4-6].

In this chapter, the design approach of the integrated oscillator antenna using a bipolar transistor in which a novel and simple method of generating AM and ASK modulations for a compact transmitter is presented. A prototype circuit has been fabricated and tested to prove the design theory. The linear and non-linear design circuit models are discussed. The results of different models are quite encouraging and agree well with the theoretical expectation.

4.2 SIMULATION OF INTEGRATED ACTIVE OSCILLATOR ANTENNA

4.2.1 Active device oscillation generation

The first stage of the design process is to select a suitable transistor. The transistor selected for this study is the Hewlett-Packard General Purpose Silicon Bipolar Transistor AT-41411. This device features have large values of S_{11} and S_{12} at intended design frequency (2.45 GHz), which is good for oscillator design since these parameters will directly contribute to instability. In order to check the stability of the transistor, the value of K needs to be calculated. If this value is greater than 1, then the transistor will not oscillate into a resonant load and a feedback might be employed to ensure $K < 1$. An analysis was performed using ADS circuit simulator, to determine the stability factor; the setup and corresponding results are shown in Figs. 4.1 and 4.2, respectively.

As can be seen in Fig. 4.2, the stability factor K of the transistor with common-emitter configurations is greater than 1 across the simulated frequency range, which implies that the transistor is unconditionally stable. In order to make the transistor become potential unstable, inductive series feedback may need to be added as illustrated in the Fig. 4.3. A parameter sweep to vary the inductance from 0.5 nH to 5 nH in 0.5 nH steps was carried out, to find the best optimum value of inductance which will contribute to the lowest value of K.

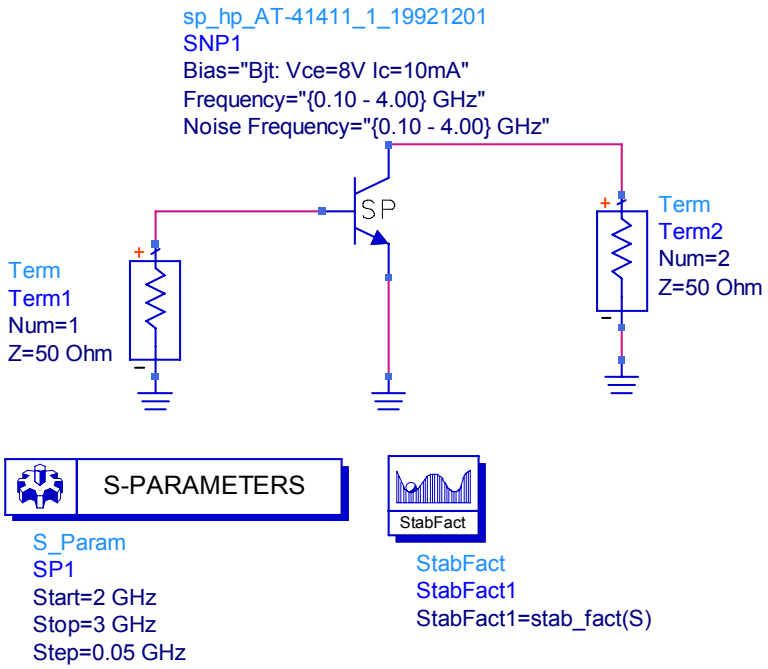

Figure 4.1 ADS circuit simulator setup for determining stability factor K.

The value of the stability factor K at 2.5 GHz is 0.895 (less than 1) when L is 4 nH, as observed. This implies that the device is now potentially stable and may be liable to oscillation. However, the value of K is not lower enough and the magnitude of S_{11} and S_{22} are still less than 1 as found in the simulation. For achieving negative resistance, the

magnitude of S_{11} and S_{22} of the active device should be larger than 1. Besides, negative values of K in the range of -1<K<0 is required because this will result in most of the smith chart being unstable. A different transistor configuration has to be employed in order to produce the required result. Subsequently, a bipolar transistor in common-base configuration was therefore chosen in this case, as shown in Fig. 4.4.

freq	StabFact1
2.000GHz	1.173
2.050GHz	1.179
2.100GHz	1.185
2.150GHz	1.192
2.200GHz	1.200
2.250GHz	1.209
2.300GHz	1.218
2.350GHz	1.228
2.400GHz	1.239
2.450GHz	1.251
2.500GHz	1.264
2.550GHz	1.255
2.600GHz	1.248
2.650GHz	1.242
2.700GHz	1.236
2.750GHz	1.231
2.800GHz	1.227
2.850GHz	1.224
2.900GHz	1.222
2.950GHz	1.220
3.000GHz	1.219

Figure 4.2 Stability factor for common-emitter configuration.

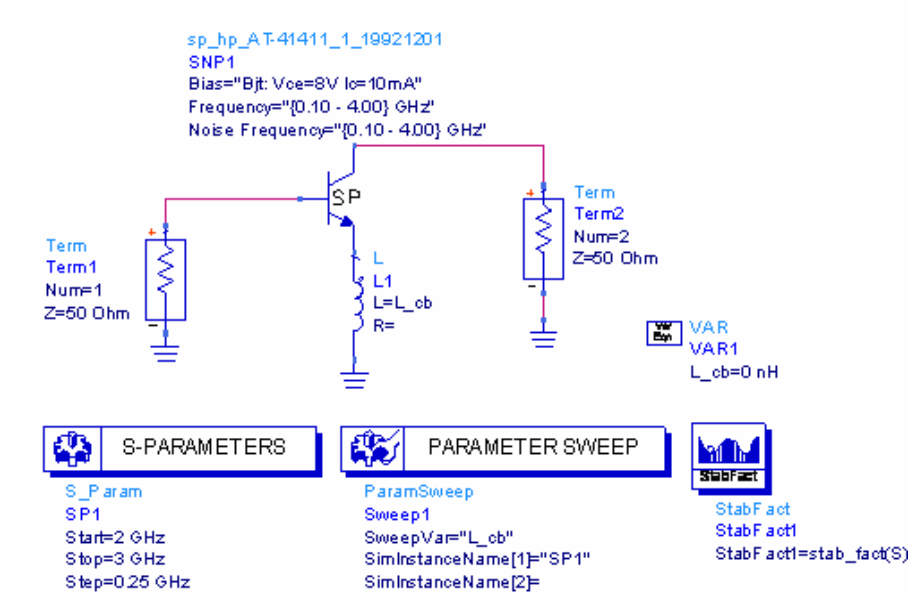

Figure 4.3 Feedback is added to increase instability.

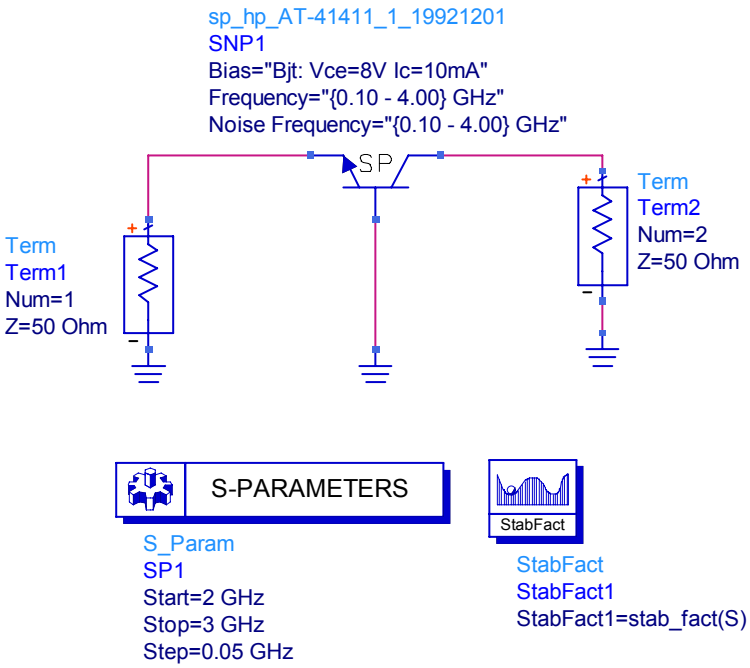

Figure 4.4 Common-Base Configurations setup in ADS simulator.

After analyzing the S parameters of the bipolar transistor with common-base configuration, the value of K now was found to be -0.850 and the magnitude of S_{11} and S_{22} were greater than 1, as observed. However, the magnitude of S_{11} is marginally 1. We can therefore subsequently further raise the magnitude of S_{11} by adding inductance L in series with the base of the transistor and perform parameter sweep to get the optimum S_{11} and S_{22} (see Fig. 4.5).

By varying the inductance L from 0.5 nH to 15 nH, the largest magnitude of S_{11} and S_{22} was obtained with L=3.5 nH. The resulting S parameters and input and output stability circles are shown in Figs. 4.6, 4.7 and 4.8, respectively.

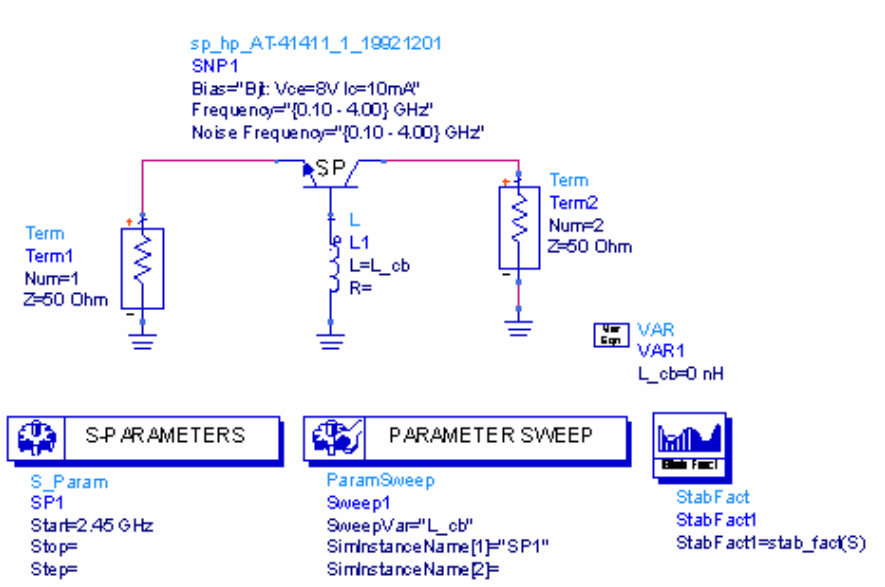

Figure 4.5 Feedback is added to increase the magnitude of S_{11} and S_{22}.

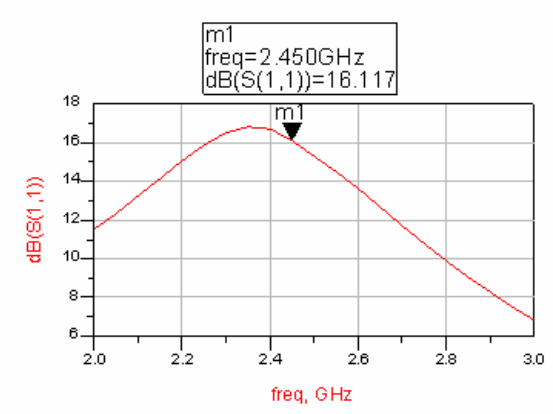

Figure 4.6 High positive input return loss required by the oscillator.

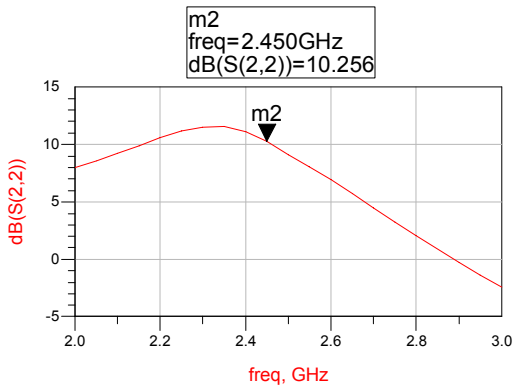

Figure 4.7 High positive output return loss required by the oscillator.

As observing the smith chart of the output stability with the S-parameters presented above, one can find that large region of instability in the smith chart. Hence we can use 50 Ω load termination Γ_L as the value of S_{22} is >1. Based on the model in Fig. 4.5, for

load termination of 50 Ω, the termination required to satisfy the oscillation obtained is (18-j*15.94) Ω. Since the transistor is operated in common-base configuration the current flowing to the load is approximately equal to the emitter current (termination network), and hence the resistor will contribute significantly to the power loss. To avoid this, a lossless element replacing the resistor was considered, using a reactive transmission line of 40 mm length, adjusted to maintain the same oscillator performance.

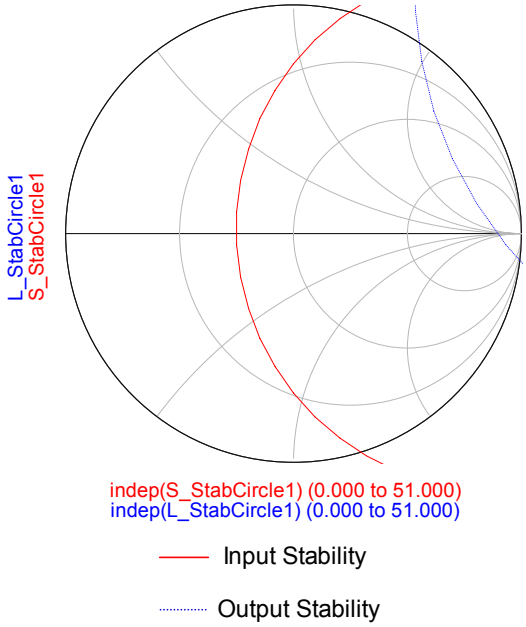

Figure 4.8 Input and output stability circles.

4.2.2 BJT DC bias network

Dc bias network play an important role in microwave transistor design. The purpose of a good dc bias design is to select the proper quiescent point and maintain the quiescent point constant over variations in transistor parameter and temperature [7]. Poor dc biasing could influence the radiation behavior of the antenna. A resistor bias network

can be used with good results over moderate temperature changes. Fig. 4.9 shows the dc biasing circuit for common-base configuration.

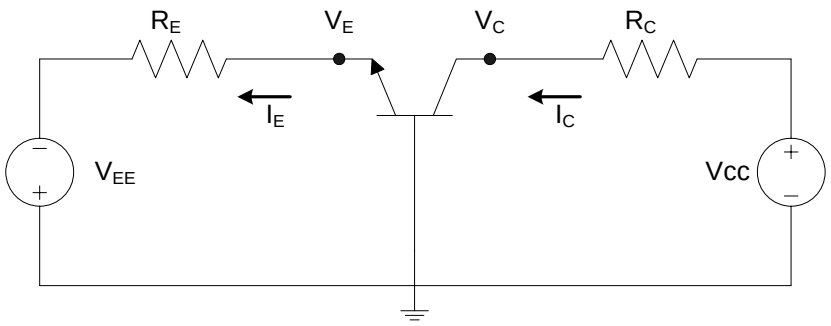

Figure 4.9 Dc bias for Common-Base Configuration.

Based on the datasheet of AT-41411, the V_{CE} =8 V and I_C=10 mA was carefully set as the biasing point for the active device. The following shows the calculation involved to obtained the biasing resistor for Vcc=9 V, V_{EE}=-3 V.

Assuming active mode

V_E = -0.7V, $V_{CE} = V_C - V_E$

Hence, V_C = 7.3V and R_C = (Vcc – Vc)/Ic = (9 – 7.3)/0.01= 170 Ω.

$I_E = Ic + I_B = Ic(1+1/150)$= 10.067 mA.

Hence, R_E = (3 – 0.7)/10.067= 228.47 Ω.

The nearest available standard value for the required bias resistors are:

Rc = 180 Ω

R_E = 220 Ω

To carry out the DC simulation the linear transistor model has been replaced with a non-linear model and the resulting bias simulation is shown in Fig. 4.10. As can be seen, a good result with Ic = 9.92 mA and Vce =8.01 V (Vc - V_E=7.21 – (-0.8)) was achieved.

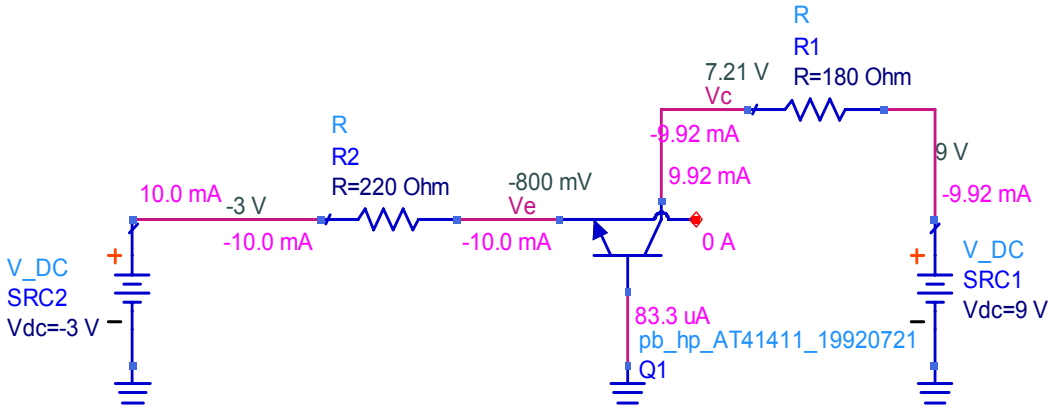

Figure 4.10 DC bias simulations.

4.2.3 Oscillation condition test Using ADS simulator

A general method of testing the steady-state oscillations is known as Nquist stability criterion [8-10]. The presence of oscillation may be tested at either the input or output port of the transistor. When the phase of the transfer function is zero and the magnitude (at the same frequency) is larger than one, the system is unstable. Let us consider the output port, then the transfer function is given by Γ_L* Γ_{OUT}, where Γ_{OUT} is the reflection coefficient seen looking into the output port of the transistor. The system stability depends on the position of poles of the transfer function Γ_L* Γ_{OUT}. If the function possesses poles in the right half plane, the system is unstable. It follows from the Nyquist criterion that the presence of poles in the right-half plane and the system instability can be determined by the encirclements of point *1+j0* by the "osctest" generated contour S_{11} = Γ_L(jw) Γ_{OUT} (jw). An equivalent test can be made using the

quantity $\Gamma_G^* \Gamma_{IN}$ and it should give the same result as above. The following schematic shows (see Fig. 4.11) how to test the Nquist stability by using ADS "OSCTEST" component.

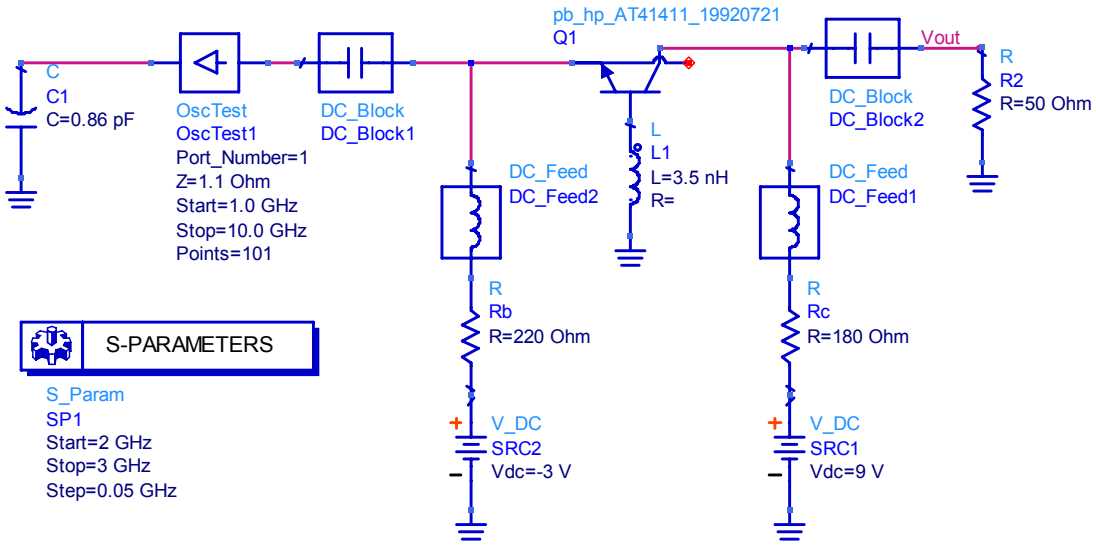

Figure 4.11 OSCTEST component used to determine if the circuit oscillates.

The dc block 1 and 2 in Fig. 4.11 are used to prevent dc bias level affecting RF port. They have low reactance at design frequency of operation, but they blocked the dc component. Moreover, both applied dc components are used to block the RF signal, but allow dc or low-frequency signal to pass through. The corresponding result of the simulation is illustrated in polar form as shown in Fig. 4.12.

The result presents that the x-axis value of 1 is circled by the trace or contour, which implies that the circuit will oscillates and the Nquist stability criterion had been met.

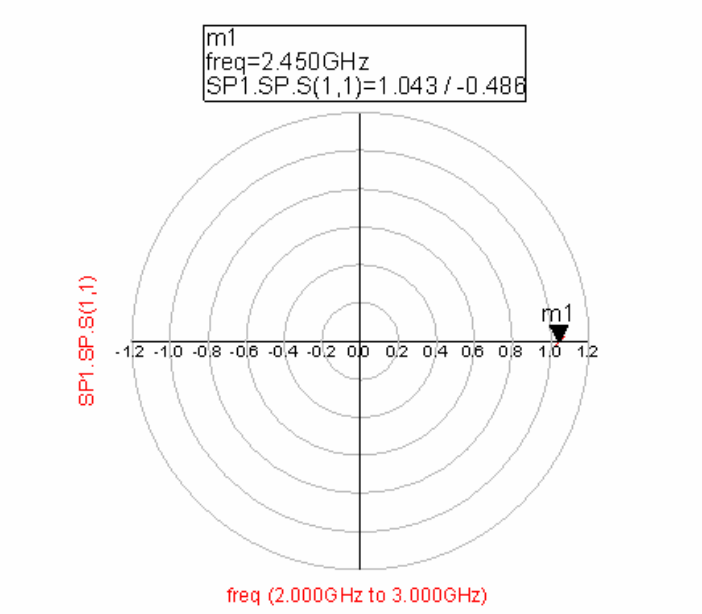

Figure 4.12 Polar plot of the S-parameter simulation using 'OSCTEST'.

4.2.4 Microstrip patch Antenna design using Momentum

The antenna was considered as a microstrip-fed offset rectangular patch (see Fig. 4.13) and was designed to resonate near 2.45 GHz. The microstrip patch acts as radiating element and an optimal bipolar transistor collector load impedance required for oscillator synthesis. The dimensions of the antenna (in mm) can be found in Fig. 4.14. Input impedance of the antenna was computed from 0.1 GHz to 12 GHz using the Agilent Momentum modelling package [11]. Fig. 4.15 presents the simulated return loss of the optimal microstrip antenna for this design. The attained antenna data was then incorporated in the circuit simulator as a one-port device and the oscillation condition at the input of the active device was observed. Then the length of the microstrip transmission line (connected with the emitter at the input) was optimised for maximum input power at the antenna port, using the HB simulator.

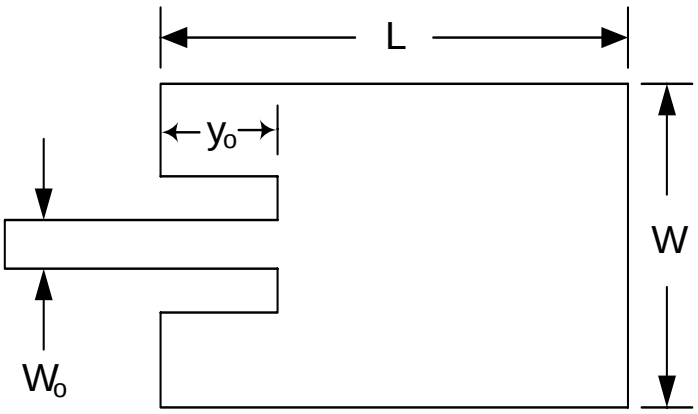

Figure 4.13 Basic antenna geometry used for optimization.

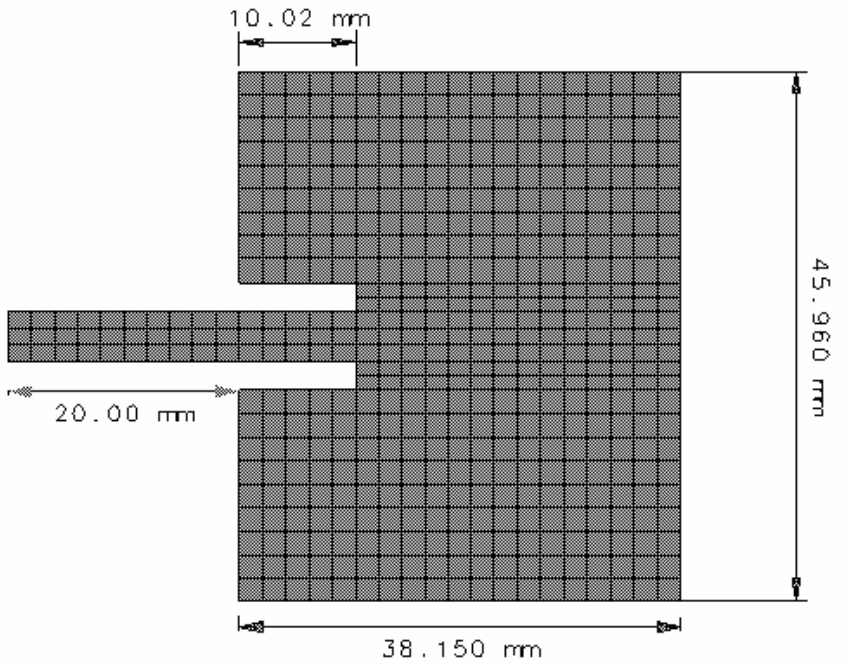

Figure 4.14 Dimensions of the designed microstrip inset-feed.

4.2.5 Simulated performance of integrated active oscillator antenna

The HB simulator was used to predict the characteristics of the active oscillator such as output power, harmonic level, frequency pushing, and phase noise. A nonlinear model

of the device was used over the first 5 harmonics operation. The load impedance at the fundamental design frequency was optimised to achieve the maximum output power and reasonable harmonic level. The schematic and the layout are shown in Figs 4.16 and 4.17, respectively.

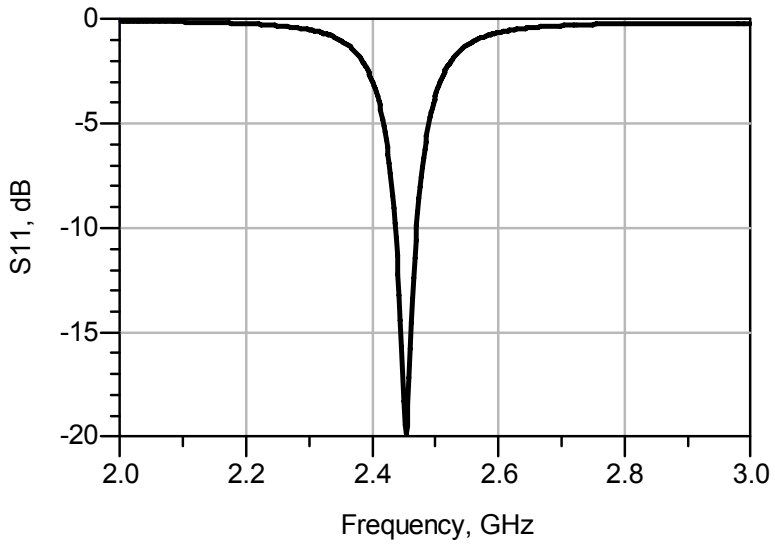

Figure 4.15 Simulated return loss of the microstrip patch antenna.

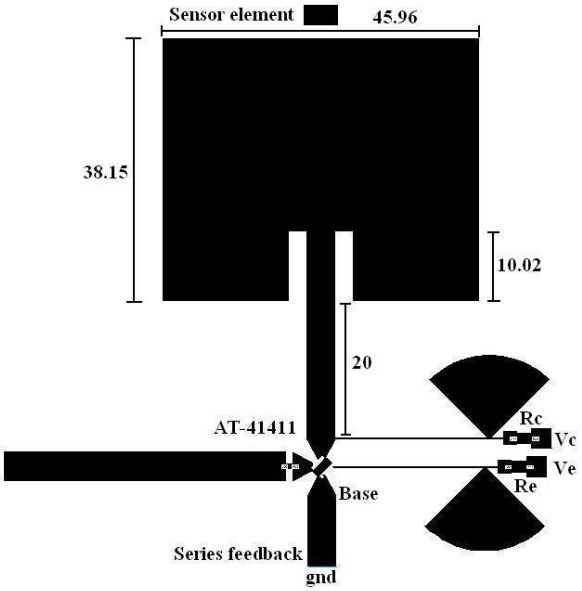

Figure 4.17 Final layout of the designed integrated active oscillator antenna.

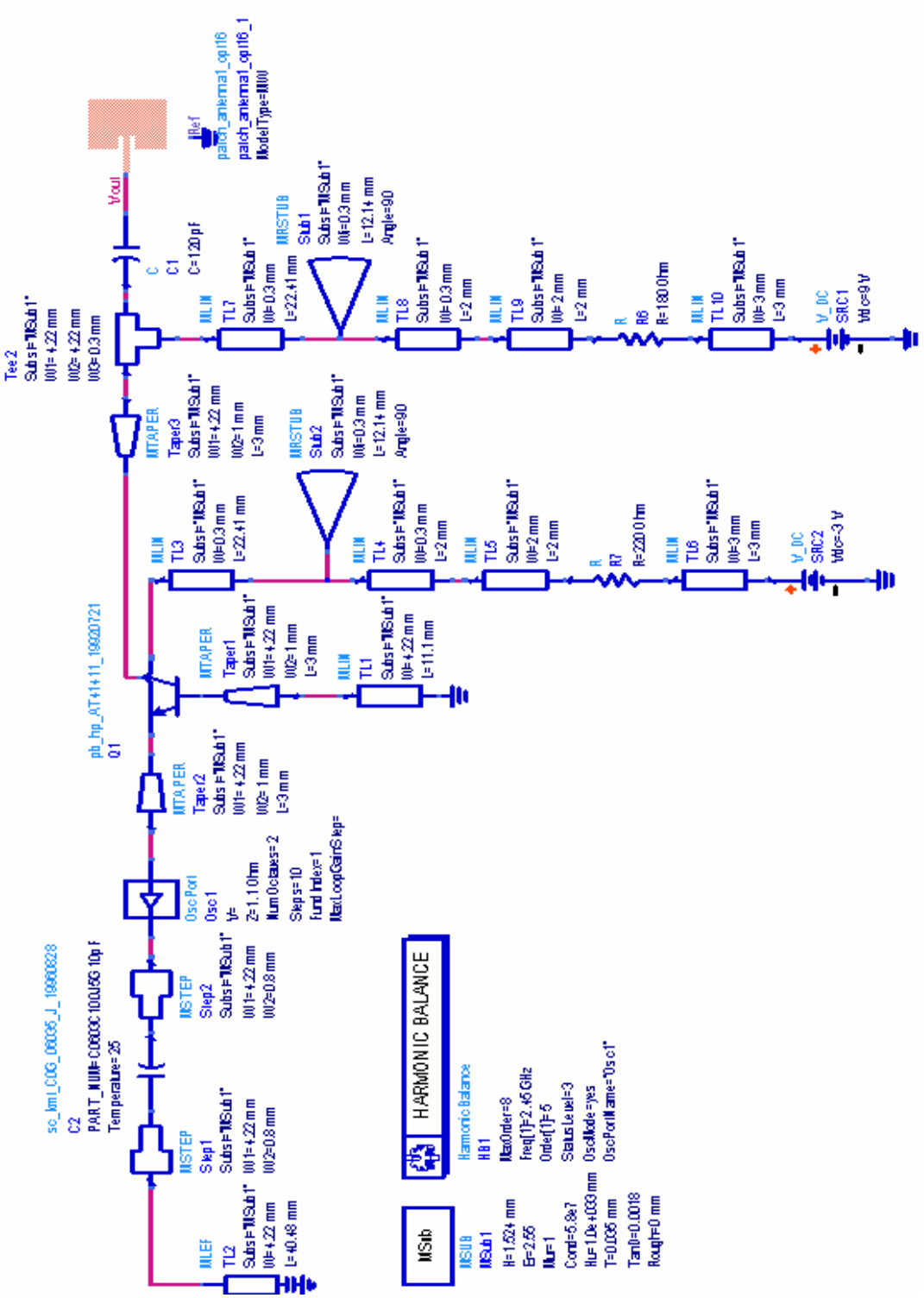

Figure 4.16 Final schematic circuit diagram of the designed integrated active oscillator antenna.

Simulated free running oscillation frequency and harmonic performance of the integrated active oscillator antenna are presented in Fig. 4.18. The waveform of the output power in time domain was predicted and shown in Fig. 4.19. As can be seen, the voltage waveform was distorted by the oscillator harmonics which is due to nonlinearity of the active device. Phase noise of the proposed integrated active oscillator antenna was also studied, as shown in Fig. 4.20.

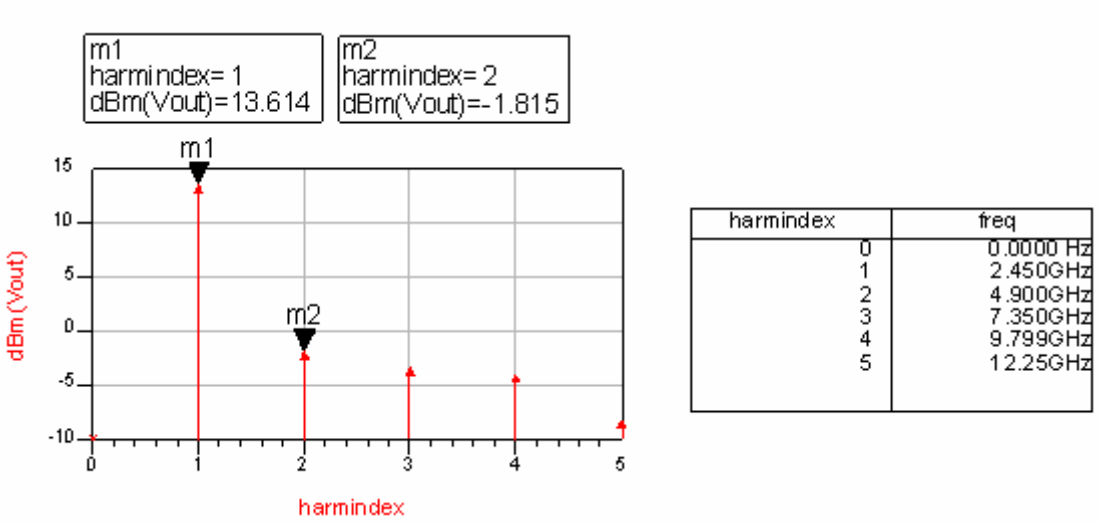

Figure 4.18 Output Power Spectrum in Frequency domain.

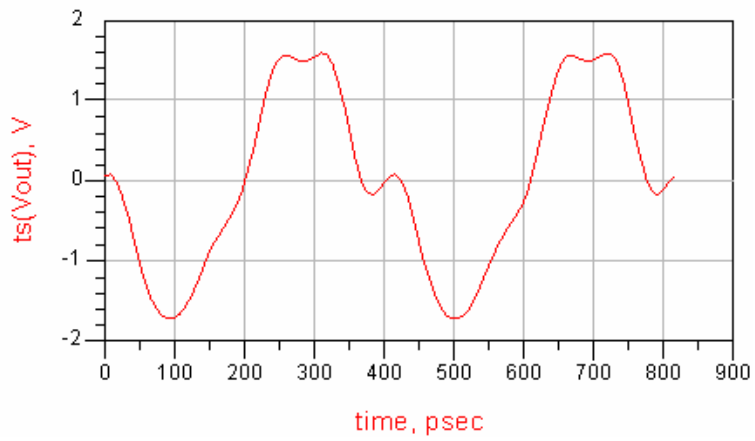

Figure 4.19 Output Power in time domain.

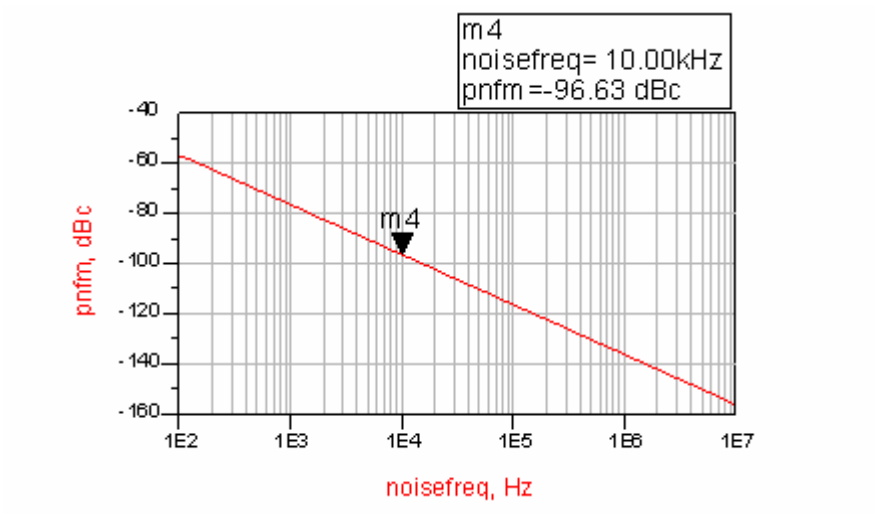

Figure 4.20 Phase Noise of integrated active oscillator antenna at 10 kHz.

4.2.6 Modulation of integrated active oscillator antenna

The increasing demand for low cost and small size radio frequency transceiver has been a growing area of research recently. The task is very challenging to the designer especially in the implementation of the circuit elements which posses multiple functionality. The circuit design (see Fig. 4.16), is not only an oscillator, but function also as a radiator.

One of the potential used of this circuit can be either in short-range communications or short-range sensing applications. However, in communication systems, we need to perform modulation in order to transmit the signal in free space. Without adding extra components, and to maintain the existing size of the circuit, we can integrate this additional function into the circuit element by placing the modulated signal into the base of the transistor. The modified schematic diagram is shown in Fig. 4.21.

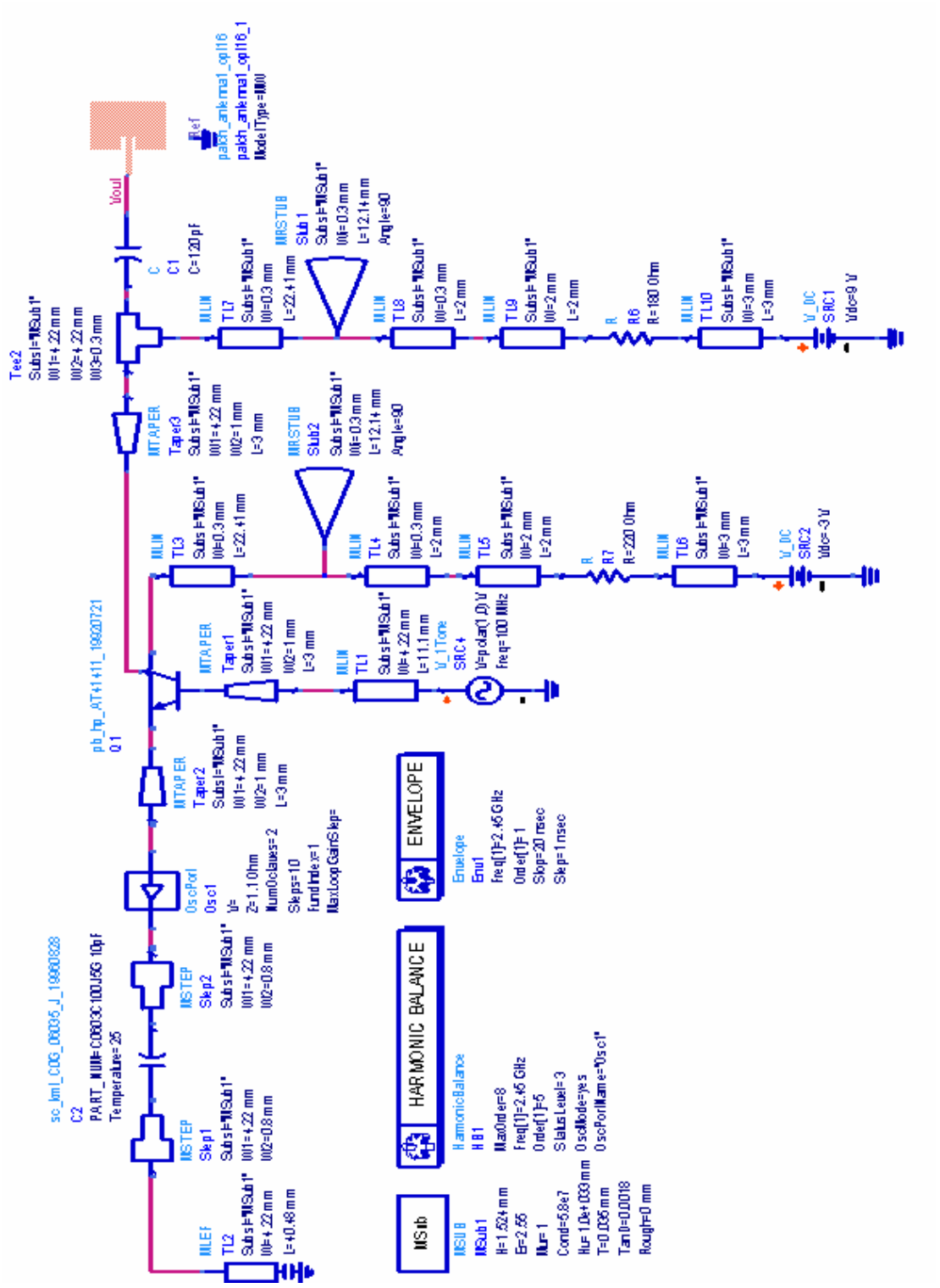

Figure 4.21 Schematic circuit of the integrated active oscillator antenna for modulation purposes.

A 100 MHz sine wave signal is used to modulate the carrier frequency. The simulation result is shown in Figs. 4.22 and 4.23. As can be seen in Fig. 4.22, the modulation has little effect on the output power of the carrier frequency. However the carrier frequency has shifted a bit. The carrier frequency can be altered by fine tuning of the input matching circuit.

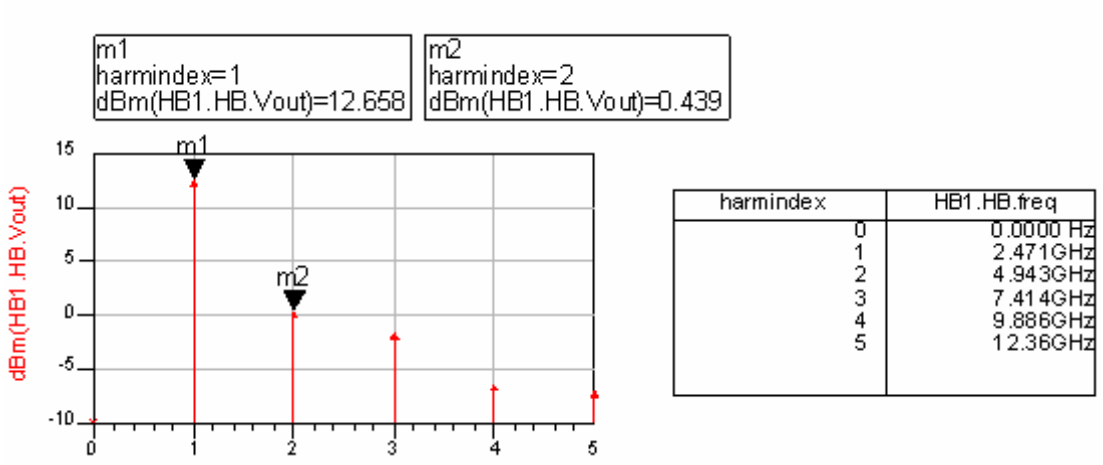

Figure 4.22 Output Power Spectrum (Amplitude Modulation).

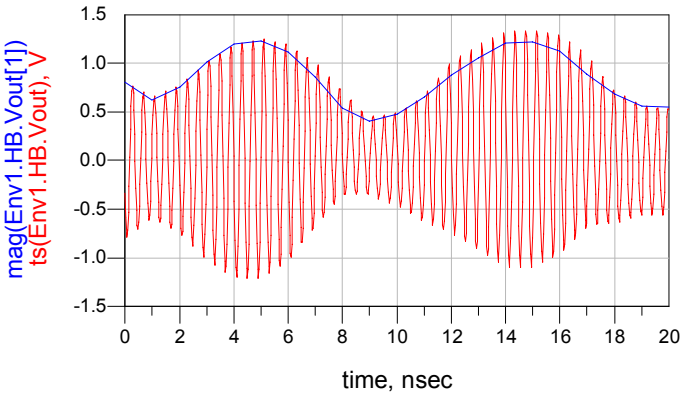

Figure 4.23 Modulated carrier in time domain (AM).

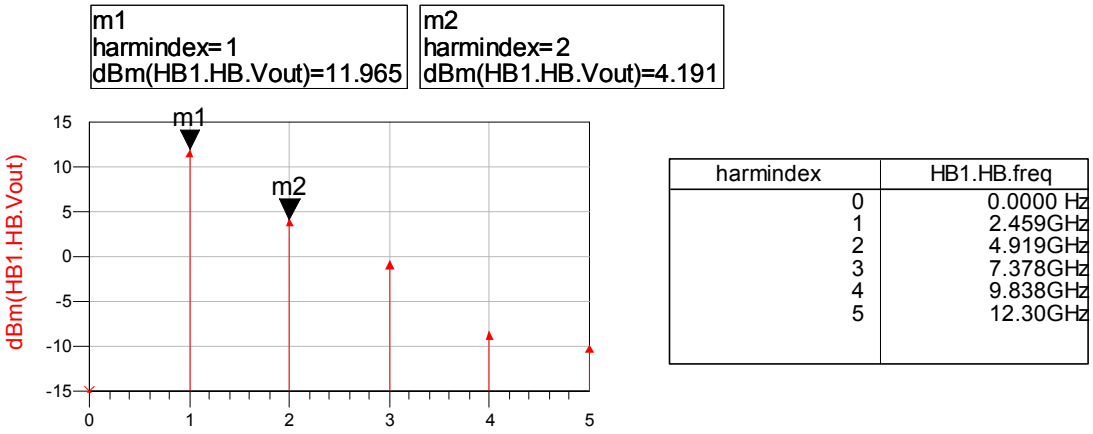

Figure 4.24 Output Power spectrum (ASK).

Another possible modulation scheme that can be integrated into the circuit element is the ASK. Instead of using 100 MHz sine wave as modulated signal, we can use rectangular signal (approximated to the equivalent digital signal) of 100 MHz. the simulation result are shown in Figs. 4.24 and Fig. 4.25.

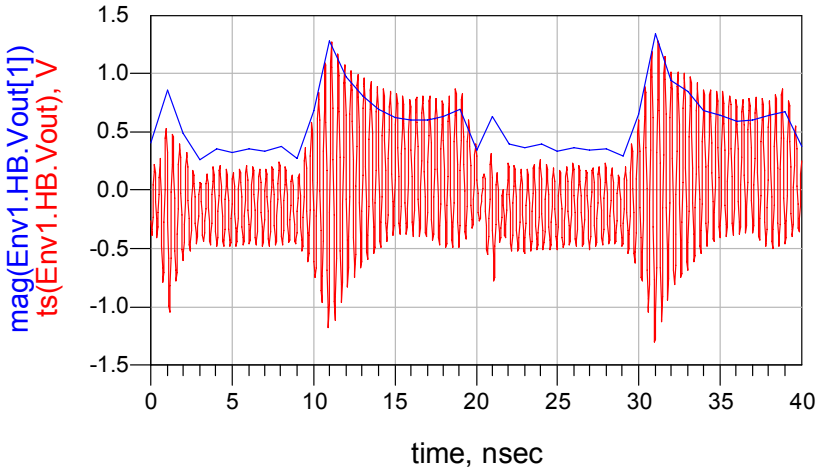

Figure 4.25 ASK modulated carrier in time domain.

4.3 MEASUREMENT OF INTEGRATED ACTIVE OSCILLATOR ANTENNA

4.3.1 Antenna and sensor patch

The antenna and the RF circuit elements were mounted on Duroid material with the following specifications: relative permittivity = 2.55, loss tangent = 0.0018 and height of the substrate = 1.524 mm. The total area of the finite ground considered for the active antenna oscillator circuit is 11 cm x 11 cm. The free running oscillation frequency and harmonic contents of the integrated active oscillator antenna were measured using the sensing patch technique. Firstly, the calibration factor was first measured when the antenna was disconnected from the RF oscillator circuit. Thus the antenna is operated as a one-port passive network. Then the feeding line of the antenna was reconnected with a coaxial probe (rear board) to the network analyzer and considered as port 1. Then the sensor patch output with a 50 Ω chip resistor across it was connected to a coaxial connector at the rear of the board and then fed to the network analyzer as port 2. Therefore the radiator and the sensor can now be considered as two-port passive network.

The S-parameter of the two-port was taken carefully on a well-calibrated network analyzer (HP 8510C), avoiding room reflections as much as possible. To achieve accurate measurement the electrical delay caused by the connector has to be taken into account. One method of measuring the electrical delay of the SMA connector is by using an identical similar element and then connects it to the probe of the network analyzer without the circuit board [12]. Then solder the centre pin of the connector to a piece of foil to make a perfect short circuit in the plane of the flange surface. The

electrical delay was adjusted until the swept frequency trace became a single point at the left of the Smith chart. The measured electrical delay obtained was 79 ps.

The resonance frequency of the antenna was found to be 2.425 GHz. Initially, the circuit did not generate stable oscillation. This is because the substrate thickness was not included in the simulation when connecting the transmission line at the base of the transistor to the ground. One way to overcome this problem is to vary the input impedance of the antenna by adding a 50 Ω microstrip line with appropriate length of about 35 mm. The modified circuit configuration is shown in Fig. 4.26. Then the two-port S parameters between the antenna input feed line and the sensor output were measured again and the results are shown in Fig. 4.27. The antenna resonant frequency now was shifted down to 2.40 GHz. The corresponding calibration factor from the measured data was computed over the band from 2 GHz to 3 GHz as shown in Fig. 4.28. As can be easily seen, the calibration factor at the oscillating frequency is about -24 dB (including cable loss of 1.33 dB).

It is notable in Fig. 4.29 that the curve shows a slowly varying magnitude over a much wider band than the resonant bandwidth of the antenna. Since the antenna impedance varies widely over this band, the curve indicates that the correction for the impedance variation is working accurately. However, on the finer frequency scale, the plot shows small magnitude variations in which can be ignored. However, this could be due to the random network analyzer errors; or could be also due to the minor room reflection. The other possibility could be due to the current flowing on the outer conductors of the network cables which produce standing waves.

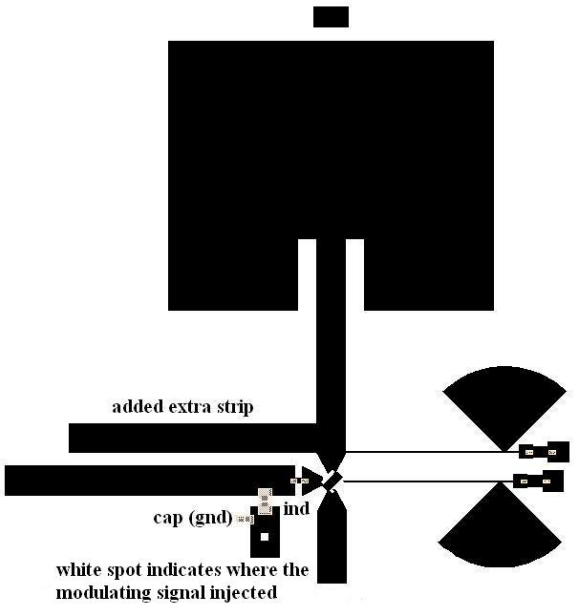

Figure.4.26 Modified layout of the oscillator for AM and ASK modulation.

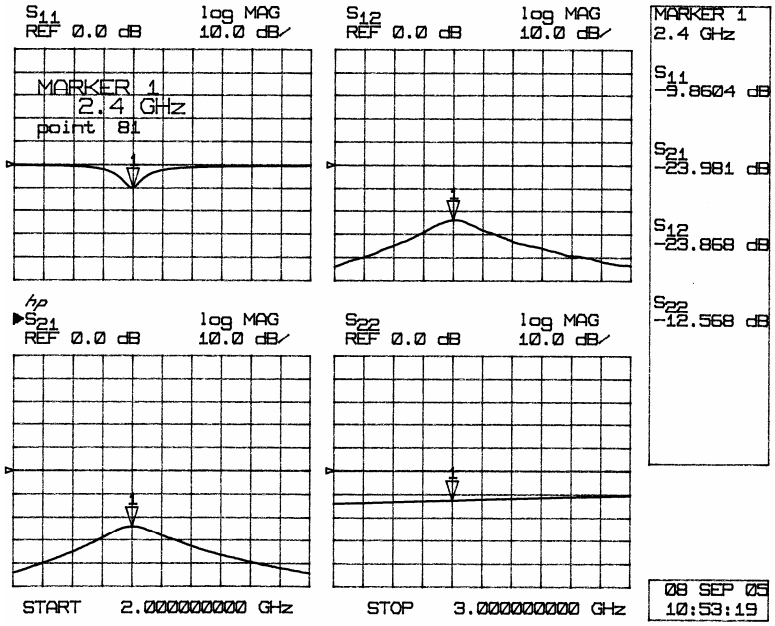

Figure 4.27 The two-port S parameters between the modified antenna input port and sensor output.

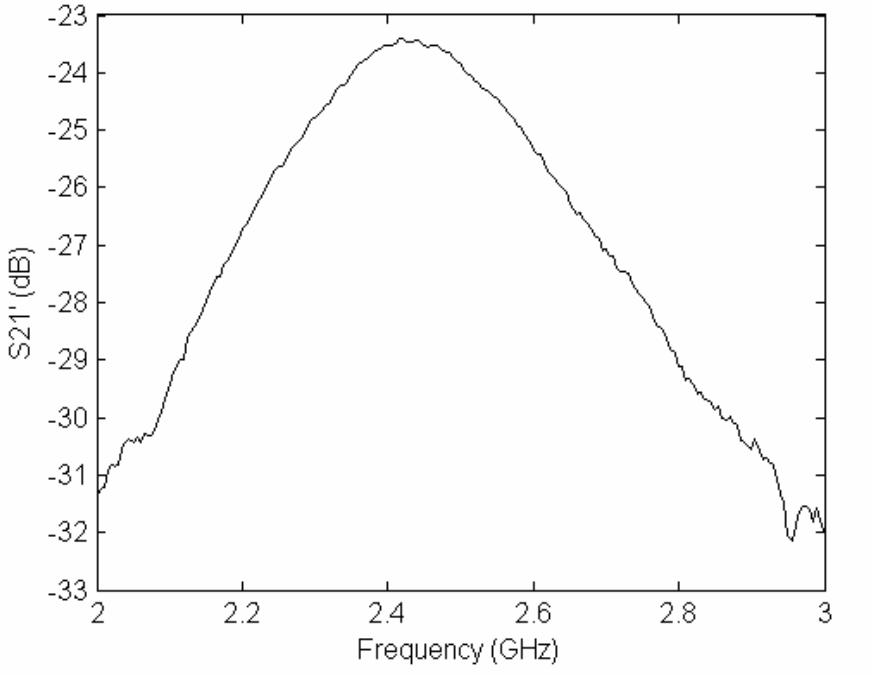

Figure 4.28 Response of calibration factor S_{21}'.

4.3.2 Measured performance of integrated-oscillator active antenna

Initially, the circuit does not oscillate because of the extra length cause by the grounding point at the base of the transistor. The circuit can be made to work by fine tuning the length of lumped element at the base of the transistor. However, this became practically impossible due to the fact that as the length of the lumped element is varied, a new hole need to be drilled. This is because the lumped element at the base of the transistor needs to be grounded. Therefore the easiest way was to vary the input impedance of the antenna, by adding a strip (see Fig. 4.26) of 50 Ω characteristic impedance; length 35 mm across the feed line of the antenna, to support the oscillation condition. The addition of the extra line will have little effect on the calibration factor of the original antenna. The antenna parameters were measured again after the edition of the metal strip.

A measurement bench setup for measuring free running oscillation frequency of the integrated active oscillator antenna is presented in Fig. 4.29. After the foregoing adjustment to the circuit, the free-running oscillation was observed at 2.36727 GHz, with about 15 dBm output power. Fig. 4.30 shows the measured free-running oscillation. The measured efficiency was about 28.7%. The choice of BJT transistor as an active element shows increase in efficiency as compared with PHEMT. Fig. 4.31 shows the output spectrum harmonic contents of the oscillator. The output power of active oscillator antenna at the 2^{nd} harmonic can be estimated using the same sensor (this will be explained in the Chapter 5). The calibration factor at the 2^{nd} harmonic was calculated to be about -20.4 dB and thus, the 2^{nd} harmonic power of the active oscillator antenna was found to be -4.43 dBm (-24.83-(-20.4)). As a result, the difference between the fundamental and the 2^{nd} harmonic in power is therefore about 19.43 dB, which is quite acceptable for practical realization. Further more, it is notable that the centre oscillating frequency has a tuning range of 20 MHz as the emitter voltage of the active device is varied.

The simplest method for measuring oscillator phase noise is to view the oscillator spectrum directly on a spectrum analyzer. To understand how to read the phase noise, refer to the definition which have been explain in chapter 3 section 3.3.2. However, this method is accurate (only) provided that the oscillator has low amplitude noise modulation in which the measured noise of the oscillator is much higher than that of the local oscillator of the spectrum analyzer. Therefore the approximate phase noise at 10 kHz offset from the centre frequency was found to be -50 dBc/Hz.

Figure 4.29 The measurement bench setup for integrated active oscillator antenna.

The phase noise can be accurately predicted and measured using the measurement setup presented in [13] as shown in Fig. 4.32. This technique gives better sensitivity than direct measurement at radio frequencies because the translation down to low RF frequencies permits the use of spectrum analyzer with lower-noise local oscillators or fast Fourier transform (FFT) analyzers. In general, the sensitivity of this system is limited by the internal noise of the frequency discriminator.

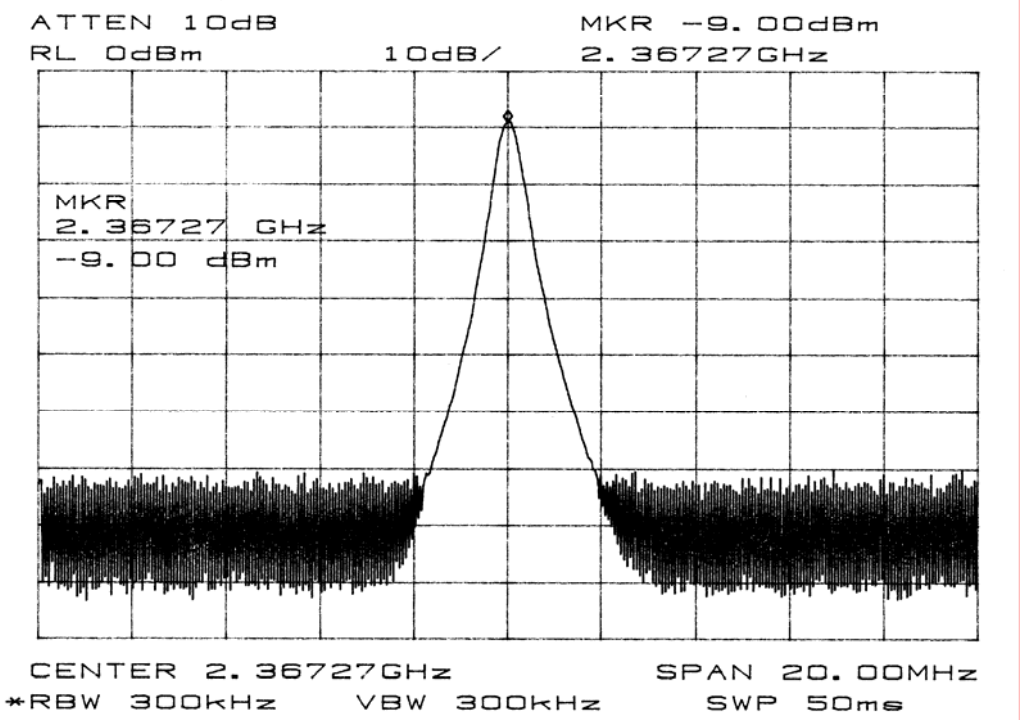

Figure 4.30 Frequency spectrum of the oscillator output.

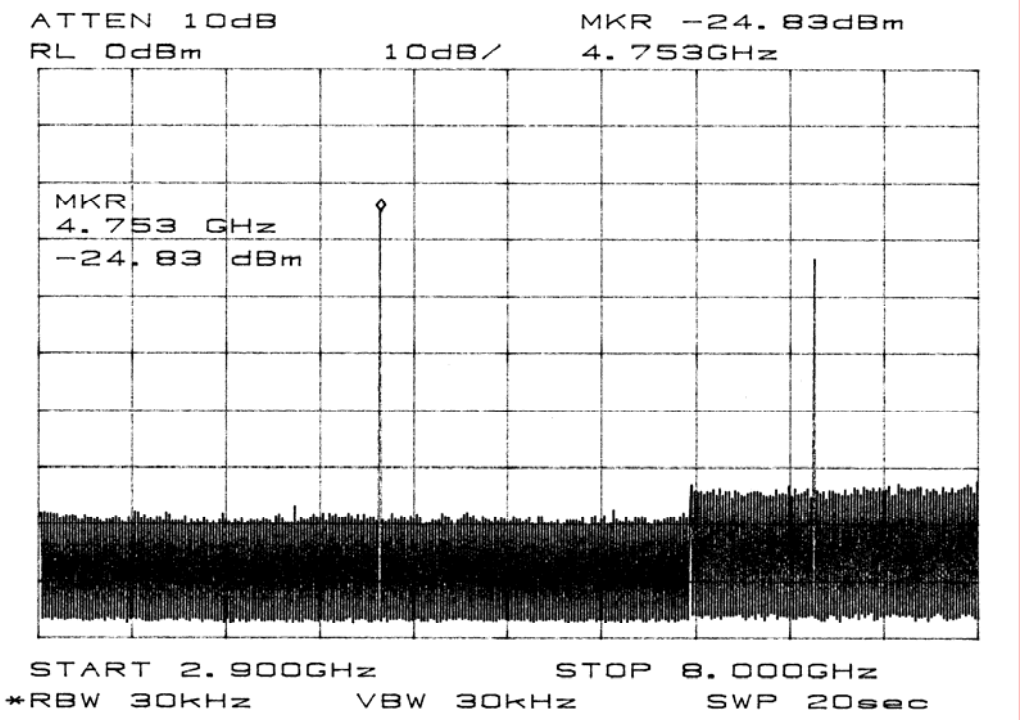

Figure 4.31 Second and third harmonics contents.

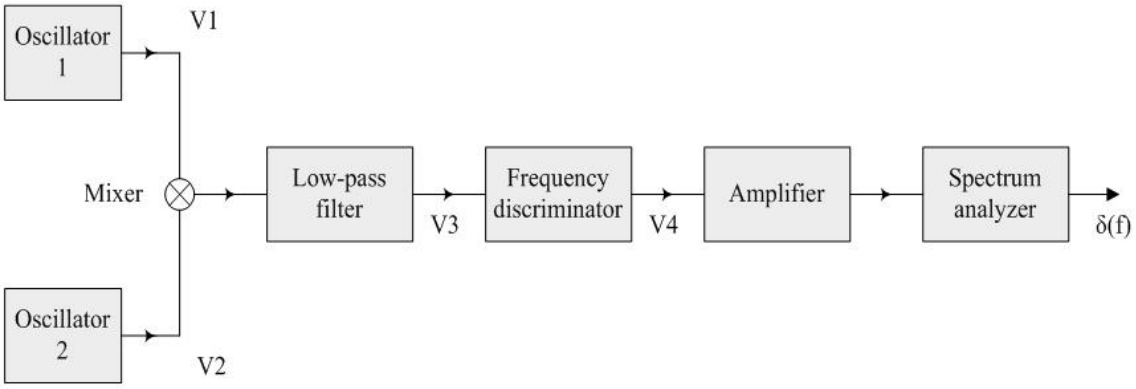

Figure 4.32 Oscillator noise measurement setup.

Another method that yields good result is suggested by LeCroy (oscilloscopes provider) technical paper [14]. Since the circuit contains antenna, it is more appropriate to measure the phase noise in anechoic chamber to avoid scattering and reflection that might be caused by the environment or nearby interferences.

4.3.3 Measured modulation performance of integrated-oscillator active microstrip antenna

In order to let the active device perform as a modulator, an attempt was first made to place the modulated signal (either analogue sinusoidal wave or digital square wave) at the base of the transistor from the rear of the circuit board, using a probe feed. It was found that modulation of the RF oscillating signal was not observed. This is mainly because oscillation frequency is so sensitive to the variation of the base inductance of the transistor. The length of the probe connector's pin contributes to the inductance at the base of the transistor, which caused the failure to generate oscillation. One alternative to overcome this problem is to place the modulated signal at the emitter of

the transistor. A piece of transmission line with dimensions of 4.2 mm x 8 mm was placed close to the emitter of the transistor and then the modulated signal was fed from the underneath of the circuit board, as shown in Fig. 4.26. It can be also seen; a 27 nH chip inductor was mounted in series across the two transmission lines, acting as a high impedance line to isolate the oscillating RF signal from the signal generator. In addition, a 10 pF chip capacitor (optional) was also added and mounted in shunt to work together with the series inductor to form a low-pass filter.

A 1 volt peak-to-peak sinusoidal wave signal of 100 MHz was first used. It was found that the oscillated signal and the two adjacent sideband signals were observed on the spectrum analyser. The spacing between the centre frequency and the two sidebands was measured to be 100 MHz. It can also be noted that the modulation has little effect on variation of the originally oscillating RF signal in terms of RF frequency. Additionally, the amplitudes of the two AM modulated sideband signals are dramatically unequal. This is probably because the antenna response over the band; or it may also be caused by the nonlinearity of the transistor. It is interesting that the difference in amplitude of the two sidebands decreases as the frequency of the modulating signal is varied from 100 MHz to 10 MHz, while the centre oscillating frequency keeps almost unchanged. Fig. 4.33 shows the AM modulated carrier in frequency domain for a 10 MHz sinusoidal input signal.

Similarly, a 1 volt peak-to-peak square wave signal of 2 MHz was fed to test the capability of the active device to generate digital ASK modulation. A Farnell low frequency signal generator was used to provide square wave and the measurement bench setup is illustrated in Fig. 4.34. The resultant modulated signal of ASK, presented

in Figs. 4.35, shows the required frequency components in frequency domain as expected: this proves the successful achievement of ASK modulation. Other frequencies (3 and 5 MHz) of the square wave were also tested for ASK modulation and the same result was observed in frequency domain (see Figs. 4.36 and 4.37).

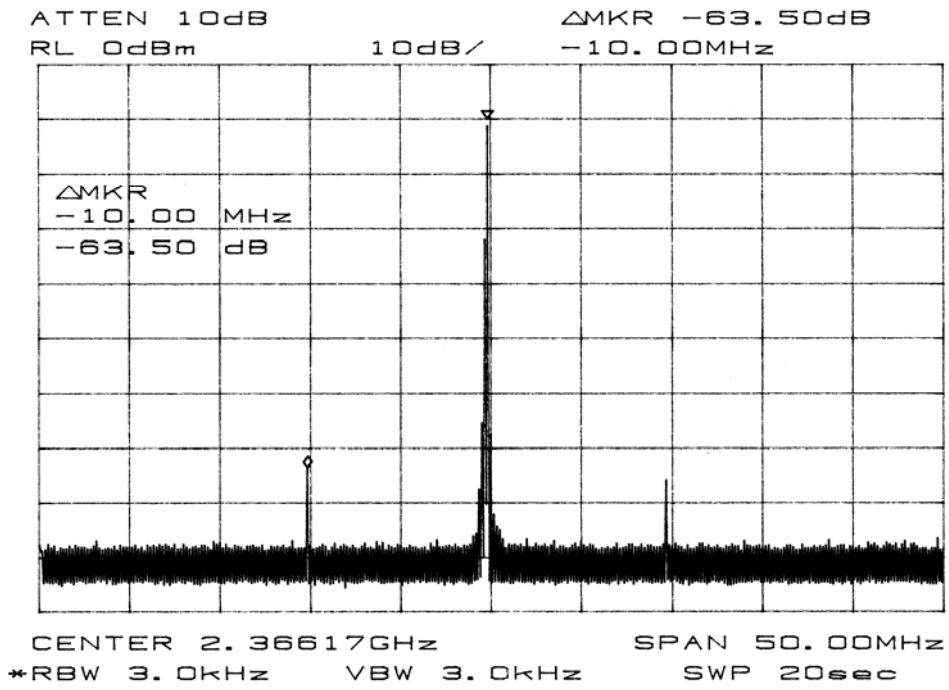

Figure 4.33 Measured spectrum of the AM modulation for a 10 MHz sinusoidal modulated signal.

Figure 4.34 Measurement bench setup for measuring ASK modulation.

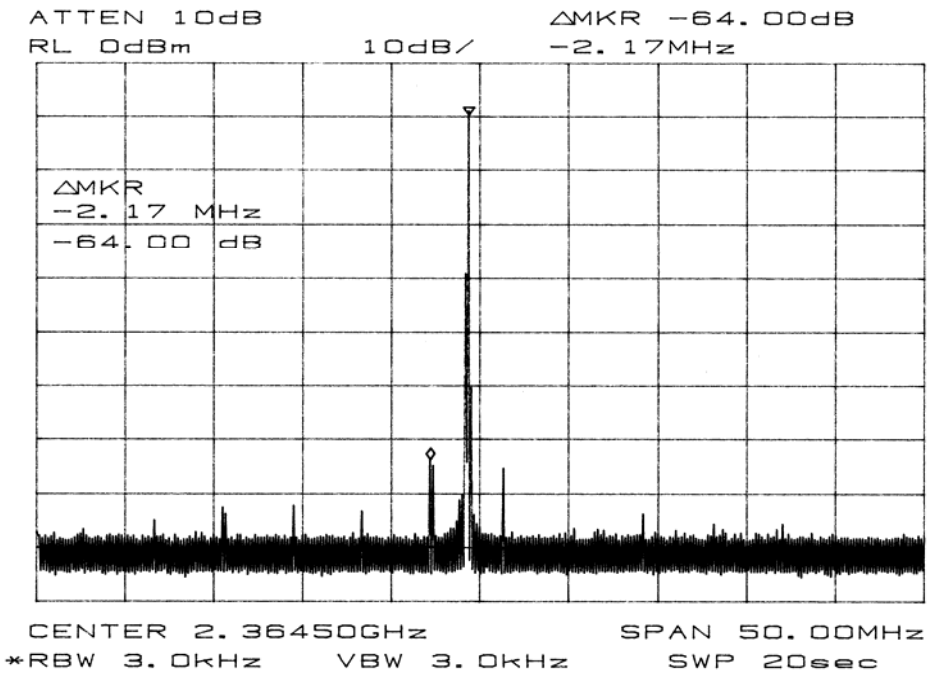

Figure 4.35 Measured spectrum of the ASK modulation for 2 MHz square wave.

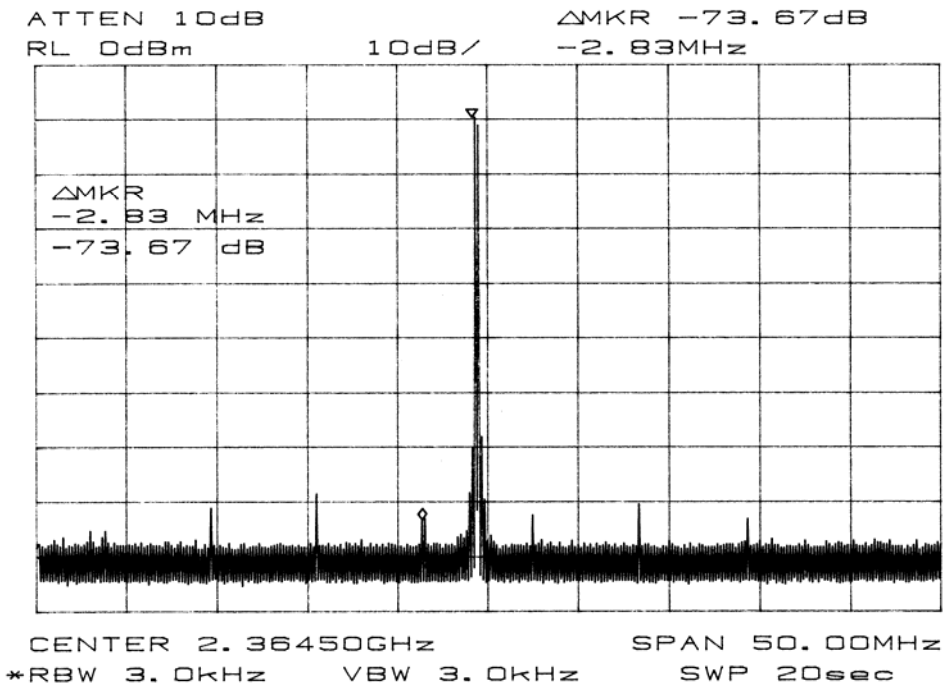

Figure 4.36 Measured spectrum of the ASK modulation for 3 MHz square wave.

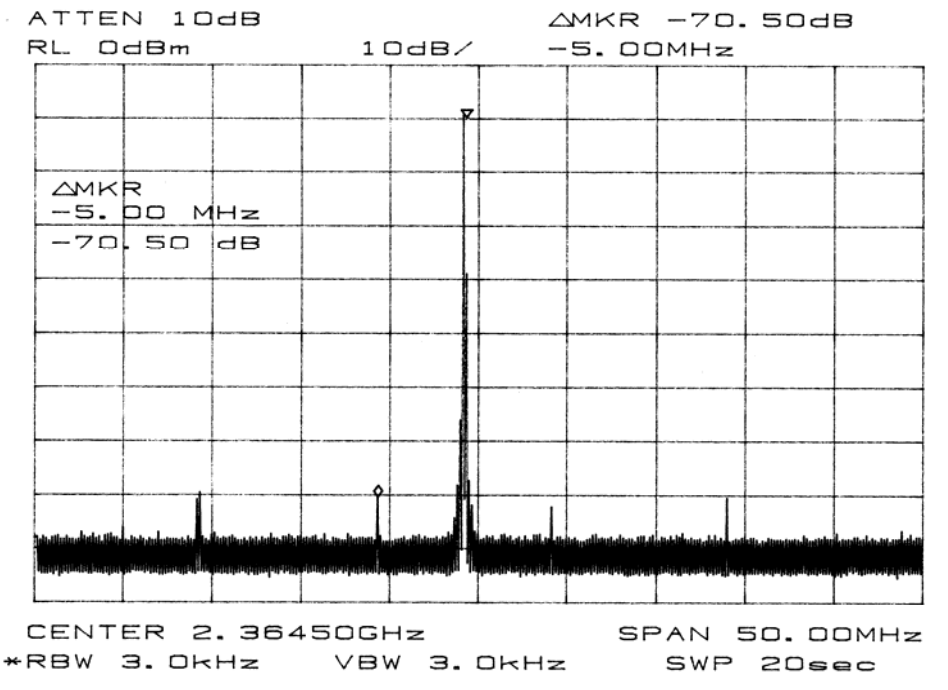

Figure 4.37 Measured spectrum of the ASK modulation for 5 MHz square wave.

4.4 CONCLUSION

The concept of AIA in designing integrated oscillator active microstrip antenna without intermediate matching circuit between the output of the active device and the antenna was studied. This type of active antenna has been developed for sensor application. Much of the progress has been generated by the interest in the potential for spatial power combiner applications to overcome the power limitations of solid state sources at high frequency. The theory of microwave oscillator is based on two-port negative resistance oscillator. The negative resistance of a two-port network was realized by circuits containing active elements like transistor. Much of the research interest has been carried out using PHEMT, FET and HBT transistor. However, in this study, BJT transistor was chosen as the active device to provide negative resistance. The measured results were quite encouraging and agreed well with the theoretical expectation using ADS software.

A novel and simple method of generating AM and ASK modulation, using an integrated oscillator antenna with positive feedback working at around 2.4 GHz, was presented and discussed. The design steps for both the oscillator and the patch antenna were carried out in parallel. The measured frequency and the forward power at the antenna input port, using a calibrated sensing patch, gave reliable results without affecting the radiation performance of the antenna or the oscillator circuit elements. The present work may find potential applications as a compact transmitter for Wireless LANs.

4.5 REFERENCES

[1] S. P. Kwok, and K.P. Weller, "Low cost X-band MIC BARITT Doppler sensor," IEEE Trans. Microwave Theory and Techniques, vol. MTT-27, pp. 844-847, 1979.

[2] Armstrong, B. M., et al., "Use of microstrip impedance-measurement technique in the design of a BARITT diplex Doppler sensor", IEEE Trans. Microwave Theory and Techniques, vol. MTT-28, pp. 1437-1442, 1980.

[3] R. Garg, P. Bhartia, I. Bahl and A. Ittipiboon, "Microstrip antenna design handbook", pp. 659-717, Chapter 11, Artech House, 2001.

[4] V.F. Fusco, "Active antenna phase modulator performance", 23rd European Microwave Conference, Madrid, Spain, pp. 248-251, September 1993.

[5] L. Dussopt, and J.-M. Laheurte, "BPSK and QPSK modulations of an oscillating antenna for transponding applications", IEE proceedings–Microwave Antennas Propagation, vol. 147, no. 5, pp.335-338, 2000.

[6] X. Zeng and Z. Chen, "Frequency multiplication and QPSK modulation with subharmonic injection-locked active antenna", Proceedings of the second annual conference on communication networks and services research, pp. 329-332, 2004.

[7] G. Gonzalez, "Microwave transistor amplifier: Analysis and Design", second edition, Prentice Hall, pp. 397-404, 1996.

[8] J.T. Aberle and D.M. Pozar, "Analysis of infinite arrays of one- and two-probe-fed circular patches," IEEE Trans. Antennas and Propagation, vol. AP-38, no. 4, pp.421-432, April 1990.

[9] R.T. Jackson, "Criteria for the onset of oscillations in microwave circuits", IEEE Trans. MTT-40, pp 566-568, March 1992.

[10] C. Schiebold, "Getting back to the basics of oscillator design", Microwave Journal, pp. 336-339, May, 1998.

[11] Agilent Technologies, Advanced Design System, ADS2003C.

[12] E.A. Elkhazmi, N.J. McEwen, and N.T. Ali, "A power and efficiency measurement technique for active patch antennas," IEEE Trans. On Microwave Theory and Techniques, vol.48, no.5, pp. 868-870, May 2000.

[13] G.D. Vendelin, "Design of amplifiers and oscillators by the s-parameter method", John Wiley & Son, pp. 145-148, 1982.

[14] LeCroy (Oscilloscope and Protocol Analyzer Provider), "Phase noise measurement", Lab744, www.lecroy.com.

CHAPTER 5

HARMONIC MEASUREMENTS ON ACTIVE PATCH ANTENNAS USING SENSOR PATCHES

5.1 INTRODUCTION

In this chapter, the possibility of using sensor patch technique to find the power accepted by the antenna at harmonic frequencies is studied. Performance of the sensing patch technique for measuring the accepted power at the antenna feed port of active patch antennas has been evaluated at harmonic frequencies. A prototype antenna such as inset-fed patch antenna used in Chapter 4, with two sensors at appropriate locations around the patch, was manufactured and tested. The test was performed to cover the designed frequency band (fundamental component) and the first two harmonics frequencies. Determination of the sensor calibration factor, for these particular sensors, for the three frequency band components will result in accurate estimation of the accepted power by the antenna. It is shown, based on experimental results, that the original technique presented in last chapter can also be employed to measure the second harmonic power [1]; measurement of the third harmonic power is also possible if another sensing patch is added in an appropriate position.

5.2 EXISTING MEASUREMENT TECHNIQUES FOR ACTIVE INTEGRATED ANTENNAS

Active integrated antennas have received much attention, due to their compact size, low weight, low cost, and multiple functionalities. They are typically classified into three types: amplifying-type, oscillating-type, and frequency-conversion-type, according to how the active device acts in the antenna [2-4].

In general, radiated power by the active integrated antenna at targeted design frequency and its harmonics can be measured using Friis transmission equation in the anechoic chamber [5]. In addition, a simple measurement technique for measuring the accepted power by the active patch antenna, using a sensing patch feeding network was first proposed in [6]. The measurement details about this technique have already demonstrated in Chapters 3 and 4. The technique eliminates many uncertainties and errors, such as cable losses, effects of the pattern, effects of nearly scatterers, and gain estimation errors, and even makes it unnecessary to operate in the far field. This technique was originally developed for the measurement of amplifying-type active patch antennas at their fundamental design frequency. It was subsequently applied to measurements on oscillating-type antennas [7] and on the microstrip dipole antennas fed by coplanar wave (CPW) for beam steering in mobile base stations [8, 9], as shown in Fig. 5.1.

5.3 SENSOR SIMULATION AND MEASUREMENT OF HARMONICS

In this study, an inset microstrip-fed patch antenna, resonating at 2.44 GHz, was chosen for the test. This type of antenna is convenient for the design purposes of active

oscillator antennas adopted for the design in Chapter 4 [8]. The performance of the sensing patch method at 2nd and 3rd harmonic frequencies was evaluated with this antenna. The current distribution on the patch at harmonic frequencies was first studied to find the proper position for the sensing patch, using Ansoft Designer SV. Figs. 5.2 and 5.3 show the corresponding harmonic current distributions on the patch. The position of the sensing patch is optimally set adjacent to a point of maximum voltage, which corresponds to a point of minimum current distribution on the patch. Thus the position of the sensing patch can be set next to the middle of the end edge of the patch for the 2nd harmonic and one-third of the way along one side of the patch for the 3rd harmonic. It was also found that the presence of the sensing patch has very little effect about ±0.1 dB on the return loss at the input port of the main patch for the fundamental and harmonic frequencies.

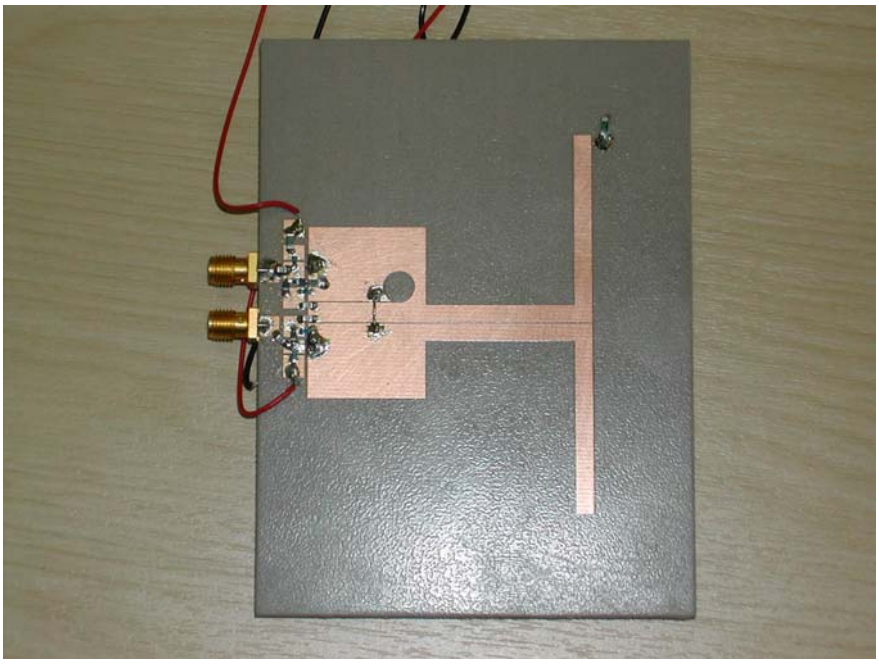

Figure 5.1 RF switched CPW-fed printed dipole, including sensor patch (for measuring radiated power by the dipole).

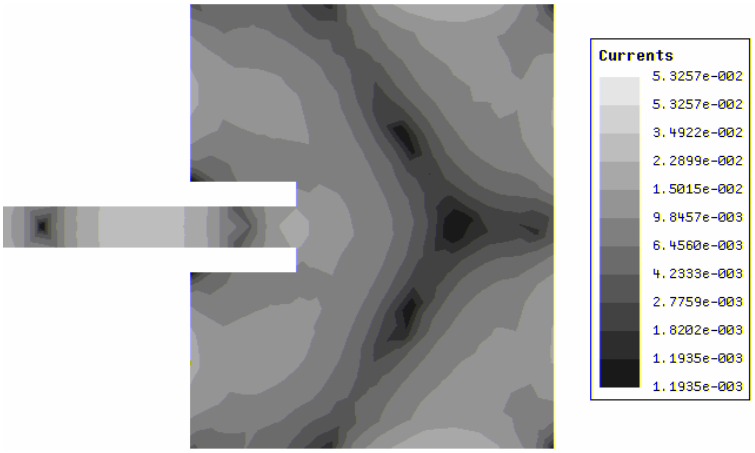

Figure 5.2 Current distribution on the patch antenna at 2nd harmonic frequency.

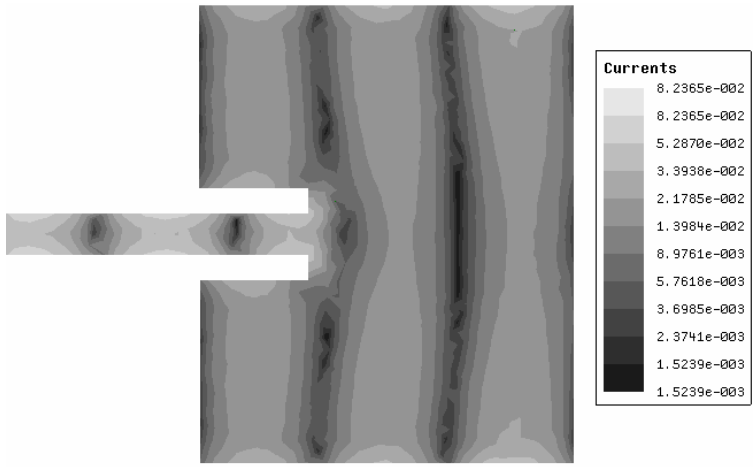

Figure 5.3 Current distribution on the patch antenna at 3rd harmonic frequency.

The antenna with two sensing patches was mounted on 1.524 mm thick Duroid substrate material with relative permittivity of 2.55 and loss tangent of 0.0018. The sizes of the sensing patches used for the 2nd and 3rd harmonic frequencies were 3 mm x 5 mm and 3 mm x 3 mm, respectively. A spacing distance of 2 mm between the sensing patches and the antenna patch (see Fig. 5.4) was found acceptable for sufficient coupling and had no noticeable effect on the antenna input return loss. It has to be noted

that the sensing patch at the 2nd harmonic has the same location as at the fundamental. The sensing patch was connected to ground via a 50 Ω chip resistor. The inclusion of the 50 Ω resistor creates a relatively well-matched source. A 50 Ω coaxial probe was mounted at the rear of the circuit board and connected to the resistor load: this fed the sensor output to a well-calibrated network analyzer.

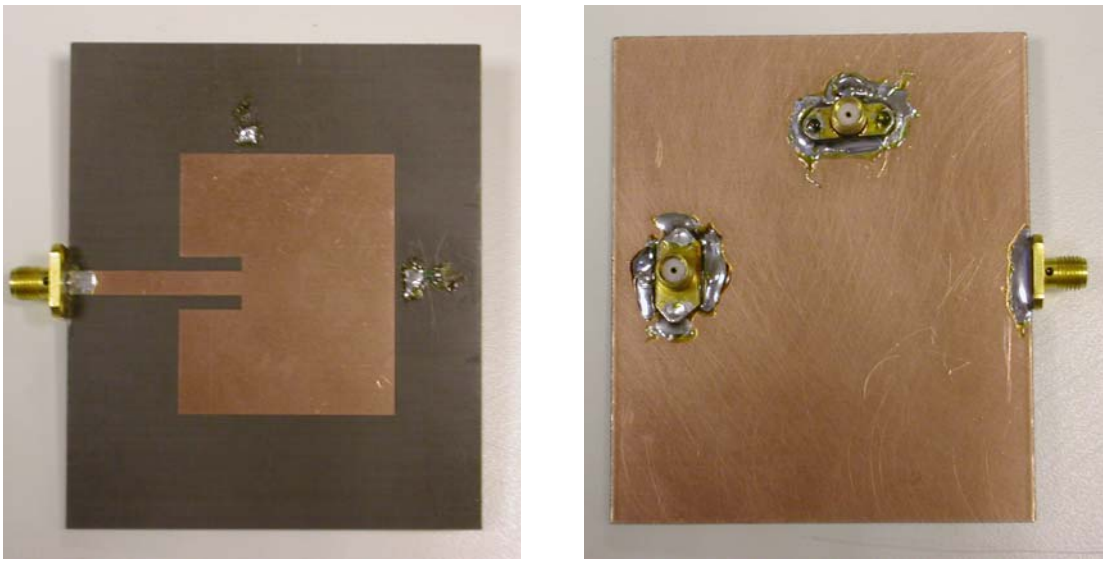

Figure 5.4 Fabricated antenna showing sensor locations: (left) Top view, (right) Underside.

The sensing patch for the 2nd harmonic was first tested. According to the work presented in [6], the performance of the sensing patch for harmonics can be evaluated using the calibration factor $|S_{21}'|$, which relates the sensor's output power to the accepted power by the antenna, as follows [6]:

$$\left|S_{21}'\right|^2 = \left|S_{21}\right|^2 \Big/ \left(1 - \left|S_{11}{}^2\right|\right) \qquad 5.1$$

Where the S parameters in Eqn. 5.1 were obtained by measuring two-port S parameters between the antenna input feed line and the sensor's output from 2 GHz to 8 GHz , using a traceably-calibrated network analyzer (HP 8510C) (see Figs. 5.5, 5.6 and 5.7); the corresponding calibration factor from the measured antenna data was computed using Eqn. 5.1. The measured return loss and computed calibration factors are presented in Table 1 at 2.44, 4.88, and 7.32 GHz, respectively. In order to evaluate sensor's calibration factor for harmonics, a 0 dBm RF signal was fed into the main patch from a sweep oscillator HP 8350B at the fundamental, and harmonics frequencies (see Fig. 5.8). The Return Loss (R.L.) of the antenna tested was optimized at its fundamental frequency into an impedance of 50 Ω as shown in Table 5.1, but at harmonic frequencies, the input impedance of the antenna was greatly different from 50 Ω. Thus, the power accepted by the antenna ($P_{accepted}$) is given by:

$$P_{accepted} = P_{incident}\left(1 - |\Gamma|^2\right) \qquad 5.2$$

Where Γ is the reflection coefficient at the input of the antenna and $|\Gamma|^2 = P_{reflected}/P_{incident}$, $P_{reflected}$ is the power reflected at the antenna input, and $P_{incident}$ is the power outgoing from the signal generator (in this case, $P_{incident}$ = 0 dBm at all frequencies). The power from the sensor's output ($P_{reading}$) was observed using a spectrum analyzer (HP 8563A) (see Fig. 5.9). Care was taken to find the loss in the cable (L_{cable}) before measuring the output power from the sensor. The estimated power accepted by the antenna ($P_{accepted}'$) can be found as:

$$P'_{accepted} = P_{reading} - |S'_{21}|^2 - L_{cable} \qquad 5.3$$

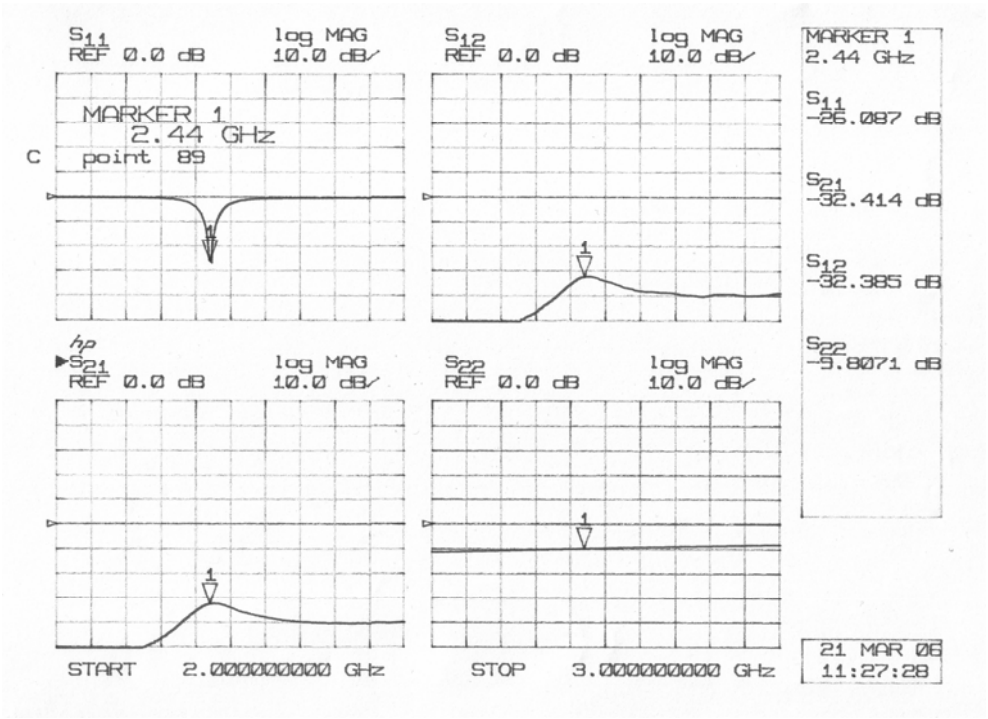

Figure 5.5 The two-port S parameters between the inset-fed patch antenna input port and sensor output at fundamental frequency band.

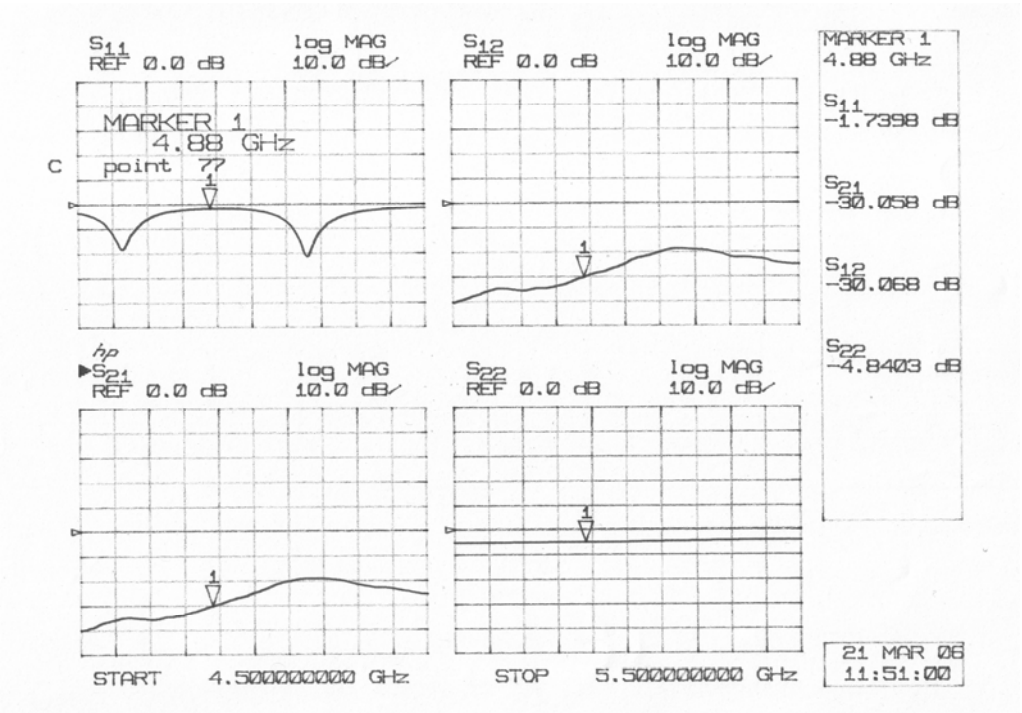

Figure 5.6 The two-port S parameters between the inset-fed patch antenna input port and sensor output at second frequency band.

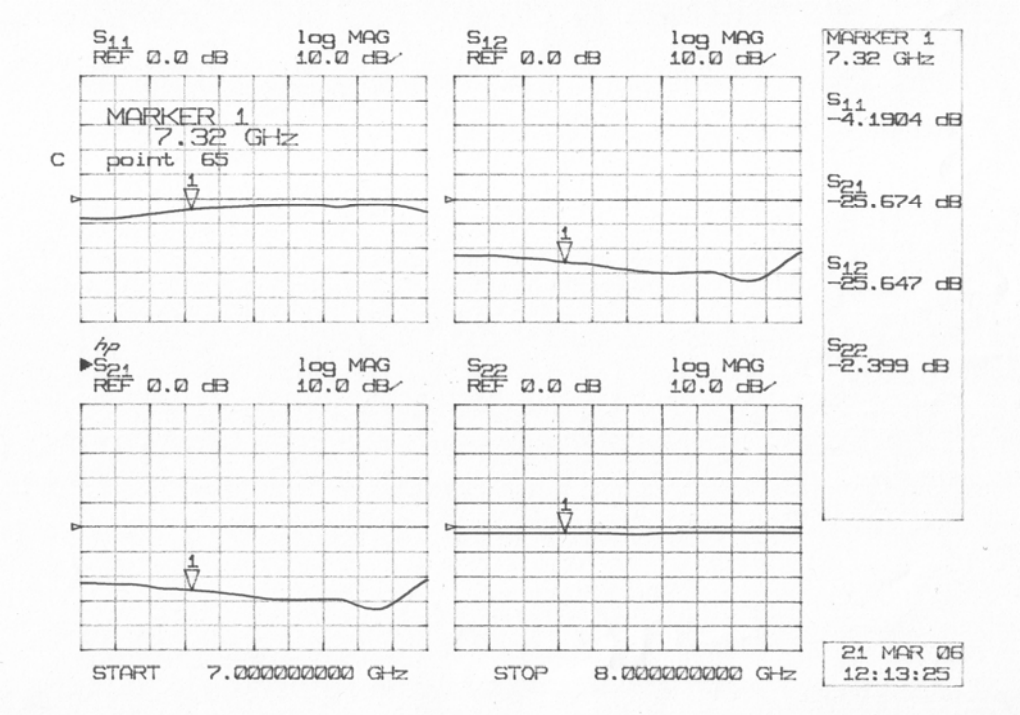

Figure 5.7 The two-port S parameters between the inset-fed patch antenna input port and sensor output at third frequency band.

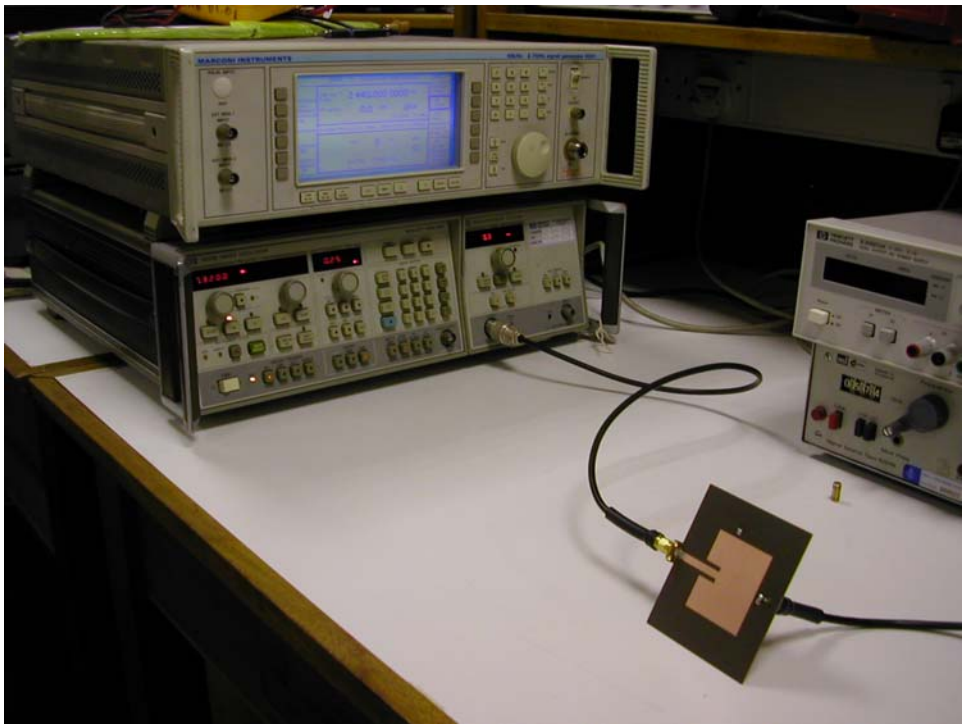

Figure 5.8 Sensor patch measurement setup for oscillating type.

A summary of measured parameters for the 2nd harmonic sensor is presented in Table 5.1. The technique is shown to be valid and the power accepted by the antenna at the fundamental and 2nd harmonic frequencies can be measured using the same sensing patch. As can be seen from Table 5.1, the accuracy of this technique is within 0.8 dB. It should be noted that the power accepted at the 3rd harmonic frequency varies greatly in the measurement and this is because the sensor is weakly coupled to the maximum voltage of the 3rd harmonic.

Similarly, for the 3rd harmonic sensor, the same process was used as with the 2nd harmonic sensor. A summary of measured parameters for the 3rd harmonic sensor is presented in Table 5.2 at the intended frequencies. It is shown that the technique is still valid within 1 dB accuracy for 3rd harmonic power measurement. In addition, this sensor can also be applied for the 2nd harmonic power measurement, with very good accuracy. This is because the current distribution at the 2nd harmonic frequency near to the location of the 3rd harmonic sensor is close to minimum, and this can be easily seen from Fig. 5.2. It is notable that the accepted power at the fundamental frequency varies greatly in the measurements.

Table 5.1 2nd harmonic sensor measurement results for the fundamental and harmonics.

Freq (GHz)	S_{11} (dB)	$\|S_{21}'\|^2$ (dB)	L_{cable} (dB)	$P_{reading}$ (dBm)	$P_{accepted}$ (dBm)	$P_{accepted}'$ (dBm)
2.44	-24.86	-23.20	1.33	-25.33	-0.0144	-0.8
4.88	-1.75	-20.42	2.67	-28.5	-4.796	-5.412
7.32	-4.241	-23.45	4	-27	-2.052	0.45

Figure 5.9 Accepted power measurement setup.

Table 5.2 3rd harmonic sensor measurement results for the fundamental and harmonics.

Freq (GHz)	S_{11} (dB)	$\|S_{21}'\|^2$ (dB)	L_{cable} (dB)	$P_{reading}$ (dBm)	$P_{accepted}$ (dBm)	$P_{accepted}'$ (dBm)
2.44	-26.09	-32.403	1.33	-33	-0.0109	0.733
4.88	-1.74	-25.25	2.6	-33	-4.814	-5.155
7.32	-4.19	-23.59	4	-30.67	-2.084	-3.08

5.4 CONCLUSION

The measured accepted power of microstrip patch antenna, using sensing patch measurement technique, was presented at the fundamental and harmonics frequencies. A prototype antenna, including two sensors at appropriate locations around the patch,

was fabricated and tested at three designated frequencies to estimate the power accepted by the antenna, using a calibration factor. The results of the present work were shown to be acceptable and agreed with direct measurements. The techniques were shown 0.8 dB and 1 dB relative accuracy for the 2nd and 3rd harmonics measurements respectively.

5.5 REFERENCES

[1] D. Zhou, R.A. Abd-Alhameed, N.J. McEwan and P.S. Excell, "Investigations on second harmonic measurements using a sensor patch for active patch antennas", In proceeding of the seventh informatics workshop for research students, pp. 200-201, Bradford, UK, 29th March 2006.

[2] H. Kim, I.-J. Yoon, and Y.J. Yoon, "A novel fully integrated transmitter front-end with high power-added efficiency", IEEE Trans. Microwave Theory and Techniques, Vol. 53, No. 10, pp. 3206-3214, October 2005.

[3] J. Birkeland and T. Itoh, "Planar FET oscillators using periodic microstrip patch antennas", IEEE Trans. Microwave Theory and Techniques, Vol. 37, No. 8, pp. 1232-1236, August 1989.

[4] K. Cha, S. Kawasaki, and T. Itoh, "Transponder using self-oscillating mixer and active antenna", IEEE MTT-S Int. Microwave Symp. Digest, pp. 425-428, 1994.

[5] C.A. Balunis, "Antenna Theory: analysis and design", Third edition, John Wiley & Sons Inc., pp. 94-96, 2005.

[6] E.A. Elkhazmi, N.J. McEwan, and N.T. Ali, "A power and efficiency measurement technique for active patch antennas", IEEE Transactions on Microwave Theory and Techniques, Vol. 48, No. 5, pp. 868-870, May 2000.

[7] R.A. Abd-Alhameed, P.S. Excell and E. Elkhazmi, 'Design of integrated-oscillator active microstrip antenna for 2.45GHz', XXVIIth General Assembly of URSI, Maastricht, Paper No. 1181: 1-4, August 2002.

[8] M.M. Abusitta**,** D. Zhou, R.A. Abd-Alhameed and P.S. Excell, "RF switch design for beam-steering antenna-array mobile communication base stations", In proceeding of the eighth Informatics workshop for research students, University of Bradford, Bradford, UK, 28th June 2007.

[9] M.M. Abusitta, D. Zhou, R.A. Abd-Alhameed and P.S. Excell, "Simulation and measurement of controlled RF switch for beam steering antenna array", National URSI symposium, University of Portsmouth, Portsmouth, UK, 2–3 July 2007.

CHAPTER 6

NUMERICAL SOLUTIONS ON ACTIVE PATCH ANTENNAS FOR HARMONIC SUPPRESSION USING GENETIC ALGORITHMS

6.1 INTRODUCTION

Active transmitting antennas normally contain significant non-linearity and are always integrated compact design. Therefore, the transistor drain (or collector) will be producing harmonic currents directly into the radiator, and these would be expected to be radiated fairly unwanted power [1]. In active antenna design, the unwanted harmonic contents can be terminated (or eliminated) using the radiating element. In this way, active circuit does not request any additional circuitry for harmonic tuning, and thus, can simplify the circuit design and ended with small compact design. In [2], the modified rectangular patch antenna with a series of shorting pins added to the patch centre line was applied to shape the radiated second harmonic from the active amplifying-type antenna, in order to increase the transmitter efficiency. Unfortunately, the proposed design does not provide the termination for the third harmonic. A circular sector patch antenna with 120° cut out (see Fig. 2.6) in [3] was investigated and proved to provide additional harmonic termination for the third harmonic, claiming a further enhancement in the transmitter efficiency. Moreover, an H-shaped patch antenna for

harmonic suppression was designed and applied in oscillator-type active integrated antennas for the purpose of eliminating the unwanted harmonic radiation [4, 5].

In this chapter the harmonic suppression antennas, used to reduce unwanted outputs at the second and third harmonics of an active microstrip patch antenna, were designed and optimised using genetic algorithms. Genetic algorithm driver, written in FORTRAN, was adopted in this work in conjunction with the industry-standard NEC-2 FORTRAN source code, which was used to evaluate the randomly generated antenna samples [6, 7]. Therefore, firstly, a summary on the sophisticated genetic algorithms (GA) and its application in collaborating with NEC-2 for antenna designs and optimization was described. Secondly, two examples on antennas using GA were briefly demonstrated to prove the capability of GA as a quick optimization tool in antenna designs. Finally, a novel FORTRAN program for adaptively meshing any planar antenna as wire-grid like structure is developed and is exploited in designs of harmonic suppression antennas for active antennas.

6.2 THE GENETIC ALGORITHM

6.2.1 Introduction to genetic algorithms

Genetic algorithms are stochastic search procedures orchestrated by natural genetics, selection and evolution [8]. They are modelled on Darwinian concepts of natural evolution thus making them more inspiring during use [9]. After it's first introduction in 1960's by J. Holland, it has become an efficient tool for search, optimization and machine learning, but in the pre – GA era, concepts of it had been looming and applied

in game playing and pattern recognition [10]. Over the recent years, it has proven to be a promising technique for different optimizations, designs and control applications.

Basically, GA exerts pressure on a set or population of possible solutions managing them to evolve towards a global optimal point. This is achieved by a fitness weight selection process and severe exploration of the solution search space attained through recombination (crossover) and mutation of the characteristics present in the particular population considered.

When the GA is used as an optimizer, it was found very effective and robust especially if the goal of the operation is to locate an approximate global maximum in complex combinatorial and search related problems. The powerful heuristics of the GA are essentially efficient to dynamically update the parameters applied to the input measurements, operates on them and produce near optimal solutions.

Genetic algorithms show more promises because among other search algorithms, it examines all possible solutions in the search space of unknown parameters and eventually identifies the most suitable and fittest solution to the complex problem. Due to the unique ability to rigorously search the entire defined search space, it's always been referred to as a robust and highly efficient technique with better performances; capable in solving complex problems in various engineering applications and fields.

6.2.2 Why genetic algorithms?

At this point, it is highly necessary to point out the reasons why GA is mostly used nowadays in different optimization processes. Majority of the optimization methods are classified as either;

- Global techniques with familiar examples such as Genetic Algorithms, random walk, simulated annealing and Monte Carlo.
- Local techniques with familiar examples such as conjugate gradient, quasi Newton and simplex methods.

A major difference between these two optimization techniques is that the local techniques tend to produce results extremely dependent upon initial start conditions and they couple tightly to the solution domain thereby converging relatively fast and producing local maximum results. On the other hand, global techniques are independent of these starting conditions and place certain constraints on them. Thus, this makes the global techniques to be robust and perform better even if there are discontinuities in the solution domain. Furthermore, it's been observed that there are three main situations when the genetic algorithms tend to be more useful. These are;

- If the problem at hand requires quite a number of parameters.
- There are multiple local optima solutions present.
- A non – differentiable objective function.

From this point of view, a deeper look into these two groups of optimization process shows that the local techniques converge faster than the global techniques [8]. However,

in the electromagnetic design problems, the rate of convergence is relatively less important but optimal results are vital. Amongst the global techniques, the GA is more suitable for electromagnetic design issues. It is faster, reliable, robust and easily programmed and readily implemented [11].

6.2.3 Terminologies in GA

To be able to appreciate and have a common understanding of this particular discussion about GA, we ought to dive more deeply into some fundamental definitions. The following summarizes the most important concepts many of which are similar and borrowed from the concepts of natural evolution.

- Generation: A set of fit individuals which were successively created.
- Parent: These are members selected in a probabilistic manner from a particular initialized population. They are usually weighted relative to their fitness values [8].
- Children: Usually generated by initially selected parents to form a new generation. They are products of the major genetic operators; crossover and mutation.
- Fitness: A value that dictates the measure of the goodness of each individual.
- Genes: Coded parameters required for optimization.
- Chromosomes: A couple of genes in string format.
- Objective function: Basically a numerical representation in simple equation formats, of the required goal in an optimization problem [12]. It defines if the complex problem is been maximized or minimized and could also be referred to as the cost function or fitness function.

- Search space: It's the region that contains all possible solutions assumed by the design engineer [12]. Due to the chances of flexibility during optimization, the search space might contain solutions outside the feasible conditions. The intelligent GA tends to isolate them and select the appropriate optimal solutions from this pool. In addition to this, the format of the search space boundaries must be carefully taken to prevent early convergence on less optimal results.

From all described so far, the whole optimization process involves some basic tasks which are enumerated below as follows:

- Solution parameters are encoded as genes.
- Chromosomes are formed from strings of genes.
- A random initiation to create a starting population.
- Individuals in the population are evaluated and assigned fitness values.
- Reproduction of the fit individuals selected.
- Genetic operators, crossover and mutation, to generate new set of individuals.

6.2.4 GA step by step implementations

In general, a typical genetic algorithm optimizer consists of three main phases as described by Rahmat–Samii etc [8]. These stages include initiation, reproduction and new generation (i.e. generation replacement).

The whole process of Genetic Algorithm is kicked–off by encoding the parameters into either a binary or real-valued format. The coding of the parameters (real values or binary) is highly required as this enables the GA to proceed in a style independent of the

parameters themselves and thus independent of the solution space [12]. Genes are then allocated to represent these parameters which are used throughout the process to model the evolutionary algorithm. A set of population is selected randomly from the allocated genes and this is called the initiation stage.

After the generation of the initial population, the fitness values of the individuals are evaluated. The evaluation of these values determines the survival of the individuals in this randomly generated generation to proceed to the selection stage. In simple terms, the fitness values describes or measures how good the individuals (i.e. antenna samples generated GA in this study) are able to produce desired results to an extent after combination with themselves. This stage is usually referred to as the evaluation stage.

The selection stage tends to identify the genes with the highest fitness values to enable them migrate unto the mating phase in which a more ideal and better generation is produced by the algorithm. It is a stage whereby pressure is applied upon the population in an approach similar to those of natural selection [8]. This stage is usually executed with different techniques such as; tournament selection, population decimation and proportionate selection also known as roulette wheel. For the roulette wheel, the individuals are selected based on fitness proportional to a probability equation written in Eqn. 6.1, where $f(parent_i)$ is the fitness of the i_{th} parent [8].

$$p_{selection} = \frac{f(parent_i)}{\sum_i f(parent_i)} \qquad 6.1$$

It could be inferred from this equation after a close look that the probability of identifying and selecting an individual from the pool of population by the algorithm is solely a function of the relative fitness of the particular individual. The selection procedure is usually applied twice in an attempt to obtain a set of individuals suitable for the GA operators to act on appropriately [9].

The second popular technique is the tournament selection because it is relatively straight forward. A subpopulation of N individuals is chosen randomly from the selected population. These individuals in the subpopulation then compete with their fitness values and the one with the highest fitness value wins the tournament and is selected and isolated. The remaining less fit of the subpopulation is then replaced back to the former pool of individuals and the whole process repeated until all the members of the subpopulation are selected. It is a faster mode of selection and it is used in the GA optimizer implemented in this study.

The preceding stage after selection is the reproduction phase in which a new generation is produced by crossovers and mutation operators. They are implemented in straightforward code segments. Simply put, crossover is the process by which the genes of a parent are combined with those of another parent to produce children with better genes. Several modes of crossover have been tried but the simplest of all is the single-point crossover demonstrated briefly below in Fig. 6.1 [13]. A random location is selected in the parent's chromosomes and swapped to produce the children.

Split Position ……+

Fathers genes: 11101000111001100110 10101

Mothers genes: 10101110011101010111 00110

Left side genes from father + right side genes from mother

Child A's genes: 11101000111001100110 00110

Left side genes from mother + right side genes from father

Child B's genes: 10101110011101010111 10101

Figure 6.1 Single point crossover illustrations.

It is obvious that the individuals in the generation that are not selected for crossover operations are acted upon by mutation. It also changes part of the chromosomes string in order to maintain at least some traits in the new generation formed.

All these processes are continued until a new generation is formed by replacing the old generation totally or partially and their fitness values evaluated intermittently. After some certain runs and considering the input search space, GA tends to identify the near optimal value. Fig. 6.2 is the pictorial diagram illustrating the GA optimizer that summarizes all processes described earlier.

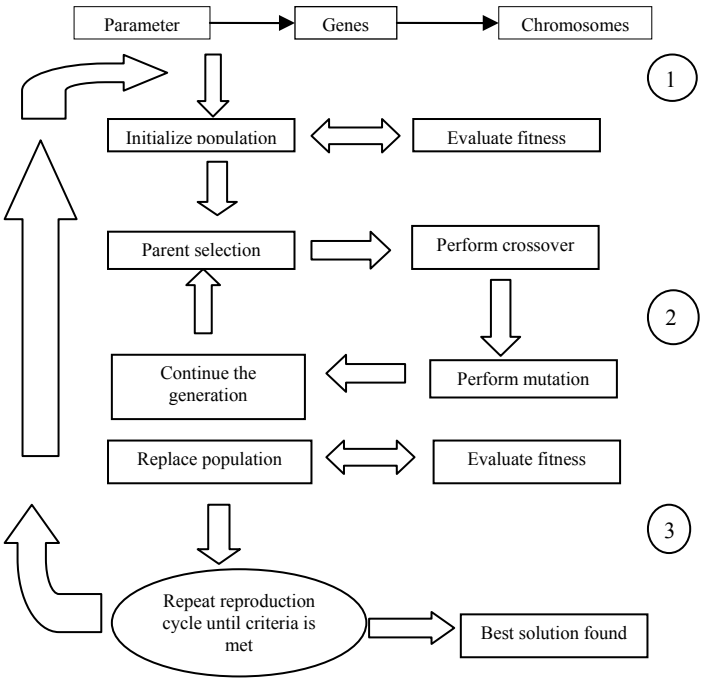

Figure 6.2 Design procedure of the GA optimizer.

6.2.5 The genetic algorithm driver and implementation

During the current research, it was noticed that various versions of the Genetic Algorithms driver are available for use as an optimizer, in which they are implemented in C, MATLAB and FORTRAN 77. From our experiences on home programmes, FORTRAN 77 seemed more friendly and easier to manipulate and thus was chosen for this optimization processes. The FORTRAN 77 version of the GA driver, written by David L. Carroll of the CU Aerospace USA [6], uses the randomized approach to initialize its start individuals and the tournament selection with shuffling techniques in choosing random pairs for mating. Binary coding is also enabled the uniform and non-uniform process of single point crossovers.

Each one of the GA parameters presented, the GA driver can be controlled and adjusted through an associated file called GA input. Fig. 6.3 illustrates a sample of GA driver input file. As can be seen, some of the parameters in the input file have been highlighted and explained. These variables are the most important and influential to the GA driver in the antenna design and should be adaptively adjusted according to the various design types or objectives, in order to maximize the GA driver performance in searching for solutions in antenna designs. It is notable that this GA driver is for maximize the design target objective.

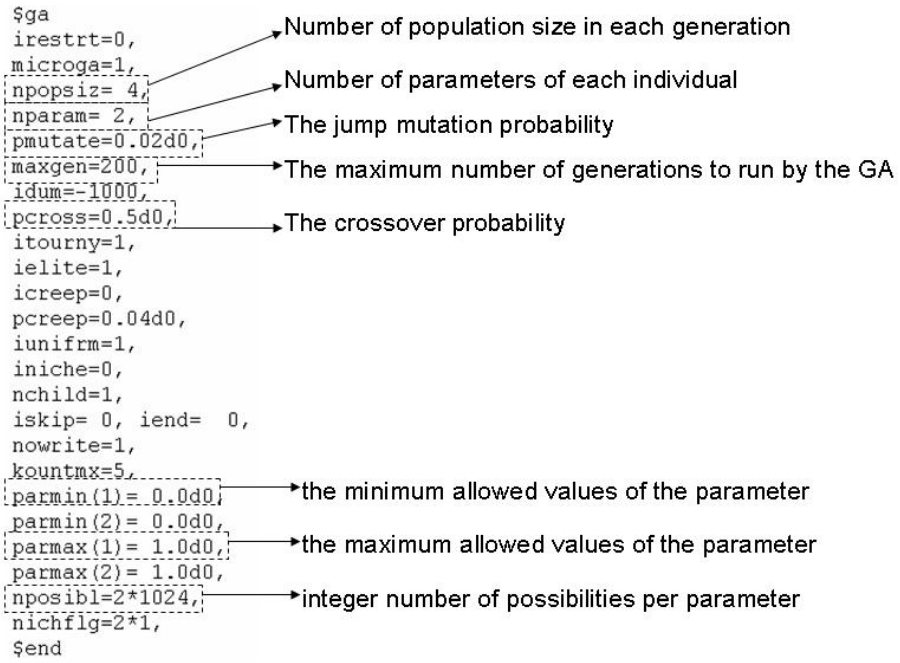

Figure 6.3 A sample of GA driver input file.

6.2.6 Implementation of antenna designs using GA driver

It is well known that, NEC-2 FORTRAN source code was adopted inside the GA fitness function to perform the required calculations answers for the cost functions. The source

code was modified to process the input data file in which to support the calling function required. These modifications are found very helpful to reduce the execution processing time and manipulate the output data files.

However, before the process of optimization is initiated, one required defining the target objectives and number of parameters required of the whole process in order to achieve the optimum desired goal. In simple terms, some of the most important antenna parameters which are directly targeted were selected for optimization and the desired objectives were those usually required by the end users.

Sometimes a relationship was required to define a threshold for the GA which enables it to evaluate the designed antenna performance and terminate where necessary. Usually, this is a complex procedure to be applied; however, one can apply a certain constraints inside the cost function to support the data processing when nearly reaching the optimal design requirements. The cost function is usually included in the algorithm and it measures the fitness of the individuals produced in each generation of the algorithm [14].

A flow chart to represent the easiest way in which the GA optimizer coordinates its functions is represented in Fig. 6.4. The algorithm randomly initiates its population and converts the parameters of the initiated individuals into a file in a card format which can be called by NEC to determine the performance of these individuals. The results from NEC are fed again to the GA engine to evaluate individual fitness if the maximum value is obtained for convergence, if otherwise the whole process is repeated until optimal results are produced [15].

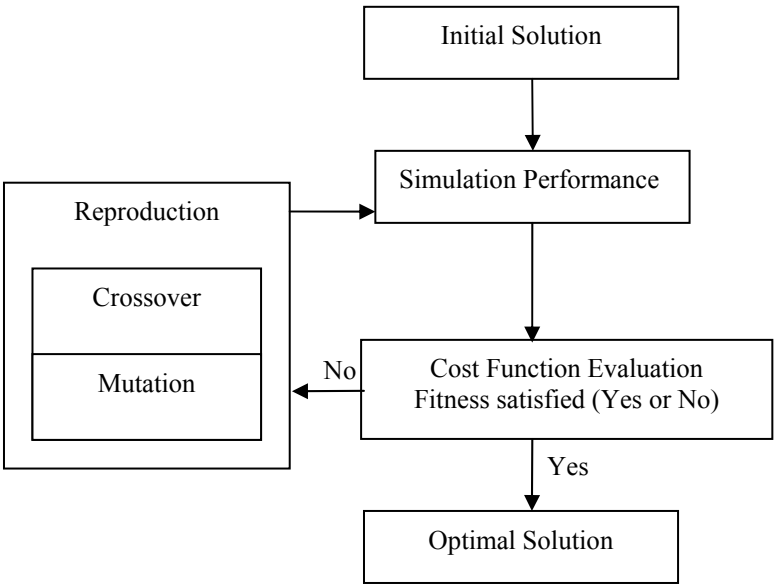

Figure 6.4 Flow chart of the genetic algorithm adopted in this study.

6.3 NEC-2 SOURCE CODE

NEC-2 was originated by the US Department of Defence and more specifically, it was developed at Lawrence Livermore National Laboratory in California under the sponsorship of the Naval Ocean Systems Centre and the Air Force Weapons Laboratory [16, 17]. NEC is an advanced version of the antenna modelling program (AMP) developed in early 1970's. NEC-2 is the most popular and widespread electromagnetic code in the public domain. This is because it is free and easy to use with scripting programs. In addition to the full source code of NEC is available and can be modified without any restriction. Generally, NEC-2 is applied for thin wires (the basic modelling used as short straight segments) and surfaces antenna structures (the basic modelling

used as flat surface patches) and based on solving integral equations by the Method of Moments (MoM).

In most cases, the Method of Moments is used to form equations like the integral equations or the integro-differential ones. The essential idea in using MoM is the discretization of the problem into smaller linear bounded elements, which are treated as independent by using many functions, known as “basis functions”. Then the inner integral of the corresponding resulted functions is taken by applying the proper weighting functions. At the end, the linear equations can take the form of a matrix and can be solved by a simple matrix inversion [18].

6.4 EXAMPLES ON ANTENNA DESIGNS USING GA

6.4.1 Design of Quadrifilar helix antenna using GA

In this section, two examples on antenna designs using the genetic algorithm driver in collaboration with NEC-2 source code are presented. They are the quadrifilar helix antenna (QHA) for the use in mobile satellite communications and balanced folded loop antenna (FLA) for mobile handsets. The antennas firstly attempted to be designed and optimized using a genetic algorithm and then subsequently the performance of the optimal GA antennas was verified using a HFSS simulator. At last, a prototype of GA-optimized antenna was fabricated and tested in order to validate the GA solution.

The quadrifilar helix antenna is a very attractive candidate antenna and has been widely used for satellite mobile handsets due to the symmetry of their geometry, properties of balanced feeding and their ability to provide circular polarization over a broad angular

region [19]. The QHA is a circular polarised (CP) antenna consisting of four helices and fed with equal amplitude signals and with 90° phase difference between the feeding sources (i.e., 0°, 90°, 180°, and 270°). The presented results in this section are a case study in which GA are applied to design and optimise circular polarized QHA in the presence of a small size satellite mobile handset (2 x 5 x 10 cm). The QHA antenna (see Fig. 6.5) can be defined by four parameters, including axial length (h), Pitch distance (P_d), Radius at bottom (R_b) and Radius at the top (R_t), as illustrated in Fig. 6.6.

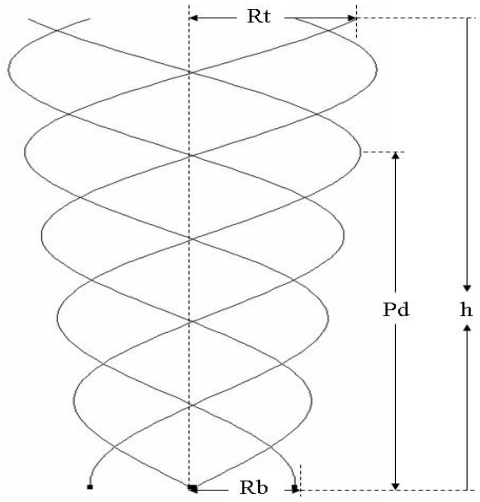

Figure 6.5 QHA antenna configuration used by GA optimization.

Real-valued GA chromosomes were used for this optimisation. Two most important antenna parameters such as VSWR and axial ratio (AR) are optimized at a single frequency (f_o = 2.4 GHz). The antenna AR was calculated at f_o at $\theta = 0°$ and $\phi = 0°$. Each antenna sample was computed using NEC-2 source code and its results were compared with desired fitness using a cost function, as follows:

$$F = W_1 \times (1/VSWR) + W_2 \times A.R. \qquad 6.2$$

$$VSWR = (1+\Gamma)/(1-\Gamma) \quad 6.3$$

$$\Gamma = \left|(Z_{in} - 50)/(Z_{in} + 50)\right| \quad 6.4$$

Where F is the Fitness of the cost function, VSWR is the voltage standing wave ratio, A.R is the axial ratio, Z_{in} is the input impedance, Γ is the reflection coefficient and W_1 and W_2 are the weighting coefficients.

Table 6.1 Comparative results of VSWR, AR and Fitness as the values of the weighting coefficients are varied.

Weighting (W_1, W_2)	0.2, 0.85	0.3, 0.75	0.4, 0.75	0.5, 0.75
VSWR	1.74531	1.66912	2.03473	1.49462
AR	0.92561	0.92665	0.98089	0.92493
Fitness	0.90064	0.87472	0.93266	1.0282

Using Eqn. 6.2 the algorithm ensures that the maximum value of F is obtained through the combination of all the antenna parameters, although it should be noted that during all optimization designs, trade offs are usually expected. The parameter quantities of each helical antenna design were coded into chromosomes inside the source code of the algorithm. It has to be noted that the two weighting coefficients are optimally found to be 0.5 and 0.75 respectively for optimum design after a few tries, as illustrated in Table 6.1. It presents the comparative results of VSWR, AR and Fitness as the values of the weighting coefficients are varied. Within the maximum generation, the values of maximum fitness function for QHA design reached to be about 1.03. Moreover, a comparison of maximum fitness versus generations of different combination choice of the two weighting coefficients is shown in Fig. 6.6. The value of best fitness for the cost function tends to reach optimum solution after around 150 generations. Fig. 6.7 presents

the progress of best fitness and average fitness against the number of generations for some selected values of weighting coefficients.

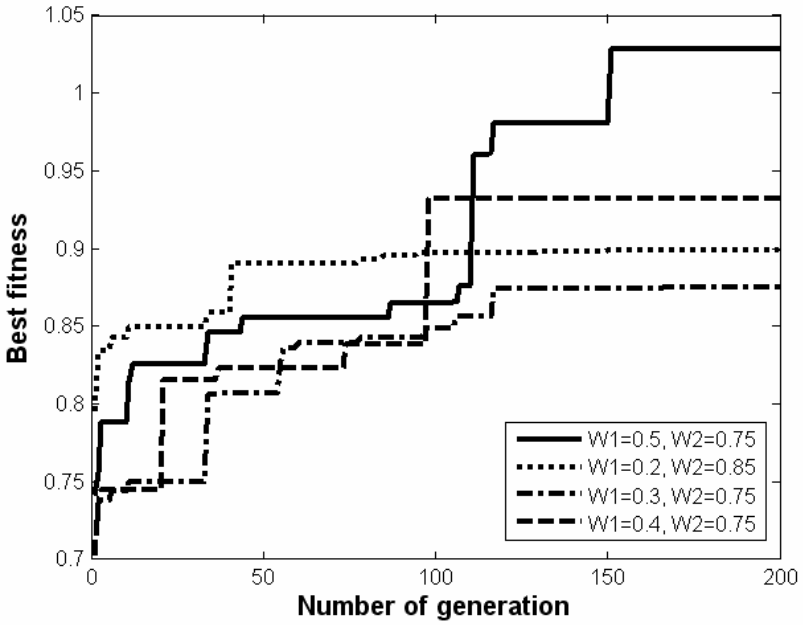

Figure 6.6 Maximum fitness versus generations
(4 populations in each generation).

Configurations for the GA-optimal QHA antenna, with Excellent VSWR and AR values were found within the maximum generation; the optimal values for each specified parameter are shown in Table 6.2. This Table also includes a summary of the GA input parameters and their constraints. The attained optimal antenna geometry for QHA antenna is presented in Figs. 6.8 and 6.9.

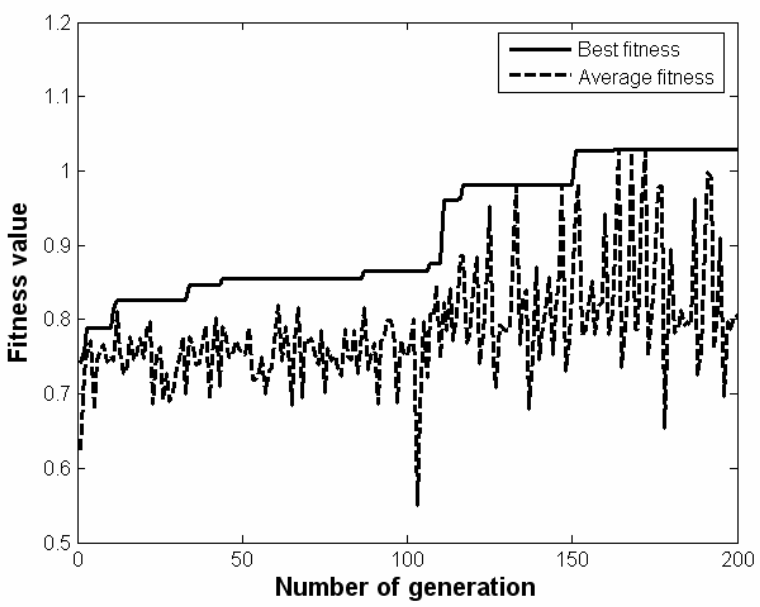

Figure 6.7 The progress of best fitness and average fitness for w1 and w2 are 0.5 and 0.75, respectively.

Table 6.2 Summary of GA input parameters, antenna variables and optimum values with the handset included.

GA parameters	QHA Design with the handset	
	Parameters (m)	Optimum (m)
Number of population size = 4	Pitch distance (P_d) (0.01-0.048)	0.03026
Number of parameters = 4	Axial length (h) (0.05-0.12)	0.06294
Probability of mutation =0.02	Radius at the bottom (R_b) (0.005-0.015)	0.00721
Maximum generation =200	Radius at the top (R_t) (0.01-0.02)	0.01194
Number of possibilities=32768	Radius of wires Distance above handset	0.00075 0.005

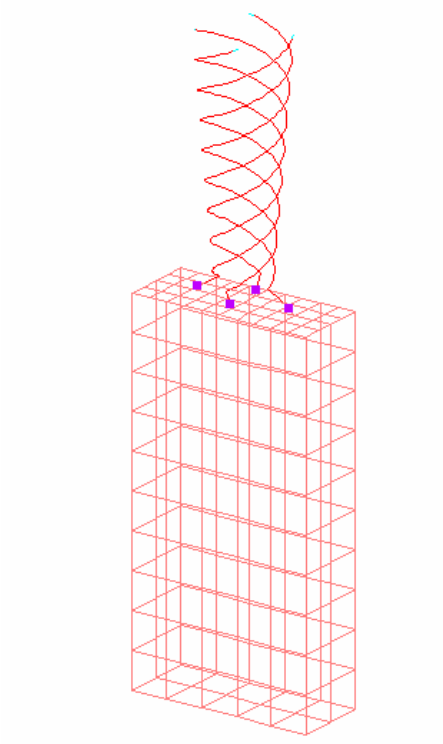

Figure 6.8 The NEC-2 model of the QHA.

Figure 6.9 Prototype QHA antenna; internal view of the completed assembly (left) and overall complete assembly (right).

For validation, a prototype of the GA-optimised QHA antenna was built up and tested. Photographs of prototype antenna, including an internal view of the hybrid feeding network and an overall view of the complete assembly, are presented in Fig. 6.9. The QHA arms were made of copper wires with radius of 0.75 mm. The measured return loss of the designed antenna is shown in Fig. 6.10. As can be seen, the QHA antenna is resonant at 2.347 GHz, which is about 60 MHz shifted compared to the targeted design frequency. This is mainly due to the mechanical error in fabrication since the total length of the prototype antenna is slightly greater than the prediction figures. It is interesting to note that the resultant measured impedance bandwidth was found to be about 150 MHz (referring to 2:1 VSWR). It should be noted that the antenna bandwidth was not considered in the GA cost function, the resultant GA-optimized QHA antenna appear to have an excellent impedance matching.

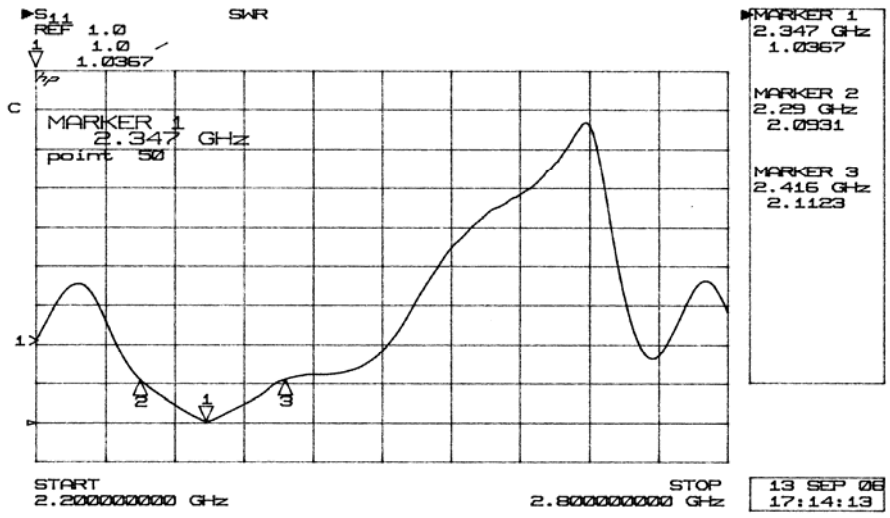

Figure 6.10 Measured VSWR of the QHA.

One way to recognize whether a given antenna design is optimum for the best AR is to look at the input impedance loci plot of the antenna on a Smith Chart. If there is a kink (extremely small loop) in the impedance plot corresponding to the excitation of the two orthogonal modes, it will yield the best AR at the kink frequency [20]. It is noticeable in Fig. 6.11 that there is kink around intended design frequency of 2.4 GHz on the Smith Chart, where the best AR is achieved and in addition to verify the initial design objective of an antenna with circular polarization.

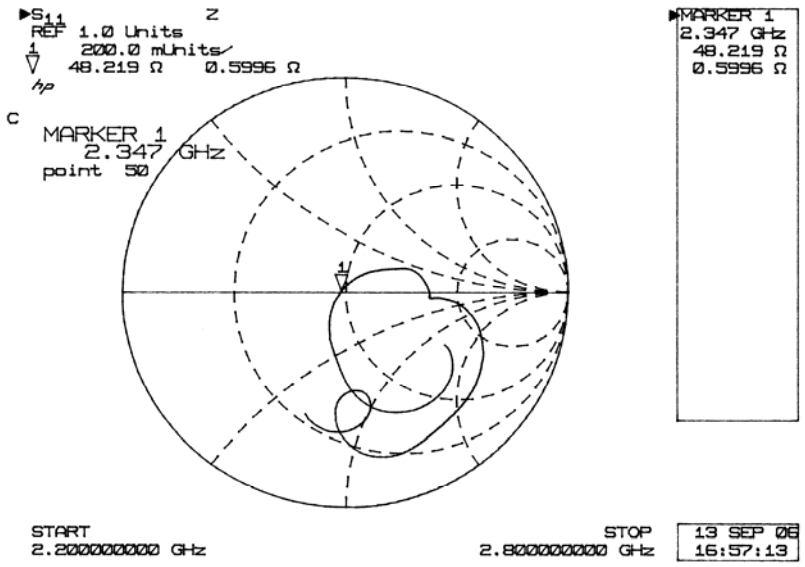

Figure 6.11 Input impedance loci plot of the antenna on a Smith Chart.

The attained results in simulation and measurement indicate that the optimal antennas met design objectives under several certain constraints. Moreover, the capabilities of GA are shown as an efficient optimisation tool for selecting globally optimal parameters to be used in simulations with an electromagnetic antenna design code, seeking convergence to designated specifications.

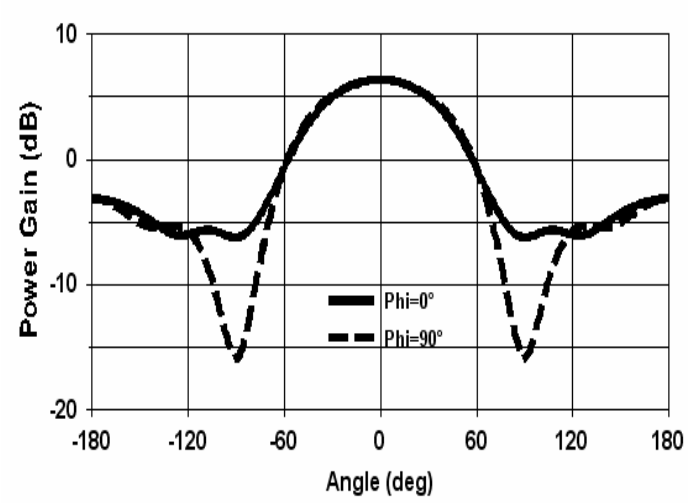

Figure 6.12 Computed power gain of the GA-optimized QHA antenna in θ plane at φ =0° at 2.4 GHz using NEC-Win professional package.

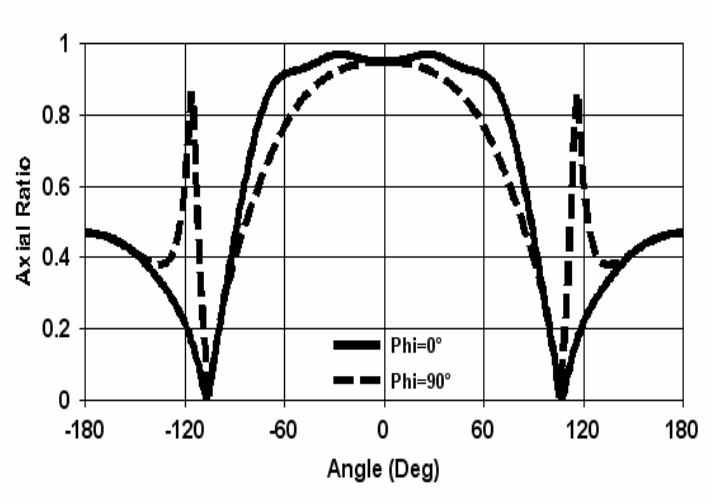

Figure 6.13 Comparison of AR results for QHA with the handset at 2.4 GHz in θ plane for φ =0° and φ =90°.

The computed AR and power gain, for the GA-optimized QHA antennas at 2.4 GHz, are shown in Figs. 6.12 and 6.13. As can be seen, good beamwidth angles and power gain over theta plane for circular polarization characteristics were observed.

6.4.2 Design of a balanced folded loop antenna using GA

A FLA for mobile handsets with relatively wideband impedance was designed and optimized using GA. The geometry of proposed FLA was adopted from the Morishita's work [21] (see Fig. 6.14) and applied here for this study. Parameters, used to define the FLA, were optimized and evaluated using GA in collaboration with NEC-2. Finally, GA optimal antenna structure was verified and compared using the commercial EM simulator HFSS and a good agreement in VSWR was observed. A prototype antenna was also fabricated and tested in order to validate the results obtained in the prediction.

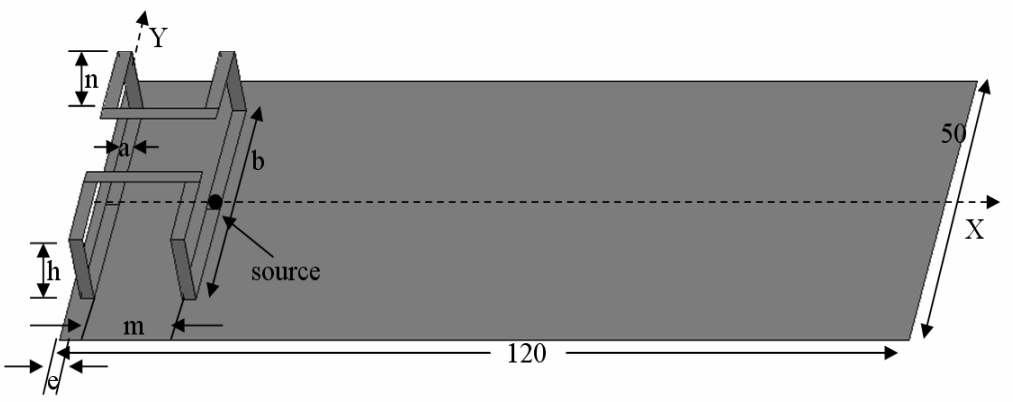

Figure 6.14 Geometry of the folded loop antenna with ground plane, modelled in HFSS.

The FLA was optimized with GA using real-valued chromosomes. The intended antenna was designed for Global System for Mobile Communications (GSM) applications (1710-1860 MHz). Performance of the randomly generated antenna samples was computed using NEC-2 and its result was compared with desired fitness using a cost function, as follows,

$$F = \sum_{n=1}^{3} W_n \cdot \left(1/VSWR\right)_{fn} \qquad 6.5$$

Where, W_n (n=1…3) are weighting coefficients for the cost function. All the weighted coefficients are set to be 1. Three pre-set specific frequencies f_n (1710, 1785, and 1860 MHz) were applied for NEC-2 and GA to run the calculation and evaluation for each erratically produced antenna structure, in order to ensure the optimal antenna covers the required impedance bandwidth.

GA input parameters, their constraints and the optimal values for each specified parameter of the design geometry are presented in Table 6.3. Since there is no graphical abilities in NEC-2, GA generated antenna structures can be viewed using the NEC-Win Professional simulator.

The basic geometry of the optimal FLA antenna with excellent VSWR covering entirely required GSM1800 frequencies bands was shown in Fig. 6.15. This was found within the maximum generations for which the antenna parameters of the best designs are shown in Table 6.3. HFSS simulator, based on the finite element method (FEM), was used to verify and validate the GA-optimized antenna structure. It should be noted that thin strip lines were employed in the HFSS model instead of thin wires used by GA optimization, due to the fact for the purpose of practical implementation (see Fig. 6.14).

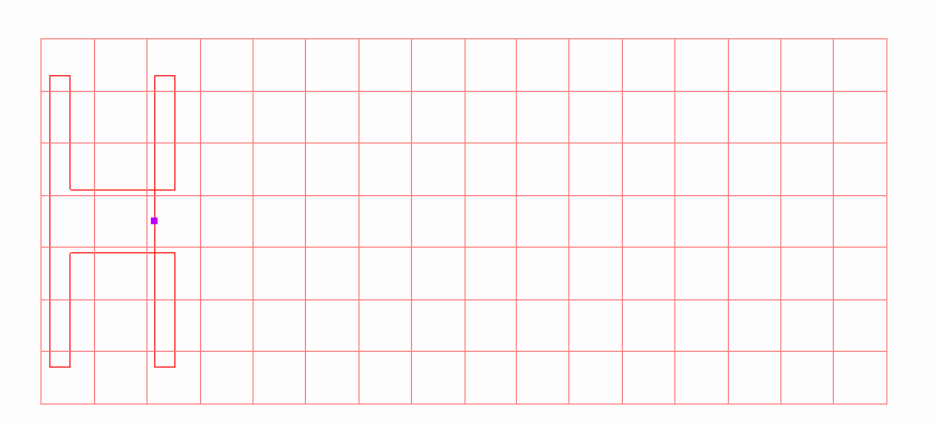

Figure 6.15 Folded loop antenna model using NEC Win Professional.

Table 6.3 Summary of GA input parameters, antenna variables and best solutions.

GA parameters	FLA for GSM1800		FLA for UMTS	
	Parameters (m)	Optimal (m)	Parameters (m)	Optimal (m)
Number of population size = 6	Wire radius (a) (0.0004-0.0008)	0.00074	Wire radius (a) (0.0004-0.0008)	0.0007905
Number of parameters = 7	FLA length (b) (0.03-0.04)	0.03978	FLA length (b) (0.03-0.04)	0.03690
Probability of mutation =0.02	FLA height (h) (0.003-0.012)	0.01173	FLA height (h) (0.003-0.012)	0.01179
Maximum generation =500	FLA arm length (n) (0.002-0.015)	0.008785	FLA arm length (n) (0.002-0.015)	0.009881
Number of possibilities=32768	Parallel wires distance (m) (0.005-0.015)	0.01489	Parallel wires distance (m) (0.005-0.015)	0.013599
Ground plane size (120 x 50 mm)	FLA distance to GP edge (e) (0.0-0.002)	0.0008643	FLA distance to GP edge (e) (0.0-0.002)	0.001137
Distance between FLA and GP (h_0) (not shown in Fig. 1) (0.001-0.003)		0.001112	h_0 (0.001-0.003)	0.001146

The calculated antenna VSWR against frequency over the interested bands is shown in Fig. 6.16 and was compared using two EM packages. As can be seen, an excellent agreement of antenna VSWR response was achieved. It can also be observable that impedance bandwidth (for VSWR $\leq$ 2) for the optimal antenna structure was 7.5% at centre frequency (f_0 = 1785 MHz), compared to the bandwidth of 2.7% (f_0 =1860 MHz) with a small FLA and 5.4% with using a parasitic element added, as reported in the

research work in [21]. The reason is comparatively broadened is because the effect of capacitive coupling between the antenna and the ground plane in which it was enlarged and tuned by varying the distance of the two parallel wires "m".

In addition, the same design principle and antenna geometry was applied to design and optimize antennas for the third generation (3G) wireless mobile communication system application. The comparative antenna VSWR (see Fig. 6.17) shows a good impedance matching over the intended band (11.3% at f_0 =2030 MHz).

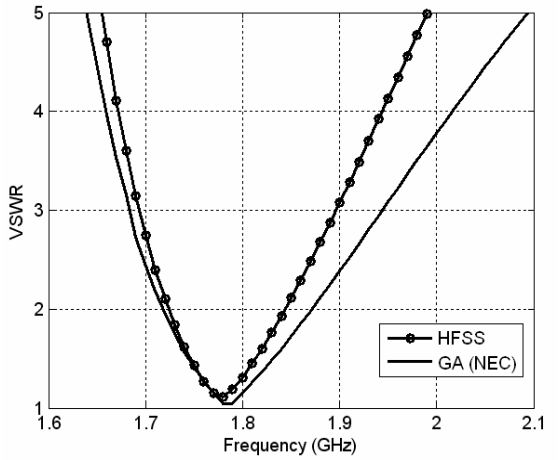

Figure 6.16 VSWR against frequency (a= 2.0705, b= 37.8802, h= 9.9991, h_0=1, n= 13.884, e= 0.9409 and m= 12.8052, all dimensions in mm).

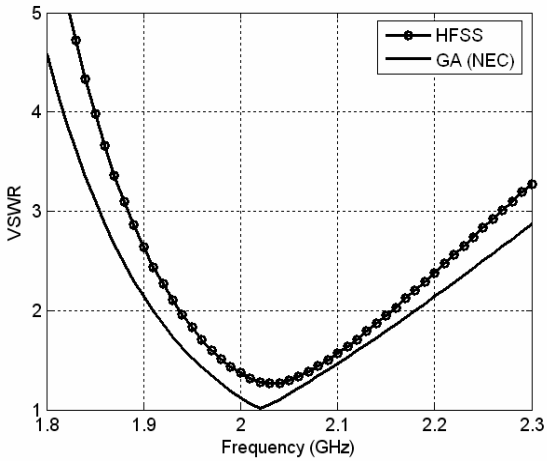

Figure 6.17 VSWR against frequency (a= 1.95144, b= 37.0052, h= 9.9966, h_0=1, n= 11.1638, e= 1.8835 and m= 12.9884.

A prototype of the GA-optimised antenna for GSM 1800 was shown in Fig. 6.18. The conducting copper thickness of 0.15mm and 0.5mm was used for fabricating the balanced antenna and the ground plane, respectively. The measured return loss of the prototype antenna is presented in Fig. 6.19. As can be seen, the resultant measured impedance bandwidth was found to be about 7.4% at f_0 =1765 MHz (referring to -10 dB

return loss), which is very encouraging, compared to the simulated result. Further work using GA for harmonic suppression antenna design was considered in the following sections.

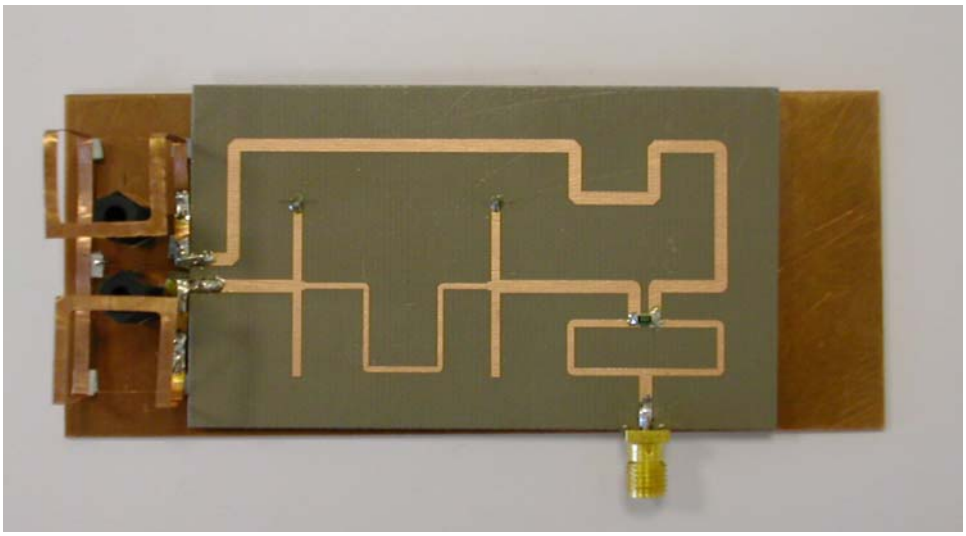

Figure 6.18 Photograph of the prototype antenna for GSM1800, including the feeding network (balun).

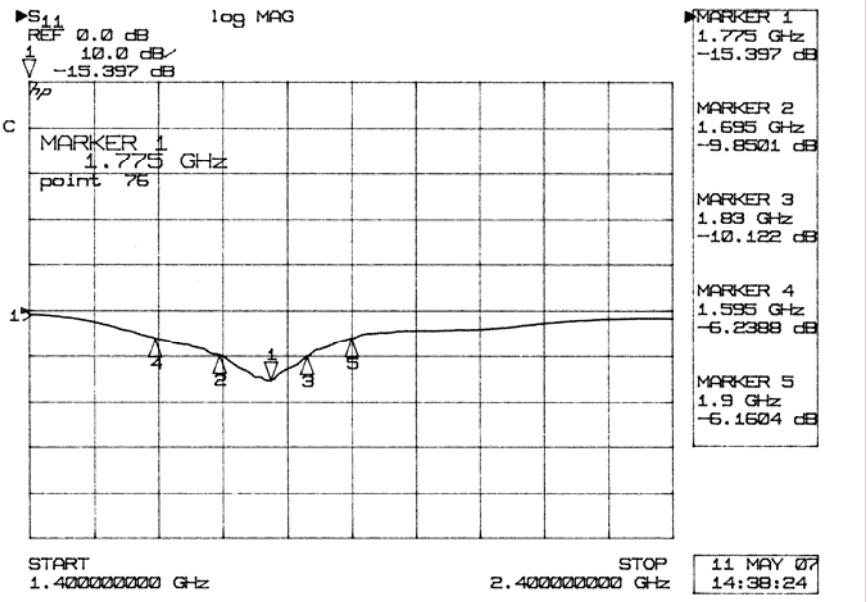

Figure 6.19 Measured return loss of the prototype antenna for GSM1800.

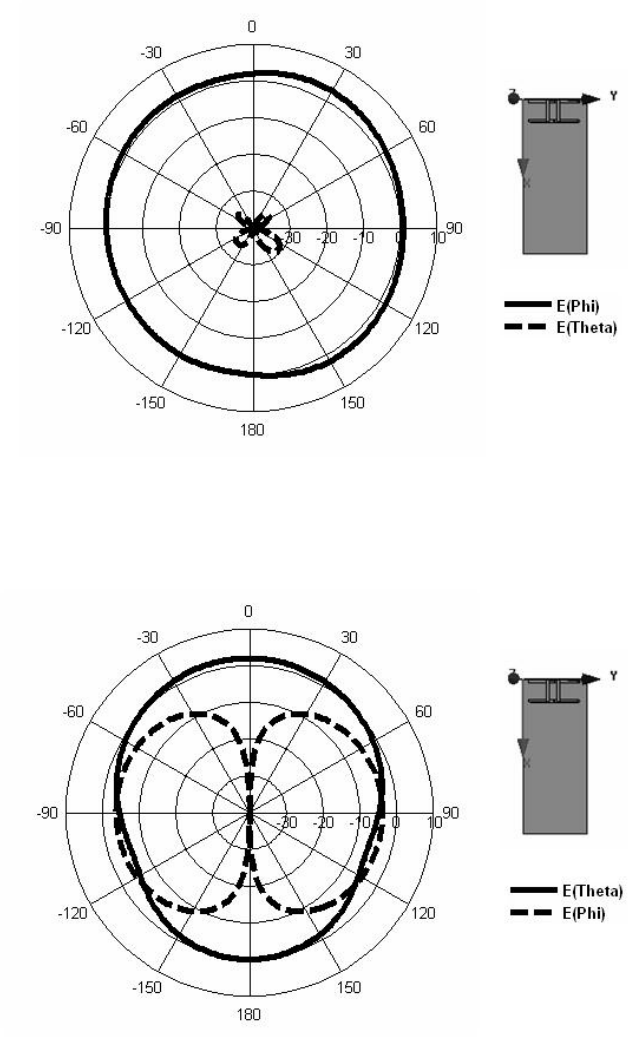

Figure 6.20 Simulated radiation pattern of the GA-optimized FLA at φ =0° (top) and φ =90° (bottom); normalized to 1 Watt input power.

Fig. 6.20 shows the simulated radiation pattern of the GA-optimized FLA using HFSS. As can be seen, the omni-directional pattern was achieved for this dipole antenna. The maximum gain at φ =0° (top) and φ =90° in simulation was found to be 4 dBi and 3 dBi, respectively.

6.5 ADAPTIVE MESHING FOR NUMERICAL ANTENNA DESIGNS USING GA

6.5.1 Motivation on development of adaptive meshing program

In the NEC-2 code, a conducting surface can be modelled using multiple, small flat surface patches similar to the segments used to the model wires. However, although NEC-2 allows the use of surface patches for modelling a conducting surface that is incorporate with the magnetic field integral equation in which a closed surface can be implemented. In addition, another alternative way for open and closed surfaces modelling can be implemented through the use of wire grids [22].

The wire-grid is an effective approach to employ thin wire to achieve the modelling of metallic planar structures using NEC for patch antenna designs. This technique, it requests a careful selection of parameters, such as segment length and the segment radius. A program to adaptively generate equivalent wire-grid structures for patch antennas for electromagnetic simulation of 2D structures has been developed and presented here. The main purpose of this program is to simulate planar microstrip patch antenna designs, using the NEC-2 code in collaboration with a genetic algorithm. In order to demonstrate how this program operates in meshing planar structures, two examples are illustrated, both involving design of circular-polarized coaxially-fed antennas. It has confirmed that the performances of both GA-optimized antennas were excellent and the presented examples show the capability of the proposed program in antenna design using GA.

6.5.2 Principle of adaptive meshing program

This program is written in FORTRAN and added as a subroutine to the GA driver, with the primary objective of simulating planar microstrip patch antenna designs, using the NEC-2 code in cooperation with a genetic algorithm. In addition to microstrip patch designs, the program can support design of any type of planar antenna structure.

To begin with, the intended antenna under optimization needs to be defined by a number of parameters that can comprise the antenna configuration. Subsequently, the antenna geometry is adaptively divided into optimum numbers of trilateral and quadrilateral polygons by the code user. Each polygon can be represented using either three or four nodes and each node is specified by its x, y and z co-ordinates written in the format using the previous defined antenna parameters. Then, the fictitious wire boundaries of these polygons can then be optimally segmented to a pre-set segment length and connected to each other using a designated algorithm. The pre-set segment length (delta) can be carefully stated according to antenna operating frequency. As constrains for accurate modelling using NEC, this figure should not empirically be greater than 0.1λ (λ is wavelength in free space).

Assuming that the surface area of the wire grid should approximate the surface area of the polygons plane being modelled, the segmented element radii can be decided using a relationship that the grid wire radius should equal the segment length divided by 2*PI. Obviously, the more wires in a grid of a certain set of polygon plane dimensions, the smaller the segment length becomes and hence, the smaller the wire radius needs to be. It is notable that segmentations on the adjoining lateral of neighbouring polygons are expected to be overlapped. If a model contains duplicate elements it will not be apparent from the graphical display, but it may significantly corrupt the accuracy of the NEC

analysis. Another algorithm for checking and removing duplicate elements of these overlapped segments is consequently applied.

Adaptive meshing code creates the required wire grid models of antennas and structures that might be used by other antenna modeling programs. Once the antenna model has been created, its wire grid geometry is saved as an ASCII text file that can be read by NEC-2 source code.

In addition, this FORTRAN code has also the capability to calculate the total number of segments in the discretised structure and allowing the user to determine whether the size of the model is still within the limits of maximum number of wires used by NEC (it should be noted that no duplicate segments of the overlapping laterals are counted). Since the NEC-2 source code adopted in this work is restricted to the maximum number of segments of 2000. The presentation of the adaptive meshing to any randomly generated antenna configurations using GA can be viewed using graphic support available from NEC-Win Professional Package for checking.

6.5.3 Design examples on implementation of adaptive meshing

In order to demonstrate how this program operates in meshing planar structures and how it is subsequently applied in antenna designs using GA, two examples are illustrated, both involving design of air-dielectric circular-polarized (CP) coaxially-fed patch antennas. The first antenna design, having two cutoffs at the diagonal corners, is shown in Fig. 6.21. In a first pass, the antenna is subdivided into three quadrilaterals, requiring six parameters to define it (including the height h). Fig. 6.22 demonstrates the adaptive segmentation results as delta was chosen to be 3 mm and was viewed using

NEC-Win Professional package. The other example considered a two square-slot CP antenna (see Fig. 6.23). This design was first adaptively segmented into four trilaterals and three quadrilaterals and requires eight parameters. Its meshing can be seen Fig. 6.24, where delta was also set to be 3 mm. The automatically-generated meshes are generally of a good shape (high area-to-perimeter ratio), although there are a few exceptions.

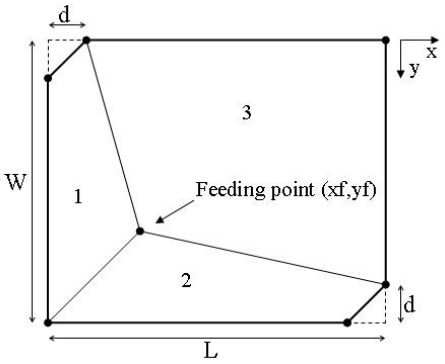

Figure 6.21. Geometry applied for adaptive meshing using GA.

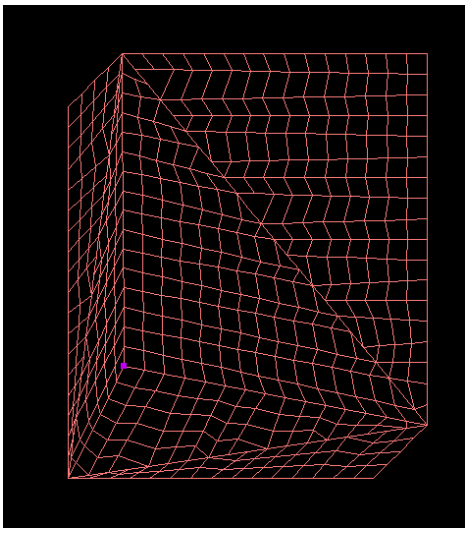

Figure 6.22 Mesh used for Fig. 6.21 using GA (the dot indicates the optimal feeding point).

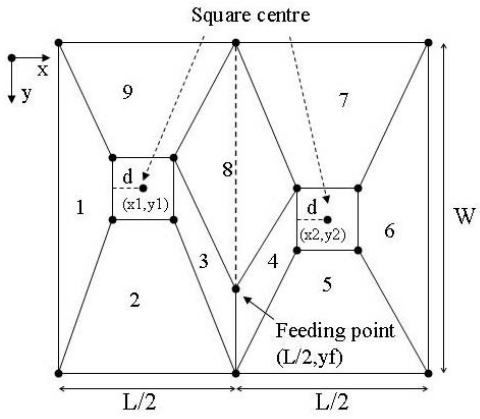

Figure 6.23 Two square slot CP antenna geometry applied for adaptive meshing using GA.

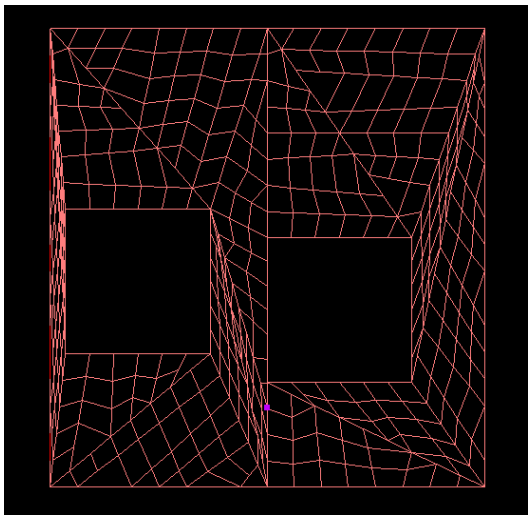

Figure 6.24 Mesh used for Fig. 6.23 using GA (the dot indicates the optimal feeding point).

For this optimisation, real-valued GA chromosomes were used and antenna parameters of VSWR and AR are optimized at a single frequency of 2.44 GHz (f_o). The antenna AR was calculated at f_o with θ= 0° and ϕ=0°. The antenna performance of each antenna was computed using NEC-2 source code and its input impedance (Z_{in}) and AR were evaluated for desired fitness using the same cost function presented for QHA antenna design.

Configurations for both optimal circular polarized microstrip antennas, with excellent VSWR and AR, were found within the maximum generations. The attained optimal antenna geometries for each of the antennas in wire-grid meshing are presented (see Figs. 6.22 and 6.24). Tables 6.4 and 6.5 present the GA input parameters, their constraints and the optimal values for each specified parameter of the design geometry. It is notable that the two weighting coefficients were found to be 0.4 and 0.8 correspondingly for both designs after a few attempts. Within the maximum generation, the values of maximum fitness function for the two designs reached to be about 1.08 and 1.03.

Table 6.4 Summary of GA input parameters, antenna variables and best solutions.

GA parameters	Air-dielectric CP antenna with two corners chopped	
	Parameters (m)	Optimal (m)
	Antenna length (L) (0.03-0.07)	0.05185
No. of population size = 4,	Antenna width (W) (0.03-0.07)	0.06127
No. of parameters = 6,	Truncated length (d) (0.002-0.01)	0.0077
Probability of mutation =0.02,	Antenna height (h) (0.003-0.01)	0.00608
Maximum generation =100,	Feeding position at x-axis (xf) (0.0-0.024)	0.00806
No. of possibilities=32768,	Feeding position at y-axis (yf) (0.0-0.024)	0.01613

Table 6.5 Summary of GA input parameters, antenna variables and best solutions.

GA parameters	Air-dielectric CP patch antenna with two square slots	
	Parameters (m)	Optimal (m)
	Antenna length (L) (0.04-0.07)	0.04667
No. of population size = 4,	Antenna width (W) (0.04-0.07)	0.04931
No. of parameters = 9,	Antenna height (h) (0.004-0.01)	0.00830
Probability of mutation =0.02,	Slot centre position at x-axis (x1) (0.008-0.015)	0.00940
Maximum generation =200,	Slot centre position at y-axis (y1) (0.01-0.034)	0.02210
No. of possibilities=32768,	Slot centre position at x-axis (x2) (0.028-0.035)	0.03112
	Slot centre position at y-axis (y2) (0.01-0.034)	0.01896
	Distance from slot centre to side (d) (0.005-0.008)	0.00779
	Feeding position at y-axis (yf) (0.0065-0.02)	0.00846

For validation, prototypes (see Figs. 6.25 and 6.26) of the GA-optimised proposed antennas for CP were fabricated and tested. The copper of thickness 0.5 mm was used for fabrication for both the patch antenna and the ground plane. The ground plane size was chosen to be 150 x 150 mm. Return loss of the GA-optimized antenna structure for each design achieved by the algorithm was validated and the results were compared using measurement data with Ansoft Designer [23], which is based on MoM. Figs. 6.27 and 6.28 present the resulting return loss of the GA-optimized antennas for comparison. As can be seen, performance of the optimal antennas is excellent and presented results are in close agreement with the GA expectation.

Finally, the far field properties of the GA-optimized patch antennas for CP were analyzed using Ansoft Designer simulator. The resulting air-dielectric circularly polarized microstrip antennas are with excellent axial ratio ($\leq$ 3 dB) and bandwidth at intended design frequency. Regarding the polarization type, it was found that both antennas are left-hand circular polarized (LHCP). The right-hand circular polarization (RHCP) level for both antennas is at least 20 dB below the LHCP level in the broadside direction.

Figure 6.25 Photograph of a fabricated prototype antenna with two cutoffs at corner for CP.

Figure 6.26 Photograph of a fabricated prototype antenna with two slots for CP.

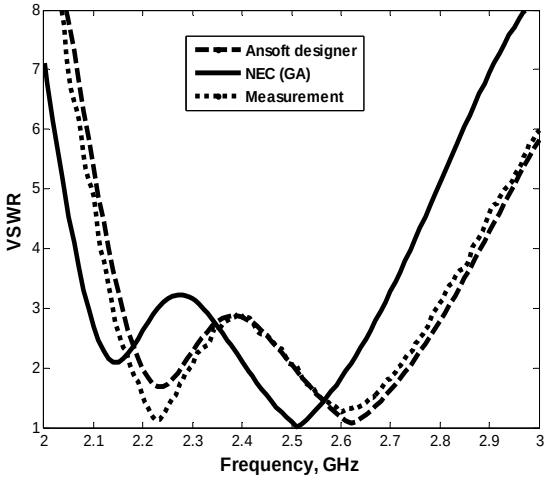

Figure 6.27 Comparison of simulated and measured return loss of GA-optimized antenna with two-corner cutoffs.

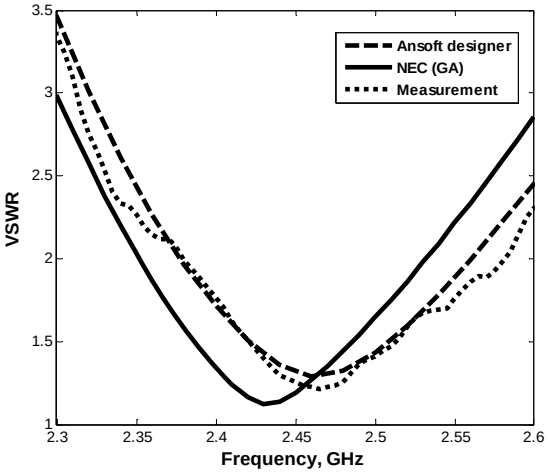

Figure 6.28 Comparison of simulated and measured return loss of GA-optimized antenna with a square slot.

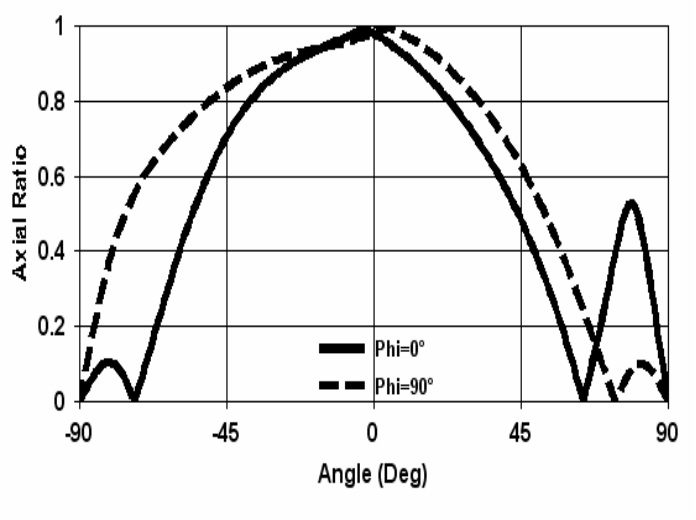

Figure 6.29 Comparison of AR results for CP patch antenna with two-corner cutoffs at 2.4 GHz in θ plane for φ =0° and φ =90°.

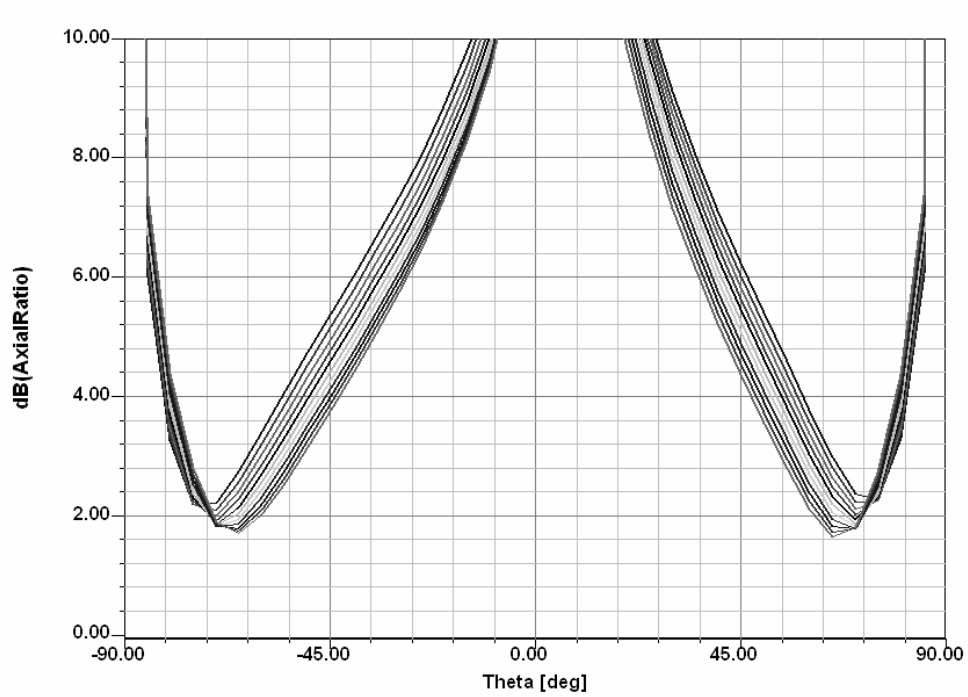

Figure 6.30 Comparison of AR results for CP patch antenna with two slots at 2.4 GHz in θ plane for φ =0° and φ =90°.

The computed AR and power gain, for the GA-optimized QHA antennas at 2.4 GHz, are shown in Figs. 6.29 and 6.30. As can be seen, excellent AR over theta plane for both optimal antennas of circular polarization characteristics was observed. It is notable that Fig. 6. 30 indicates the GA-optimzed antenna is a conical beam CP antenna.

6.6 DESIGN OF HARMONIC SUPPRESSION ANTENNAS WITH ADAPTIVE MESHING USING GA

6.6.1 Design objectives for harmonic suppression antennas

In the scenario of designing the active integrated antenna, the microstrip patch antenna not only acts as a radiator, but also provides some circuit functionalities such as matching circuit and band pass filter as in active amplifier-type antenna. In this case, without proper designs to suppress the harmonic radiation from the radiator, some possible unwanted harmonic power can be radiated, which could cause detrimental electromagnetic interference (EMI) to the system [24]. In order to overcome this problem, several techniques have been proposed and demonstrated to control such harmonics for patch antennas, for example: using shorting pins, slots, Photonic Bandgap (PBG) structures, or matching stubs on the antenna feeding line [24-37]. Above these proposed techniques, one interesting fact can be found is that most of the modified patch antennas for harmonic suppression were achieved based on a specific reference antenna. It implies that the proposed techniques for successfully rejecting harmonic radiation has certain constrains applied on them, such as the type of feeding used (microstrip line or slot feed) for the patch. In [34], a microstrip-line fed slot antenna was developed for harmonic suppression without using a reference antenna and this was achieved with a rather complex geometry for 5 GHz operation. Assuming the operating frequency was changed, and then the whole antenna structure has to be redesigned, which is believed to be long and complicate in process. Therefore, there is a motivation to develop a novel technique to design harmonic suppression microstrip patch antennas for active integrated applications. It has no much constrains on feeding types or antenna geometries. Moreover, it has to be easily manufactured and redesigned if there is a

request on the antenna design specification for different applications (i.e. different operating frequency). In this study, a technique in designing microstrip patch antennas for harmonic suppression is presented and implemented using a genetic algorithm.

An antenna that presenting a good impedance matching at the fundamental design frequency (f_o) and an ideally maximum reflection at harmonic frequencies (mainly considering the first two harmonics ($2f_o$ and $3f_o$)), is said to be a harmonic suppression antenna (HSA). Strictly speaking, the response of the HSA in terms of antenna return loss (S_{11}) is mostly like a band pass filter having a perfect rejection outside the interested frequency bands. It has to be noted that in some HSA designs [26, 30 and 37], the proposed antenna can still have resonances at frequencies other than the targeted frequencies (i.e. f_o, $2f_o$ and $3f_o$); but they are still claimed as antennas for harmonic suppression as long as the designs present good termination at the intended frequencies.

In addition, another constrain to the HSA is that in theory, the input impedance of any HSA design has to be purely reactive at the harmonic frequencies [3]. This is because originally HSA was developed for harmonic termination in order to achieve a Class F operation for the amplifying-type active antennas [3], as we demonstrated in Chapter 3. In this way, antenna will not radiate any power at the harmonic frequencies and the unwanted power will be reflected back to the active device.

The design objectives of antennas for harmonic suppression are necessary to satisfy the two aspects in terms of return loss and input impedance. In the following, four designs of coaxially-fed air-dielectric microstrip patch antenna for rejecting harmonics using a genetic algorithm were presented, including patch antenna with a fully shorted wall, or

partially shorted wall, with a folded shorting wall and with a folded patch. They are all designed to operate at 2.4 GHz. The presentation of the antenna geometry and adaptive meshing for the optimal antenna configuration using GA for each one of the designs were presented. For the first two designs, prototype antennas of optimal antenna configurations using GA for each one of the designs were fabricated and tested. The return loss was validated and the results were compared using measurement. For the other two designs, however, the return loss was validated and the results were compared using two different simulation packages.

6.6.2 Microstrip patch antenna with a fully shorted wall

A simple coaxial-fed air-dielectric patch antenna with a fully shorted wall, operating at 2.4 GHz, was firstly attempted for this study as a simple technique to provide the acceptable harmonic rejection [2]. A FORTRAN adaptive meshing subroutine, used to adaptively generate equivalent wire-grid structures to support the structure design of this antenna was added to the GA program. This subroutine provides the suitable link of the GA cost function to the NEC-2.

The proposed antenna design is shown in Figs. 6.31 to 6.34. For our design proposal the antenna is subdivided into four trilaterals and two quadrilaterals (including the conducting shorted wall). This proposal was requiring six parameters (including the patch height h) to be defined. Fig. 6.32 and 6.34 demonstrates the top view and 3D of the adaptive wire grid segmentation results.

Table 6.6 presents the GA input parameters in which the possible range of parameters magnitudes were shown. For this optimisation, real-valued GA chromosomes were used.

In this work, the Fundamental, first and second harmonic frequencies were considered inside the GA cost function. The randomly generated antenna configurations were evaluated for maximum fitness using a cost function is given as follows:

$$F = w_1 \frac{1}{VSWR(f_o)} + \sum_{i=2}^{n} w_i \left|\Gamma(if_o)\right| \qquad 6.6$$

Where F is the fitness of the cost function; W_1, W_2 and W_3 are the weight coefficients of the cost function and were optimally found to be 0.6, 0.4 and 0.4 after a few attempts. The geometry configuration of optimal antenna was found within the maximum generations and presented in Fig. 6.34, where the white-grid surface represents the infinite ground plane. The computation time consumed for each of the erratically generated antenna samples varied between 60 to70 seconds, according to the different combination of length, width and height of the patch antenna selected for comprising the antenna configuration. This was achieved by using a PC: 2.8 Pentium IV of 1 GB RAM.

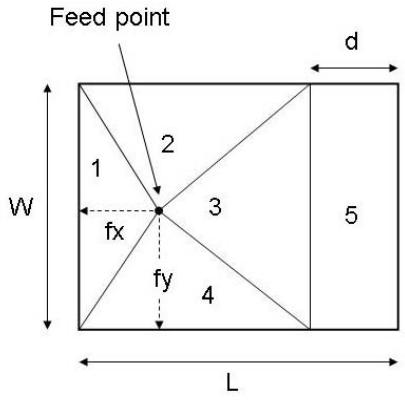

Figure 6.31. Top view subdivision of the antenna geometry used for adaptive meshing using GA.

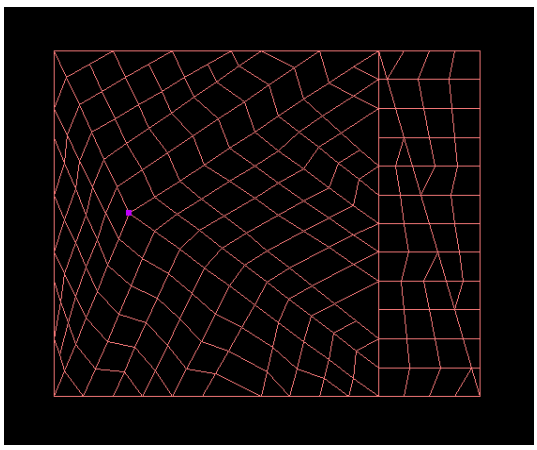

Figure 6.32 Top view of resulted wire mesh used for Fig. 6.31.

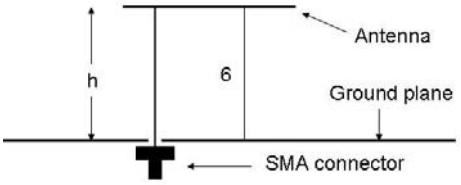

Figure 6.33. Side view of the antenna geometry of Fig. 6.31.

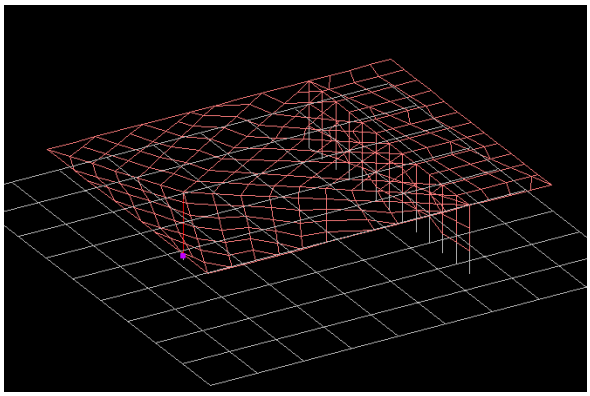

Figure 6.34 3D view of the resulted wire mesh using GA.

Table 6.6 Summary of GA input parameters, antenna variables and best solutions.

GA parameters	Air-dielectric patch antenna with a shorting wall	
	Parameters (m)	Optimal (m)
	Antenna length (L) (0.03-0.06)	0.04093
No. of population size = 4,	Antenna width (W) (0.02-0.06)	0.03305
No. of parameters = 6,	Shorting wall position (d) (0.002-0.03)	0.00972
Probability of mutation =0.02,	Antenna height (h) (0.003-0.01)	0.0079
Maximum generation =200,	Feeding point at x-axis (fx) (0.004-0.02)	0.00723
No. of possibilities=32768,	Feeding point at y-axis (fy) (0.004-0.02)	0.01752

For validation, a prototype of the GA-optimised harmonic suppression antenna with a fully shorted wall (see Fig. 6.35) was subsequently designed and tested in the telecommunication research laboratory using Network Analyzer HP 8510C (see Fig. 6.36). A copper with thickness of 0.5 mm was used for the patch antenna, the shorting wall and the ground plane. The ground plane size was 140 mm x 140 mm and this relatively large size for the purpose of eliminating effect of the finite ground plane. The return loss was validated and measured results were compared to the one computed using a commercial electromagnetic simulator HFSS, as shown in Fig. 6.37. As can be seen, the results the rejection of 2^{nd} and 3^{rd} harmonics were quite encouraging and no other resonance or ripples were found at the harmonic frequency bands. It has to be

noted that the simulated result on return loss using NEC-2 is not presented here, however, thus to evaluate GA-optimal antenna configuration HFSS simulator was used in which it has shown the capability in accurately predicting the antenna performance by the author's previous research work [38].

Figure 6.38 shows the performance of the measured return loss of the proposed harmonic suppression antenna at the fundamental and first two harmonic frequencies. The prototype antenna is resonant at 2.47 GHz and presents a quite wide bandwidth around 500 MHz as observed. The reflection coefficient level at the first and second harmonic frequencies was found to be 1.7125 dB and 2.4473 dB, respectively, and these results are quite acceptable, as compared with harmonic suppression antennas published in the open literature [26]. It has to be noted that the measured resonance frequency of the prototype antenna has good agreement with the predicted one obtained using HFSS package. Taking the manufacture error into the account and the errors due to the the adaptively meshing wire-grid structures the proposed antenna design for harmonic suppression presents a fairly good accuracy and minimum computation time to evaluate the antenna performance using NEC-2 source code.

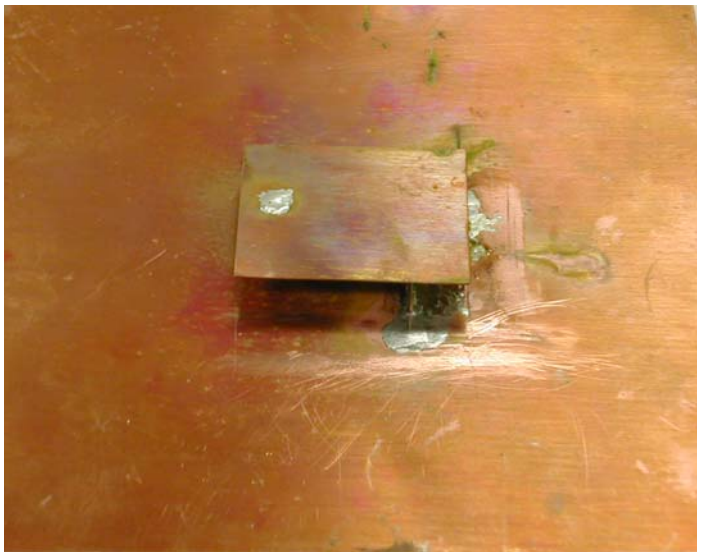

Figure 6.35 Photograph of the fabricated harmonic rejection antenna with a shorting wall.

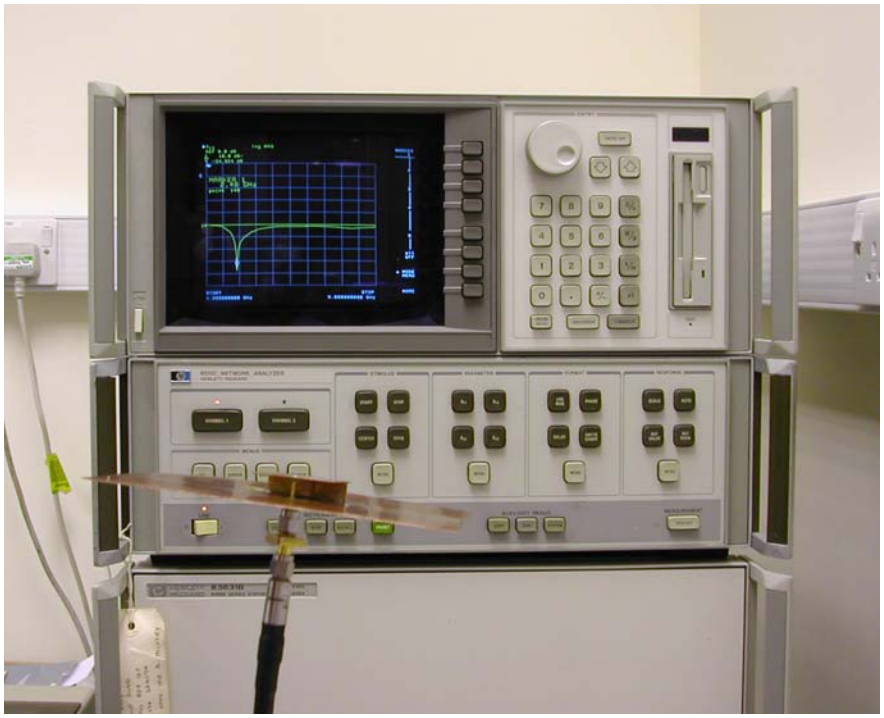

Figure 6.36 Photograph of testing bench for measuring antenna return loss.

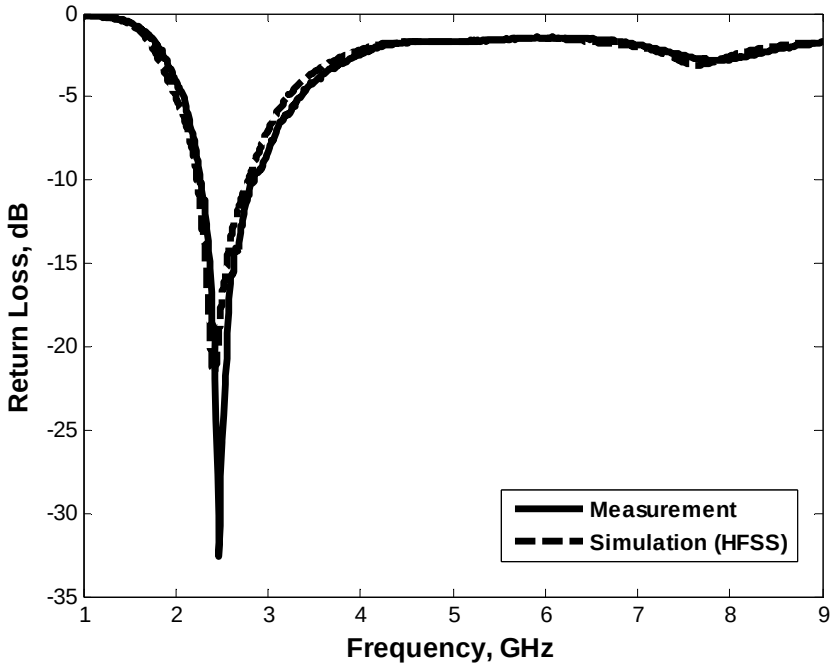

Figure 6.37 Comparison of the measured and simulated return loss of the patch antenna with a shorting wall.

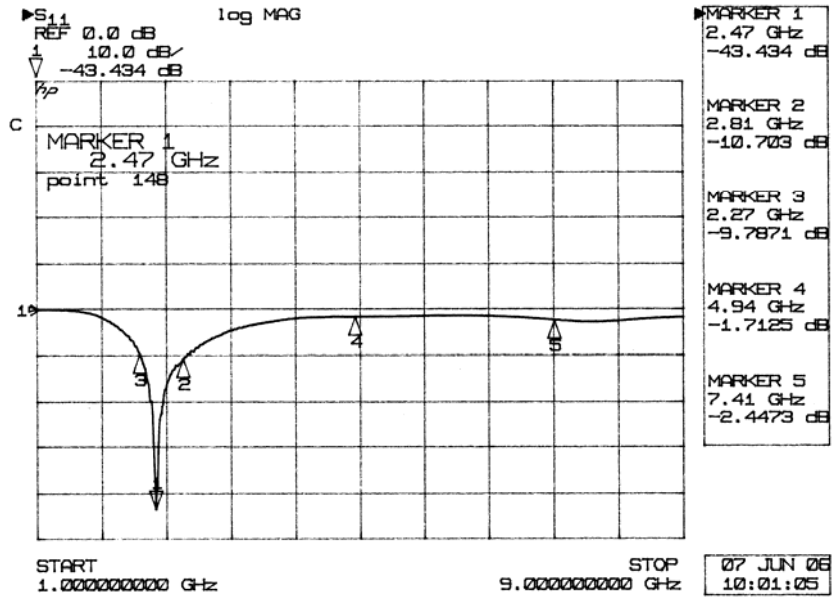

Figure 6.38 Performance of the measured return loss of the patch antenna with a shorting wall at the fundamental and first two harmonic frequencies.

In addition, input impedance of the prototype antenna was also measured over a wide frequency band, as shown in Fig. 6.39. A different-scaled input impedance plot is also

presented in Fig. 6.40, in order to precisely observe the variations of the input impedance over the frequencies of interest. As can be shown in Fig. 6.40, the real part of the input impedance of the proposed antenna is almost constant (less than 10 Ω) at harmonic frequency bands. This is very promising characteristic of the designed procedure of such harmonic suppression. The antenna can also achieve the harmonics rejection from the nonlinear active devices, even when the operating frequency is slightly varied. This is because the proposed antenna provides the required reactive termination around the harmonic frequencies. The measured input impedance of the harmonic rejection antenna with a fully shorted wall for fundamental frequency and its first two harmonics is summarised in Table 6.7. It shows that almost a perfect matching to 50 Ω was attained at fundamental frequency and fairly small resistive impedance at harmonics was found. This clearly shows the design objectives were met.

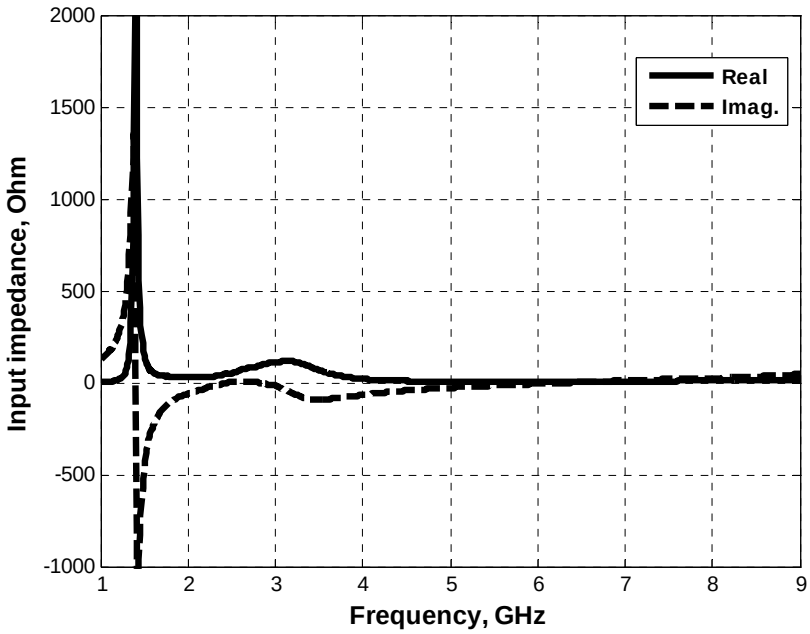

Figure 6.39 The overall measured input impedance of the patch antenna with a fully shorted wall.

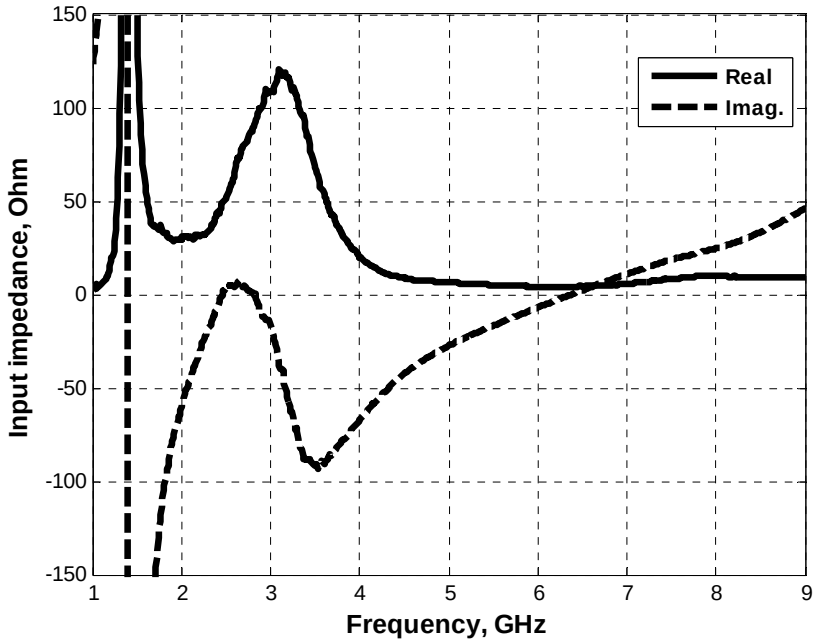

Figure 6.40 Measured input impedance of the harmonic suppression antenna (expanded scale of Fig. 6.39).

Table 6.7 Performance of antenna input impedance of the harmonic rejection antenna with a fully shorted wall at the fundamental and first two harmonics.

Frequency (GHz)	Antenna input impedance (Ω)	
	Real	Imaginary
f_o : 2.47	48.92	-0.5879
$2f_o$: 4.94	6.4834	-28.917
$3f_o$: 7.41	7.9395	17.64

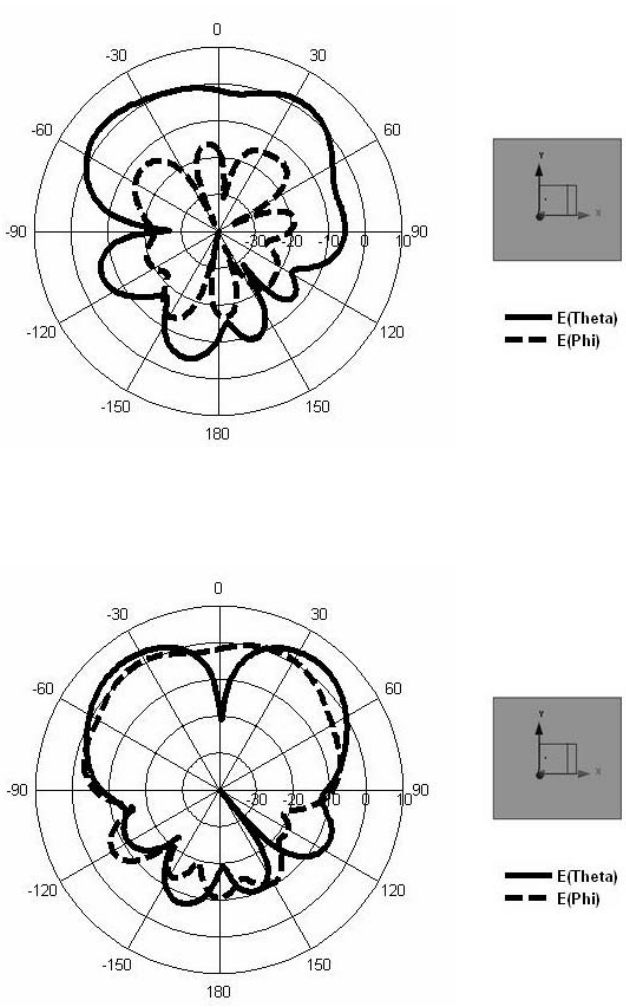

Figure 6.41 Simulated radiation pattern of the GA-optimized HSA with fully shorted wall using HFSS at φ =0° (top) and φ =90° (bottom); normalized to 1 Watt input power.

Fig. 6.41 shows the simulated radiation pattern of the GA-optimized HSA with fully shorted wall using HFSS at fundamental design frequency. The maximum gain at φ =0° (top) and φ =90° in simulation was found to be 3 dBi and 4 dBi, respectively.

6.6.3 Microstrip patch antenna with a partially shorted wall

Following a successfully development and demonstration of harmonic suppression antenna design with a fully shorted wall in the previous section, a follow-up work on investigating the possibility to control the harmonics with the variation of the width of the shorting wall is presented in this section. The design was continued to operate at 2.4

GHz. The antenna geometry for harmonic suppression, having a partially shorted wall, is shown in Figs. 6.42 and 6.44. Initially, the antenna is subdivided into six trilaterals and two quadrilaterals (including the partially shorted wall), this is requiring seven parameters to predefine including the width of the shorting wall. Fig. 6.43 demonstrates the top view of adaptive segmentation results.

Table 6.8 presents the GA input parameters for each required variable. Again real-valued GA chromosomes were used. The frequency band that covers fundamental, first and second harmonic frequencies were considered. The randomly generated antenna configurations were evaluated for maximum fitness using the same cost function stated in the previous section. The weighting coefficients (W_1, W_2 and W_3) for the cost function were still optimally found to be 0.6, 0.4 and 0.4. The geometry configuration of optimal antenna was found within the maximum generations as shown in Fig. 6.45, where the white-grid surface represents the infinite ground plane.

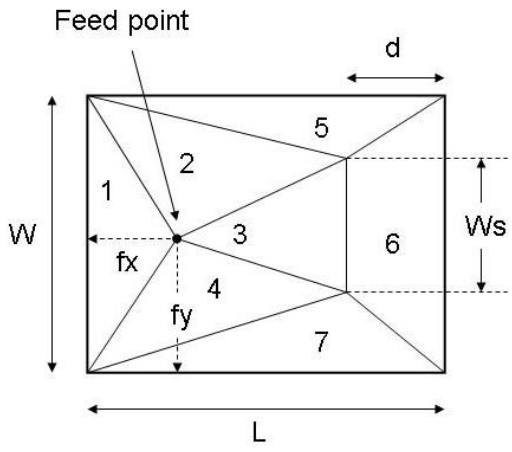

Figure 6.42 Top view of the geometry applied for adaptive meshing using GA.

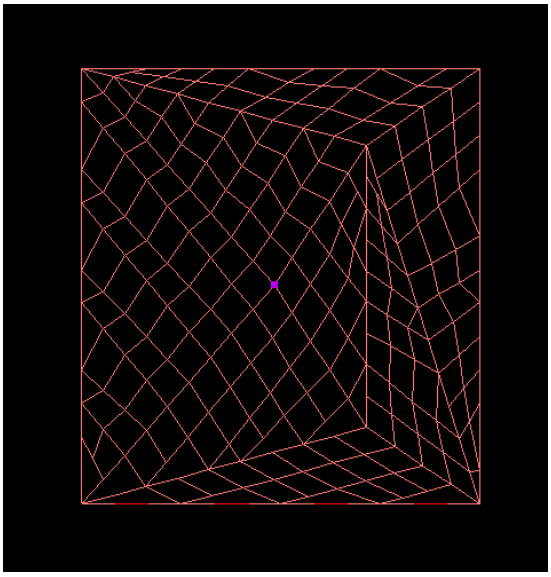

Figure 6.43 2D Mesh used for Fig. 6.42 using GA.

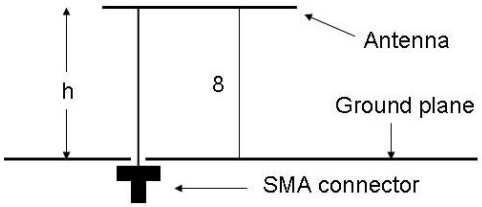

Figure 6.44. Side view of the antenna geometry of Fig. 6.42.

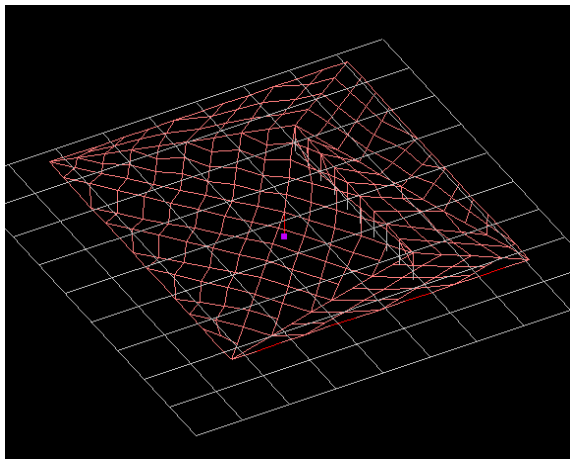

Figure 6.45 3D Mesh used for Fig. 6.44 using GA.

Table 6.8 Summary of GA input parameters, antenna variables and best solutions.

GA parameters	Patch antenna design with a partially shorted wall	
	Parameters (m)	Optimal (m)
	Antenna length (L) (0.03-0.05)	0.03486
No. of population size = 4,	Antenna width (W) (0.03-0.05)	0.03820
No. of parameters = 7,	Shorting wall position (d) (0.005-0.015)	0.00986
Probability of mutation =0.02,	Antenna height (h) (0.003-0.01)	0.00336
Maximum generation =200,	Variable shorting wall width (Ws) (0.001-0.03)	0.02474
No. of possibilities=32768,	Feeding point at x-axis (fx) (0.004-0.02)	0.01685
	Feeding point at y-axis (fy) (0.004-0.025)	0.01923

For validation, a prototype of the GA-optimised harmonic suppression antenna with a partially shorted wall was shown in Fig. 6.46. A copper sheet of thickness of 0.5 mm was used for fabrication of the patch antenna, the shorting wall and the ground plane. The ground plane size is 140 x 140 mm. The return loss was validated and measured results were compared using a commercial electromagnetic simulator HFSS, as shown in Fig. 6.47. As can be seen, the rejection levels of 2^{nd} and 3^{rd} harmonics were quite encouraging. Figure 6.48 shows the performance of the measured return loss of the proposed harmonic suppression antenna at the fundamental and first two harmonic frequencies. It can be easily noticed that the rejection level of the antenna at the second harmonic is superior to the previous design and is almost the same at the third harmonic.

In addition, other resonance was found at the third harmonic frequency bands. The prototype antenna is resonant at 2.48 GHz and presents a less wide bandwidth (around 150 MHz), compared to the first design. This is mainly because the height of this antenna is much lower (about 3.36 mm) than the first design (7.9 mm), in which the antenna height has the most important influence on bandwidth enhancement of the microstrip patch antenna. In addition the measured results were in good agreement to that predicted one obtained using HFSS package.

The measured input impedance over the frequency band of 1 GHz to 9 GHz is shown in Fig. 6.49. Extended scale plot of Fig. 6.49 is presented in Fig. 6.50. Again it can be seen that the real part of the input impedance of the proposed antenna is close to zero for a wide frequency band around the second and third harmonic frequencies. This is also indicating the influence of the reactive effects to harmonic termination at harmonic frequencies are realised. A summarised detail of the input impedance for fundamental and two first harmonics is presented in Table 6.7. Similar to previous section it is a fairly good matching to 50 Ω was attained at fundamental frequency and relative small resistive impedances at harmonics were observed.

Figure 6.46 Prototype harmonic rejection antenna with partially shorted, side view (left) and top view (right).

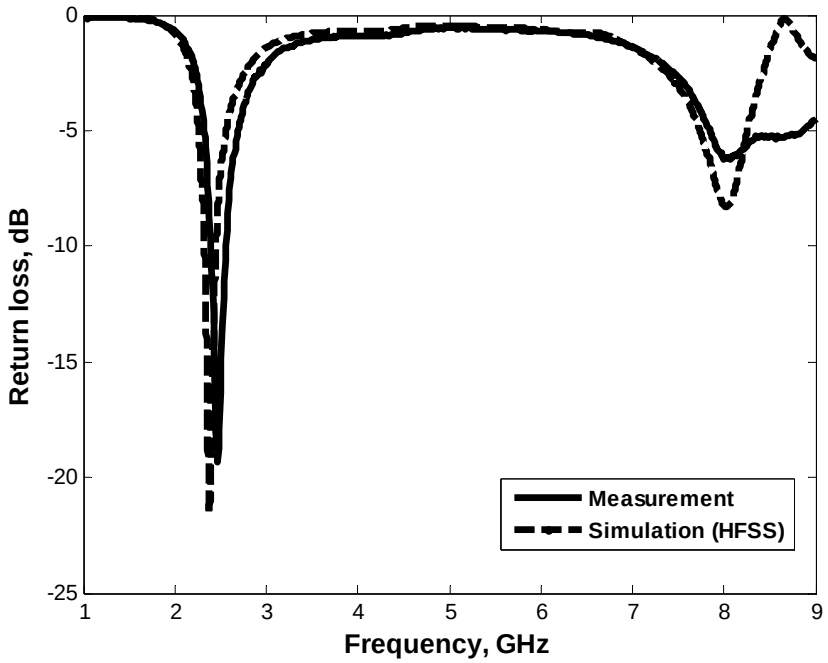

Figure 6.47 Comparison of the measured and simulated return loss of the patch antenna with partially shorted wall.

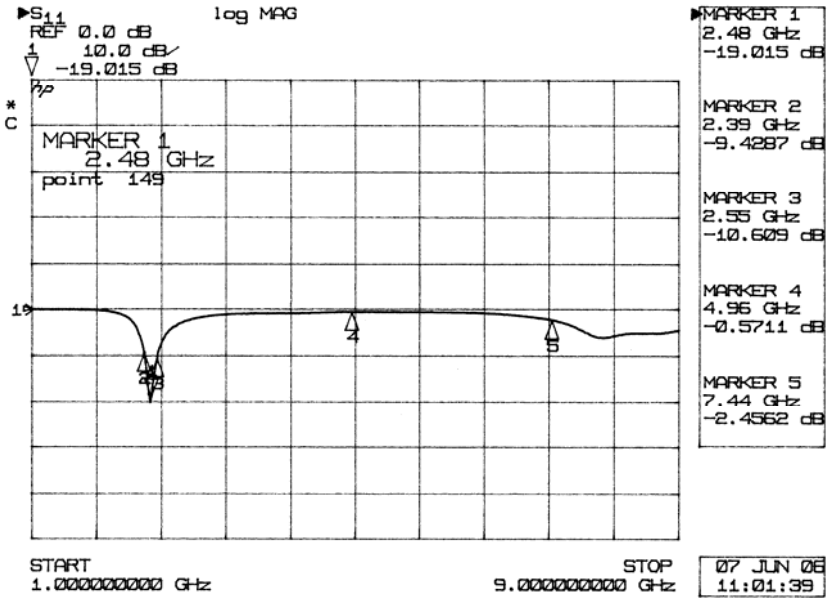

Figure 6.48 The measured return of partially shorted wall patch antenna at the fundamental and first two harmonic frequencies.

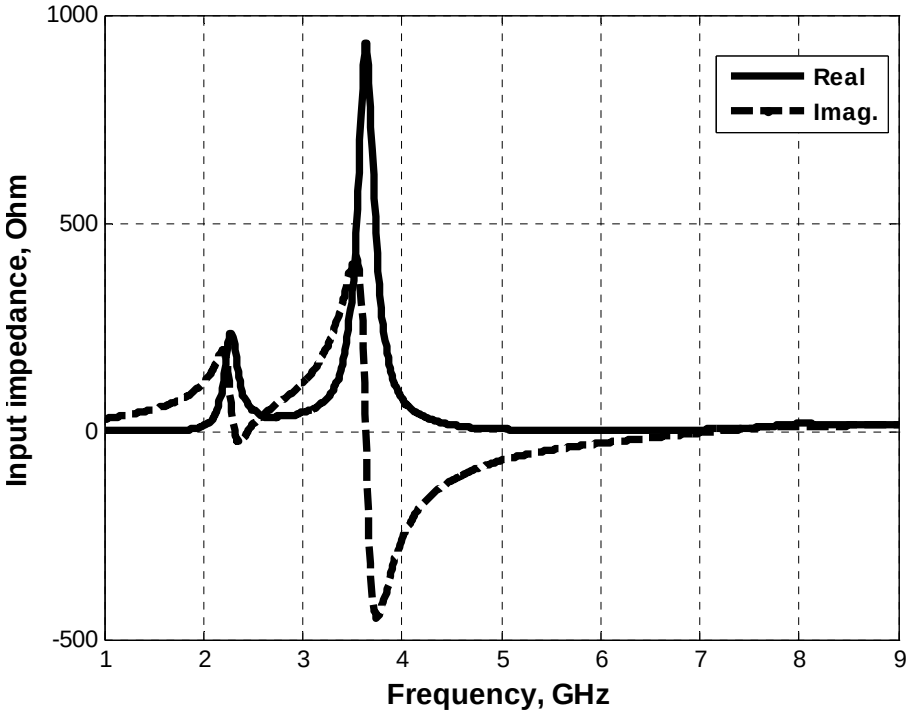

Figure 6.49 The overall measured input impedance of the patch antenna with partially shorted wall.

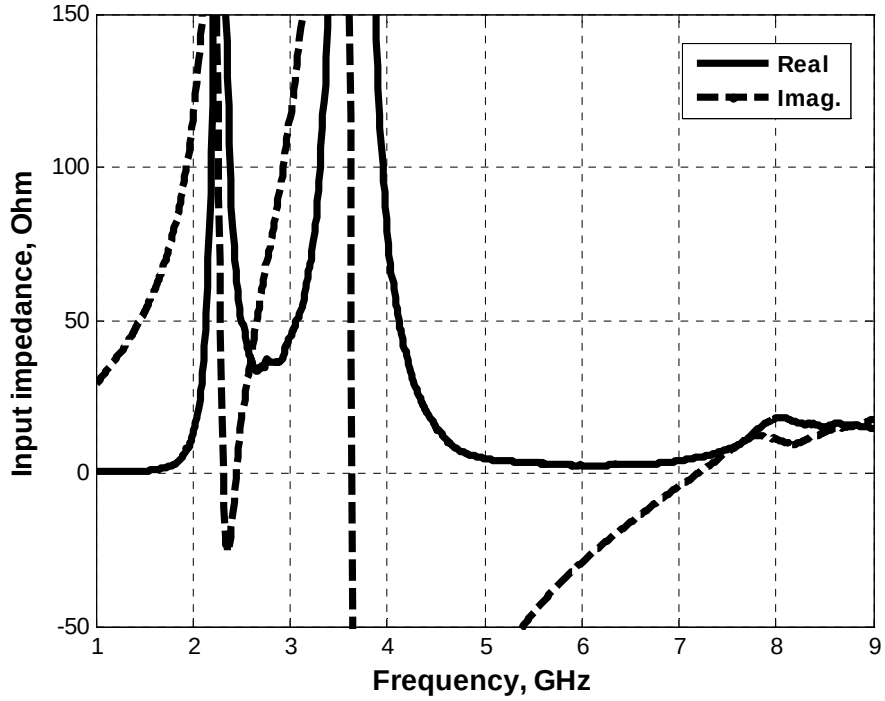

Figure 6.50 The measured input impedance of the patch antenna with partially shorted wall (expanded scale of Fig. 6.43).

Table 6.9 Performance of measured harmonic rejection antenna with partially shorted wall at the fundamental and first two harmonics.

Frequency (GHz)	Antenna input impedance (Ω)	
	Real	Imaginary
f_o : 2.48	53.852	7.8281
$2f_o$: 4.96	5.0547	-73.672
$3f_o$: 7.44	7.002	5.5452

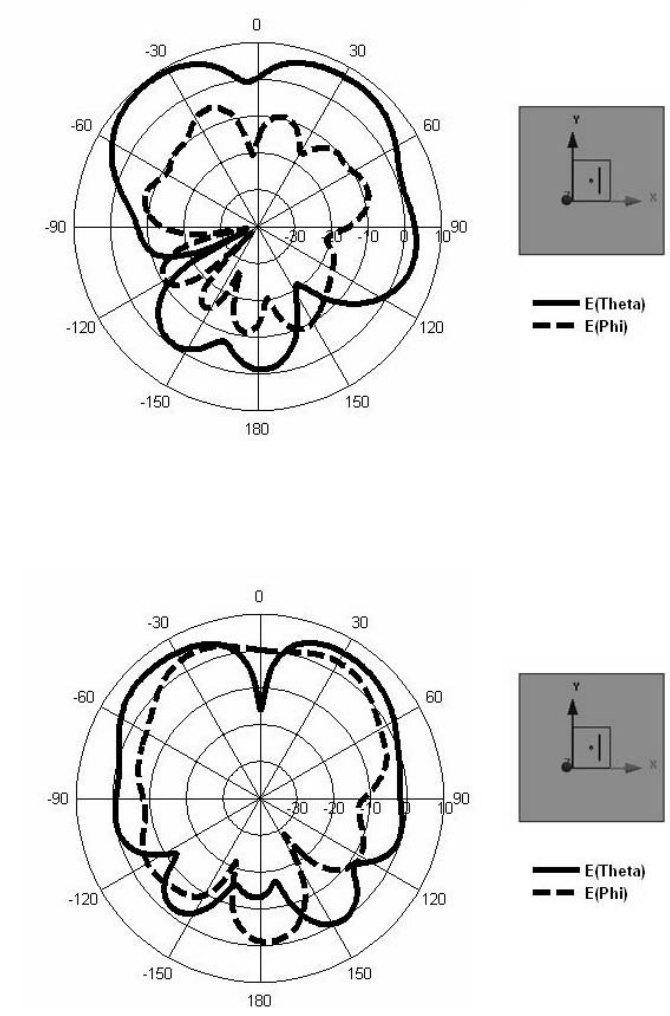

Figure 6.51 Simulated radiation pattern of the GA-optimized HSA with partially shorted wall using HFSS at φ =0° (top) and φ =90° (bottom); normalized to 1 Watt input power.

Fig. 6.51 shows the simulated radiation pattern of the GA-optimized HSA with partially shorted wall using HFSS at fundamental design frequency. The maximum gain at φ =0° (top) and φ =90° in simulation was found to be 10 dBi and 6 dBi, respectively.

6.6.4 Two New Microstrip Patch Antenna for Harmonic Suppression

In the following section, the technique in designing microstrip patch antennas for harmonic suppression using GA is extended to develop another two harmonic suppression antennas, including the patch antenna with folded shorting wall and the other with a folded patch. For validation, the return loss of the two proposed antennas was compared using the commercial EM packages.

6.6.4.1 Microstrip patch antenna with folded shorting wall

The antenna geometry for harmonic suppression, having a folded shorting wall, is shown in Figs. 6.52 to 6.55. The design frequency is 2.4 GHz. The antenna is subdivided into four trilaterals and four quadrilaterals (including the folded shorting wall), requiring eight parameters to be firstly defined. The GA input parameters regarding the above antenna structure surface subdivision is presented in Table 6.10. The same procedure used in the previous example is applied here. The three weighting coefficients (i.e. W_1, W_2 and W_3) used for cost function for optimal operation found to be 0.4, 0.4 and 0.6 respectively. The optimal geometry configuration is presented in Fig. 6.53.

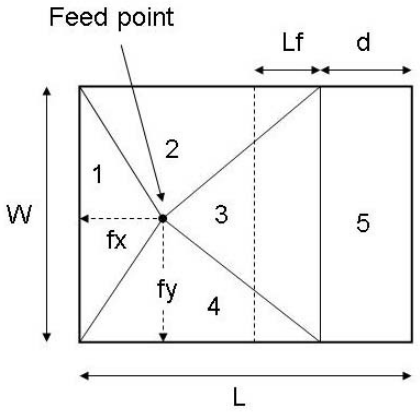

Figure 6.52 Top view of the antenna geometry applied for adaptive meshing using GA in section 6.6.4.1.

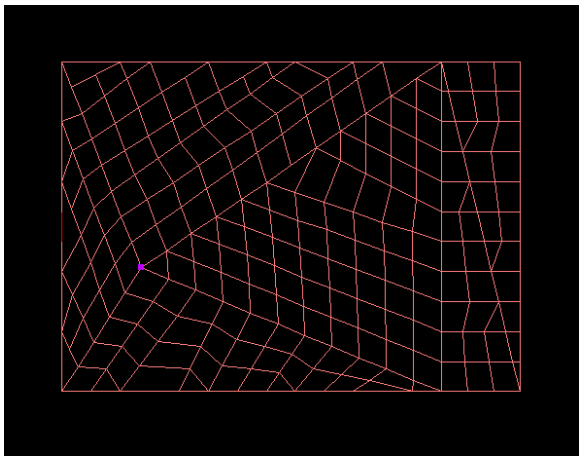

Figure 6.53 2D Mesh used for Fig. 6.52 using GA.

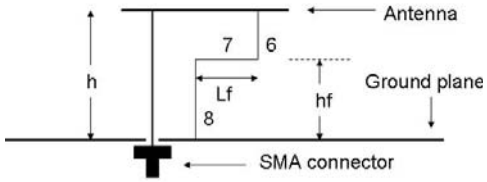

Figure 6.54. Side view of the antenna geometry shown in Fig. 6.52.

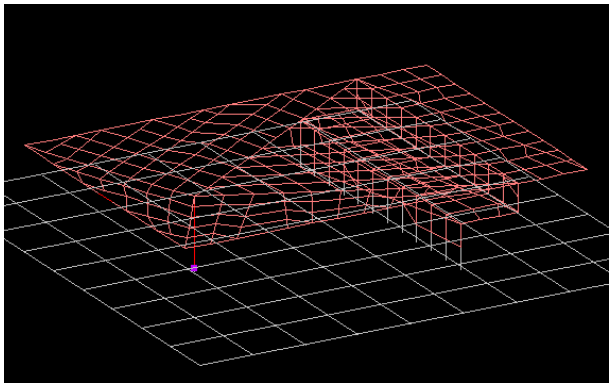

Figure 6.55 3D Mesh used for Fig. 6.54 using GA.

Table 6.10 Summary of GA input parameters, antenna variables and best solutions.

GA parameters	Air-dielectric patch antenna with folded shorting wall	
	Parameters (m)	Optimal (m)
	Antenna length (L) (0.03-0.06)	0.04367
No. of population size = 4,	Antenna width (W) (0.02-0.06)	0.03141
No. of parameters = 8,	Shorting wall position (d) (0.005-0.02)	0.00750
Probability of mutation =0.02,	Antenna height (h) (0.004-0.01)	0.00771
Maximum generation =100,	Folded shorting wall length (Lf) (0.005-0.015)	0.00624
No. of possibilities=32768,	Folded shorting wall height (hf) (0.003-0.005)	0.00466
	Feeding point at x-axis (fx) (0.004-0.02)	0.00753
	Feeding point at y-axis (fy) (0.004-0.025)	0.01174

6.6.4.2 Microstrip patch antenna with a folded patch

A novel coaxial-fed air-dielectric microstrip patch antenna for suppressing harmonics with a folded patch, resonating at the same frequency is studied. The antenna geometry for harmonic suppression, having a folded patch extended underneath the main patch, is shown in Figs. 6.56 to 6.57. The antenna is subdivided into four trilaterals and three quadrilaterals (including the folded patch), thus it requires eight parameters to be defined. Table 6.11 presents the GA input parameters for each variable used. Again the weighting coefficients W1, W2 and W3 were found to be 0.4, 0.4 and 0.6 respectively.

6.6.4.3 Results and discussions

The results were validated using HFSS and Microwave Studio (MWS) [39] that is based on Finite integration technique (FIT). Figs. 6.60 and 6.61 present the computed return loss for microstrip patch with shorted folded wall and a folded patch respectively. The results were quite encouraging especially on the required harmonic suppression. The results of both packages for each antenna were agreed very well. However, the first and second harmonic levels for shorted folded wall were found around 2.8 dB and 2.4 dB, where as for the case of folded patch for both harmonics were around 2 dB. It can be noticed that a small ripples were observed at frequencies above the third harmonic frequency band, which might be caused by the computation error from the simulators.

The resonant frequency of the GA-optimised antenna with shorted folded wall configuration was found at 2.34 GHz and 2.38 GHz from HFSS and CST respectively, which is quite close to the expected fundamental design frequency. In the case of folded patch configuration was found 2.48 from both packages. It should be noted that the operating bandwidth were around 500 MHz for both antennas under considerations.

This bandwidth totally supports the design procedure of using these antennas for wide range of wireless communication application.

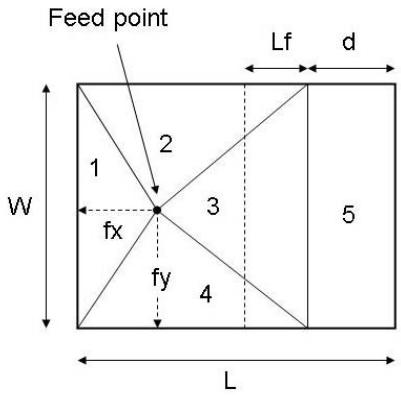

Figure 6.56. Top view of the antenna geometry applied for adaptive meshing using GA for section 6.6.4.2.

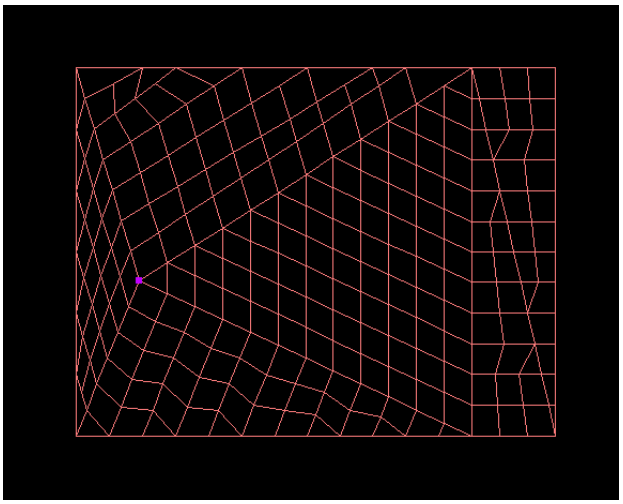

Figure 6.57 2D Mesh used for Fig. 6.56 using GA.

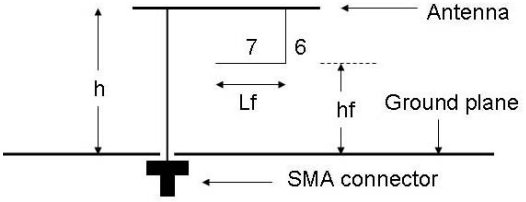

Figure 6.58. Side view of the antenna geometry applied for adaptive meshing using GA for Fig. 6.56.

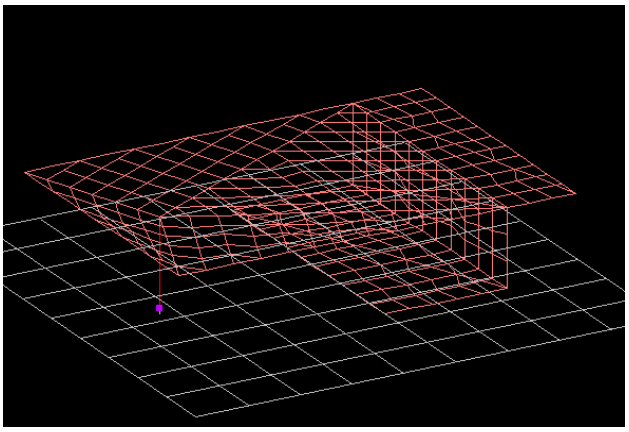

Figure 6.59 3D Mesh used for Fig. 6.58 using GA.

Table 6.11 Summary of GA input parameters, antenna variables and best solutions.

GA parameters	Air-dielectric folded patch antenna design	
	Parameters (m)	Optimal (m)
	Antenna length (L) (0.03-0.06)	0.04316
No. of population size = 4,	Antenna width (W) (0.02-0.06)	0.03006
No. of parameters = 8,	folded wall position (d) (0.005-0.015)	0.00748
Probability of mutation =0.02,	Antenna height (h) (0.004-0.01)	0.00989
Maximum generation =500,	Extend folded wall length (Lf) (0.005-0.015)	0.01327
No. of possibilities=32768,	Extend folded wall height (hf) (0.001-0.0035)	0.00159
	Feeding point at x-axis (fx) (0.004-0.015)	0.00571
	Feeding point at y-axis (fy) (0.004-0.025)	0.01392

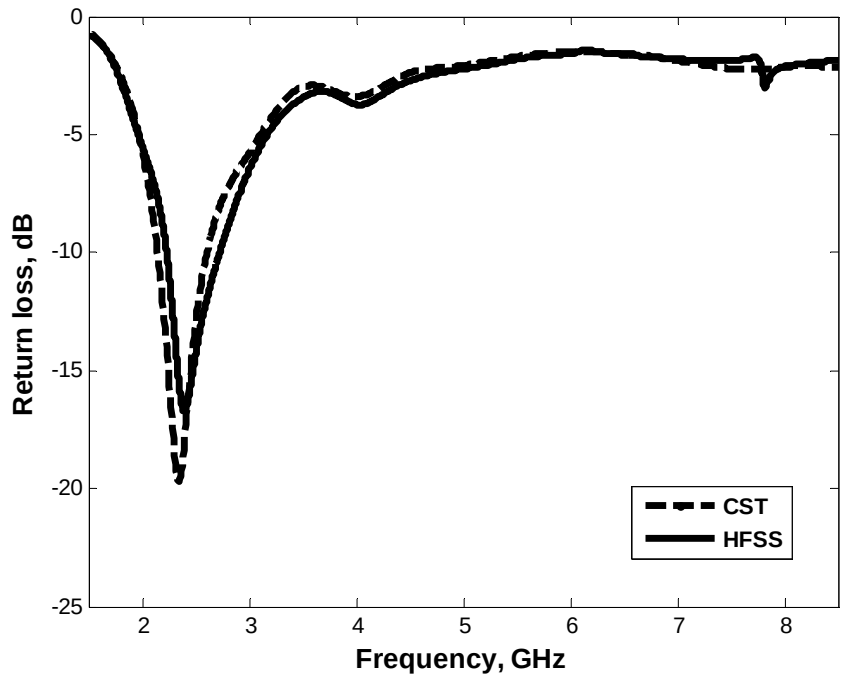

Figure 6.60 The simulated return loss of the antenna with shorted folded wall from two EM packages.

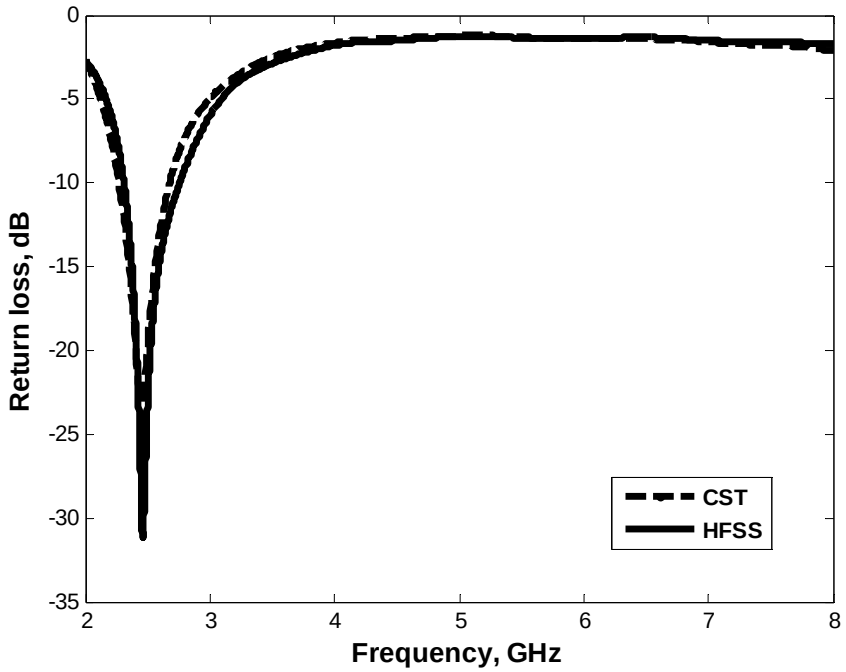

Figure 6.61 The simulated return loss of the antenna with folded patch from two EM packages.

6.7 CONCLUSION

The numerical solution technique for harmonic suppression for active integrated antennas using adaptive meshing and genetic algorithm has been presented in this chapter. A FORTRAN genetic algorithm driver was adopted in this work in conjunction with the industry-standard NEC-2 FORTRAN source code, which was used to evaluate the randomly generated antenna samples.

Several antenna designs were considered and investigated using GA. These include QHA antenna, balanced folded loop antenna, two circular polarized antennas, and four different microstrip patch antennas. For these designs the GA was successfully proved

as an efficient optimizer tool that can be adopted and used to search and find the quicker solutions for complex antenna design geometries.

A novel FORTRAN program for adaptively meshing planar antennas in terms of wire-grid structure has been implemented and embedded inside the GA source code. The programme was fully tested and applied for complex antenna structures. It was shown that the results of several examples modelled by the adaptive meshing illustrate good stability and accuracy.

In this chapter, four novel microstrip patch antennas, for which first and second harmonics were mostly suppressed, have been successfully developed using GA and adaptive meshing FORTRAN code. The results of the optimum designs of the proposed antennas exhibit an excellent harmonic suppression.

6.8 REFERENCES

[1] E. Elkhazmi, N. J. McEwan and J. Moustafa, "Control of harmonic radiation from an active microstrip patch anrtenna", Journees Intern. De Nice Sur Les Antennas, pp. 313-316, November 1996.

[2] Vesna Radisic, S. T. Chew, Yongxi Qian, and Tatsuo Itoh, "High efficiency power amplifier integrated with antenna", IEEE Microwave guided wave letter, vol. 7, no. 2, pp. 39-41, February 1997.

[3] Vesna Radisic, Yongxi Qian, and Tatsuo Itoh, "Class F power amplifier integrated with circular sector microstrip antenna," IEEE MTT-S Digest, pp. 687-690, 1997.

[4] Abdel Fattah Sheta, "A novel H-shaped patch antenna", Microwave and optical technology letters, vol. 29, no. 1, pp. 62-66, April 2001.

[5] Qin-Xin Chu and Meng Hou, “An H-shaped harmonic suppression active integrated atnenna”, International Journal of RF and microwave computer-aided engineering, vol. 16, Issue 3, pp. 245-249, May 2006.

[6] Carroll, D.L., FORTRAN Genetic Algorithm Driver, Version 1.7, Download from: http://www.staff.uiuc.edu/~carroll/ga.html, 12/11/98.

[7] Burke, G.L. and Poggio, A.J., Numerical Electromagnetics Code (NEC)-Method of Moments, Lawrence Livermore Laboratory, Livermore, CA, 1981.

[8] Y.Rahmat – Samii, E. Michielssen, “Electromagnetic optimization by Genetic Algorithms”, John Wiley & Sons, Canada, 1999.

[9] David A. Coley, “An introduction to Genetic Algorithms for scientists and engineers”, World Scientific, Singapore, 1999.

[10] H.H. Ammar and Y. Tao, “Fingerprint registration using Genetic Algorithms”, IEEE Symposium on applications specific systems and software engineering technology, pp. 148–154, March 2000.

[11] D.E. Goldberg, “Genetic Algorithms in search, optimization and machine learning”, Addison – Wesley Publishing Company, Canada, 1989.

[12] R.H. Dinger, “Engineering design and optimization with Genetic algorithms”, Northcon/98 conference proceedings, pp.114–119, October 1998.

[13] http://ai.eller.arizona.edu/%7Emramsey/ga.html.

[14] J. Johnson and Y. Rahmat–Samii, “Genetic Algorithms in engineering electromagnetic”, IEEE Antenna & Prop. Magazine, Vol. 39, pp.7 – 21, Aug. 1997.

[15] D. Zhou, R.A. Abd-Alhameed, C.H. See, P.S. Excell, and E.A. Amushan, “Design of Quadrifilar Helical and Spiral Antennas in the Presence of Mobile Handsets Using Genetic Algorithms”, The first European Conference on Antennas and Propagation (EuCAP2006), Session 3PA1, Paper no.122, Nice, France, 6-10 November 2006.

[16] Burge G. T. and Poggio A. J., “Numerical electromagnetic code (NEC): method of moments”, US Naval Ocean Systems Center, San Diego, Rep. No. TD116, pp. 1-37, 1981.

[17] Strait B. J., “Applications of the Method of Moments to electromagnetic fields”, Ed, SCEEE Press, pp. 450-457, 1980.

[18] Mangoud M. A., Abd-Alhameed R. A. and Excell P. S. “Simulation of human interaction with mobile telephones using hybrid techniques over coupled domains”, IEEE Transactions on microwave theory and techniques, vol. 48, no. 11, pp. 2014-2021, November 2000.

[19] R. A. Abd-Alhameed, M. Mangoud, P. S. Excell, and K. Khalil, “Investigations of polarization purity and specific absorption rate for two dual-band antennas for satellite-mobile handsets”, IEEE Transactions on antennas and propagation, vol. 53, no. 6, pp. 2108-2110, June 2005.

[20] Girish Kumar and K. P. Ray, “Broadband microstrip antennas”, Artech House, Inc. pp. 320-321, 2003.

[21] H. Morishita, Y. Kim, Y. Koyanagi and K. Fujimoto, “A folded loop antenna system for handsets”, IEEE AP-S Proc., vol. 3, pp. 440-443, July 2001.

[22] WireGrid for Windows: A graphic user interface for NEC, version 3.20.

[23] Ansoft Corporation, Ansoft designer SV, Pittsburgh, USA.

[24] Fu-Ren Hsiao, Tzung-Wern Chiou and Kin-Lu Wong, “Harmonic control of a square microstrip antenna operated at the 1.8 GHz band”, Proceedings of APMC2001, pp. 1052-1055, Taipei, Taiwan, R.O.C., 2001.

[25] Byoung Moo Lee, Se Woong Kwon and Young Joong Yoon, “Dual feeding active integrated antenna”, Electronics Letters, vol. 38, no. 19, pp. 1073-1075, September 2002.

[26] Sewoong Kwon, Byoung Moo Lee, Young Joong Yoon, Woo Young Song, and Jong-Gwan Yook, “A harmonic suppression antenna for an active integrated antenna”, IEEE antennas and wireless propagation letters, vol. 13, no. 2, pp. 54-56, February 2003.

[27] Y. J. Sung, M. Kim, and Y.-S. Kim, “Harmonics reduction with defected ground structure for a microstrip patch antenna”, IEEE antennas and wireless propagation letters, vol. 2, pp. 111-113, 2003.

[28] Xian-Chang Lin and Ling-Teng Wang, “A broadband CPW-fed loop slot antenna with harmonic control”, IEEE antennas and wireless propagation letters, vol. 2, pp. 323-325, 2003.

[29] Hyungrak Kim, Kwang Sun Hwang, Kihun Chang, and Young Joong Yoon, “Novel slot antennas for harmonic suppression”, IEEE antennas and wireless components letters, vol. 14, no. 6, pp. 286-288, 2004.

[30] Sin Keng Lee, Yi Qin, and E. Korolkiewicz, “Reduction of the second and third harmonics for a rectangular microstrip patch antenna”, Microwave and optical technology letters, vol. 40, no. 6, pp. 455-460, March 2004.

[31] Xian-Chang Lin, Ling-Teng Wang and Jwo-Shiun Sun, “Harmonic suppression by photonic bandgap on CPW-fed loop-slot antenna”, Microwave and optical technology letters, vol. 41, no. 2, pp. 154-156, April 2004.

[32] Haiwen Liu, Zhengfan Li, Xiaowei Sun and Junfa Mao, "Harmonic suppression with photonic band gap and defected ground structure for a microstrip patch antenna", IEEE antennas and wireless components letters, vol. 15, no. 2, pp. 55-56, February 2005.

[33] Y. J. Sung and Y.-S. Kim, "An improved design of microstrip patch antennas using photonic bandgap structure", IEEE Transactions on antennas and propagation, vol. 53, no. 5, pp. 1799-1804, May 2005.

[34] Hyungrak Kim and Young Joong Yoon, "Microstrip-fed slot antennas with suppressed harmonics", IEEE Transactions on antennas and propagation, vol. 53, no. 9, pp. 2809-2817, September 2005.

[35] Shun-Yun Lin, Kuang-Chih Huang, and Jin-Sen Chen, "Harmonic control for an integrated microstrip antenna with loaded transmission line", Microwave and optical technology letters, vol. 44, no. 4, pp. 379-383, February 2005.

[36] Kwang Sun Hwang, Hyungrak Kim, and Young Joong Yoon, "Bandwidth-enhancement approach for a small-sized harmonic-suppressed antenna", Microwave and optical technology letters, vol. 44, no. 6, pp. 585-587, March 2005.

[37] Shun-Yun Lin, "Modes-controlled slot antennas with frequency selective surface", Microwave and optical technology letters, vol. 48, no. 1, pp.47-49, January 2006.

[38] D. Zhou, R.A. Abd-Alhameed and P.S. Excell, "Bandwidth Enhancement of Balanced Folded Loop Antenna Design for Mobile Handsets Using Genetic Algorithms", IEEE AP-S symposium, Hawaii, USA, 2007 (Accepted).

[39] Computer Simulation Technology Corporation, CST Microwave Studio, Version 5.0, Germany.

CHAPTER 7

CONCLUSIONS AND SUGGESTIONS FOR FURTHER WORK

7.1 CONCLUSIONS

The present work set out to investigate, design and implement active integrated antennas comprising active devices connected directly to the patch radiators, for various applications in high efficiency RF front-ends and integrated oscillator antennas. A general CAD approach to obtaining optimal fundamental load impedance, and designing input matching circuits, in an active integrated antenna of transmitting type, has bee discussed [1]. A case study of a design for 1.6 GHz is used to confirm the design principle, and uses a previously reported patch antenna shape to achieve Class F operation with an alternative type of power transistor. Simulation and measurement in active integrated oscillator antennas with a series feed back for the oscillator circuit connected directly to the active antenna have been demonstrated. The present work had to be limited to two case studies, one using a PHEMT device and the other a low noise bipolar device [2, 3]. A better phase noise performance in active oscillator antenna circuit was attained when using BJT device and in addition to develop an amplitude modulation using the same proposed design circuit. Another development in the work has been the improvement of measurement techniques for active antennas to measure

the accepted power by the antenna at harmonic frequencies was studied. This was implemented using a sensor patch technique [4].

A parallel theme of the present research work was applied to design and optimize of harmonic suppression for active integrated antennas using a genetic algorithm. A novel numerical solution, for designing and optimizing active patch antennas for harmonic suppression using GA in collaboration with NEC-2, was presented [5, 6]. A new FORTRAN program was developed and used for adaptively meshing any planar antenna structure in terms of wire grid surface structures. The program is subsequently implemented for harmonic suppression to active antenna using the GA optimization tools. Simulation and measurements results for several surface structures were also presented.

The motivation for this work was specified on the development of active integrated antennas. Following some comments on the functional classification of active antennas and their possible merits and drawbacks, chapter 1 reviewed existing literature on active integrated antenna for various applications, including amplifying-type, oscillating-type and frequency-conversion-type [7-9].

Chapter 2 discussed what is believed to be the first published attempt to investigate on modeling aspects of active antennas of Class F power amplifier. The work presented a general CAD approach to obtain the optimal fundamental load impedance and design the input matching circuits for an active integrated antenna of the transmitting type in order to achieve Class F active amplifier antenna operation. A case study of a design for 1.6 GHz is used to confirm the design principle, and uses a previously reported patch

antenna shape to achieve Class F operation with an alternative type of power transistor [10]. It was concluded that performance could be substantially enhanced in an active integrated antenna by shaping a patch radiator to control the harmonic load impedances. Generally, the proposed CAD approach can be used as an efficient tool in applying to design and optimize the input impedance of active antennas for achieving harmonic suppression at the desired operating frequency and harmonics with any types of given transistors.

Chapter 3 introduced the design procedure in simulation and measurement of the oscillator implementation integrated with an active antenna working at 2.4 GHz for wireless LANs. Characteristics of the active devices for various applications were briefly reviewed [11]. A CAD design procedure of active oscillator antenna using ADS simulator was described in details. A common source PHEMT transistor was used, with positive feedback to enhance the instability of the active device. Two types of microstrip patch antennas were implemented. Improvement was made to connect the active antenna directly to the transistor output with no other intervening circuitry, except at most a short microstrip line.

The chapter also identified one existing simple measurement technique using sensor patch for finding the accepted power by the active patch antenna [12]. The two-port S parameters between the input port of the passive patch and the sensor were validated and the results were compared using measurement data. The novel measurement technique was adopted and employed through out other patch antenna. The measured free running frequency was observed at 2.43540 GHz with 16.17 dBm output power was observed for circular patch integrated oscillator. For a similar configuration using

rectangular patch the operating frequency and output power were found to be 2.3995 GHz and 11.5 dBm respectively. The measured efficiencies for circular and rectangular active oscillators were about 27.6% and 9.42% respectively. From the measured results presented in chapter 3, it was concluded that performance of design of integrated oscillator with circular patch is superior to the other design with rectangular patch.

Two interested phenomenon were observed in the measurements. One is that the inaccuracy of nonlinear model (provided by the manufacturer) of active device used in the simulation led to the failure to generate oscillator at the first stage of the testing. With some fine amendment to the fabricated oscillator circuit, the oscillation condition was satisfied and free running oscillation was found for both designs. The other is that phase noise level is quite high compared to the oscillator design specification. This is mostly caused by involving a sensing patch in the measurement that may degrade the phase noise performance of the active oscillator, or possibly the nature of the noise characteristic of the chosen transistor device.

Chapter 4 developed an integrated antenna oscillator, operating simultaneously as a source generator and provides AM and ASK modulators functions. A bipolar transistor was selected to provide the instability through generation of negative resistance. The design steps for both the oscillator and the patch antenna were carried out in parallel. Simulations using ADS have showed promising results. The practical results were obtained to validate the theoretical design. The measured frequency and the forward power at the antenna input port, using a calibrated sensing patch, gave reliable results without affecting the radiation performance of the antenna or the oscillator circuit elements. With the fine adjustment to the oscillator circuit, the free-running oscillation

was observed at 2.36727 GHz, with about 15 dBm output power. A superior phase noise performance was achieved compared to PHEMT device design case. It was observed that the modulating signal has little effect on the oscillation frequency that can be ignored. It was observed that the oscillating frequency was also having a tuning range of 20 MHz as the emitter voltage of the active device is varied.

In chapter 5, performance of the sensing patch measurement technique, for measuring the accepted power at the antenna feed port of active patch antennas, was evaluated at harmonic frequencies. A prototype of inset-fed microstrip patch antenna, including 2 sensors at appropriate locations around the patch, was fabricated and tested at 3 designated frequencies to estimate the power accepted by the antenna. The position of the sensing patch was optimally set adjacent to a point of maximum voltage, which corresponds to a point of minimum current distribution on the patch. It was concluded that it was appropriate to place the sensing patch next to the middle of the end edge for the 2^{nd} harmonic and one-third of the way along one side of the patch for the 3^{rd} harmonic. The interesting features of this technique are to eliminate the uncertainties of the Friis equation method and achieve a weakly frequency dependent calibration factor. It was also found that the presence of the sensing patch has very little effect about ±0.1 dB on the return loss at the input port of the main patch for the fundamental and harmonic frequencies. The results of the present work were shown to be acceptable and agreed with direct measurements. The techniques were shown 0.8 dB and 1 dB relative accuracy for the 2^{nd} and 3^{rd} harmonics measurements respectively.

In chapter 6 a genetic algorithm in conjunction with the industry-standard NEC-2 FORTRAN source code to design and optimize antennas were presented and described. Two complex antenna structures using GA were investigated and discussed. These include QHA antenna for mobile satellite communications and balanced folded loop antenna for mobile handsets. With respect to experimental results both designs have shown the capability of GA as an efficient optimization tool to predict the optimum solutions.

A novel program to adaptively generate equivalent wire-grid structures for electromagnetic simulation of 2D/3D structures was also developed in this chapter. This program was written in FORTRAN, with the primary objective of simulating planar microstrip patch antenna designs, using the NEC-2 in collaboration with a genetic algorithm. In addition to microstrip patch designs, the program can support the design of any type of planar antenna structure. The antenna geometry was adaptively divided into optimum numbers of trilateral and quadrilateral polygons for analysis purposes. The fictitious wire boundaries of these polygons can then be optimally segmented to a pre-set segment length and connected to each other using a designated algorithm. Several antenna designs were considered to demonstrate the ability of modeling complex surface structures. These include: two circularly-polarized microstrip patch antennas were accurately designed and modeled to operate around 2.4 GHz; four novel microstrip patch antennas for first and second harmonic suppression have been successfully developed. The harmonic suppression antennas include microstrip patch with fully shorted wall, partially shorted wall, folded shorting wall and folded surface patch. For two prototype antennas, the measured and simulated results were agreed very well.

In general, the numerical techniques and solutions developed have been inherently stable, as it is clear from the stable results of several antenna parameters that were obtained for various antenna structures.

7.2 SUGGESTIONS FOR FURTHER WORK

This work can be extended for further research dealing with other antenna design problems for example:

- An investigation to the harmonic suppression antenna presented in this work in terms of radiation property is necessary in order to ensure the proposed patch antennas exhibit the capability to eliminate the radiation at harmonics. The study needs to be carried out in the anechoic chamber and to measure the E plane and H plane radiation pattern at the desired fundamental and harmonic frequencies.

- Several ideas such as introducing slots (single or dual slots) on rectangular, circular or triangular shaped patches [13], in collaboration with the methods used in this work, can be employed to design and optimize using GA to achieve harmonic suppression antennas with circular polarizations.

- In the present work, the feeding type for the proposed harmonic suppression antennas was restricted to the coaxial-fed type. In the design of active transmitting antennas, microstrip line fed patch antennas sometimes are directly

integrated with the active circuit. Thus, it is interesting to continue a numerical study on designing and optimizing harmonic suppression antennas for active antennas with microstrip line feed using genetic algorithms.

- In addition, the presented work on suppressing harmonics for active patch antennas based on assumption to match the input impedance to 50 Ω at the fundamental frequency can be further extended to consider different matching load impedances. This might also include different load impedances on harmonics frequencies.

- The present work can be extended to investigate the antenna design using inverse problem. This idea can be easily implemented and can add different targets objectives to the antenna design problem. A very interested example includes low Specific Absorption Rate (SAR) antenna design for Mobile handsets.

- Using mix of scalar and binary distributed variables might be used to extend the operation tools of the cost function to handle different complex geometries.

- The present work can be easily extended to include Multiple Input Multiple Output (MIMO) antenna design using polarization concept for wireless access points and mobile handsets applications.

- Harmonic suppression of circularly-polarized wide band antennas can also be investigated.

- Antennas mounted on finite dielectrics might also a good subject for further study.

- A research on antenna design using GA in cooperation with a commercial available EM simulators such as in [14, 15], might directly be applied for further investigation to support the active circuitry to perform more functionalities in the design of active integrated antennas.

- Applications in Ultra wideband (UWB) systems could be interesting topics to extend the present work to include the design possibility of using active integrated antennas and antenna systems that can operate simultaneously in close proximity without mutual interference [16, 17].

- RFID is currently another challenging area of active research field and has been applied in some areas where identification at a distance is highly appreciated [18]. Some previous research work has demonstrated that performance of the RFID transceiver can be somehow enhanced with the proper design in applying the technique of the active integrated antennas, such as improving the responding distance for active tags [19] and implementing a compact transmitter using the oscillator-type active antenna with circular polarization. With the well understood the knowledge on the benefits in applying an AIA approach, it would be worth attempting to study these two topics together to improve the performance of the reader or the tags of the RFID systems for the various applications.

However, it is hoped, in more general terms, that this work has contributed somehow to a field of great theoretical and mathematical complexities and that the practical side of it may aid the edge of advanced technology today.

7.3 REFERENCES

[1] R.A. Abd-Alhameed, D. Zhou, N.J. McEwan, P.S. Excell and A. Ghorbani, "A CAD-oriented Approach to Design of Load Impedance and Input Matching in Active Transmitting Antennas", Microwave Journal, pp. 98-112, March 2005.

[2] D. Zhou, R. A. Abd-Alhameed and P.S. Excell, "Design of Active Oscillator Microstrip Patch Antenna for 2.4 GHz", Proceedings of the sixth informatics workshop for research students, University of Bradford, pp. 216-219, Bradford, UK, 23rd March 2005.

[3] D. Zhou, R.A. Abd-Alhameed, S.J.P. Heng and P.S. Excell, "Design of Amplitude Modulator Using Active Integrated Antennas", In proceeding of the 19th UK URSI Colloquium at Cosenor's House, the Rutherford Appleton Laboratory, Abingdon, Oxford, UK, 3-4 July 2006.

[4] D. Zhou, R.A. Abd-Alhameed, N.J. McEwan and P.S. Excell, "Investigations on Second Harmonic Measurements Using a Sensor Patch for Active Patch Antennas", In proceeding of the seventh informatics workshop for research students, pp. 200-201, Bradford, UK, 29th March 2006.

[5] D. Zhou, R.A. Abd-Alhameed, C.H. See, K. Khalil and P.S. Excell, "Adaptive meshing for numerical antenna designs using genetic algorithms", In proceeding of the 19th UK URSI Colloquium at Cosenor's House, the Rutherford Appleton Laboratory, Abingdon, Oxford, UK, 3-4 July 2006**.**

[6] D. Zhou, R.A. Abd-Alhameed and P.S. Excell, "Design of harmonic rejection antennas with a shorting wall using a genetic algorithm In proceeding of the 19th UK URSI Colloquium at Cosenor's House, the Rutherford Appleton Laboratory, Abingdon, Oxford, UK, 3-4 July 2006.

[7] H. Kim, I.-J. Yoon, and Y.J. Yoon, "A novel fully integrated transmitter front-end with high power-added efficiency", IEEE Trans. Microwave Theory and Techniques, Vol. 53, No. 10, pp. 3206-3214, October 2005.

[8] J. Birkeland and T. Itoh, "Planar FET oscillators using periodic microstrip patch antennas", IEEE Trans. Microwave Theory and Techniques, Vol. 37, No. 8, pp. 1232-1236, August 1989.

[9] K. Cha, S. Kawasaki, and T. Itoh, “Transponder using self-oscillating mixer and active antenna”, IEEE MTT-S Int. Microwave Symp. Digest, pp. 425-428, 1994.

[10] V. Radisic, Y. Qian, and T. Itoh, “Class F power amplifier integrated with circular sector microstrip antenna,” IEEE MTT-S Digest, pp. 687-690, 1997.

[11] S.A. Mass, “Nonlinear microwave and RF circuits”, Norword, MA: Artech House, 1998.

[12] E.A. Elkhazmi, N.J. McEwan, and N.T. Ali, “A Power and Efficiency Measurement Technique for Active Patch Antennas”, IEEE Transactions on microwave theory and techniques, pp. 868-870, vol. 48, no. 5, May 2000.

[13] G. Kumar and K.P. Ray, “Broadband microstrip antennas”, Artech House, Inc. Chapter 8: Broadband circularly polarized MSAs, 2003.

[14] N. Telzhensky and Y. Leviatan, “Planar differential Elliptical UWB antenna optimization”, IEEE Transactions on Antennas and Propagation, vol. 54, no. 11, part 2, pp. 3400-3406, Nov. 2006.

[15] M. John and M.J. Ammann, “Wideband printed monopole design using genetic algorithm”, IEEE antennas and wireless propagation letters: Accepted for future publication, 2007.

[16] G.R. Aiello and G.D. Rogerson, “Ultra-Wideband wireless Systems”, IEEE Microwave Magazine, vol. 4, pp. 36-47, Jun. 2003.

[17] M. Jalaili, A. Abdipour, A. Tavakoli and G. Moradi, “Performance amelioration of an active integrated spiral antenna system for UWB applications”, International workshop on Antenna Technology: small and smart antennas metamaterials and applications (IWAT07), pp. 323-326, 2007.

[18] K. Finkenzeller, “RFID Handbook: Radio-Frequency Identification Fundamentals and Applications”, John Wiley & Sons, 2nd edition, 2004.

[19] L. Cabria, J.A. Garcia, A. Tazon, and A. Mediavilla, “Taking advantage of PHEMT nonlinear behaviour for RFID applications”, 2006 International workshop on integrated nonlinear microwave and millimetre-wave circuits, pp. 42-45, January 2006.

[20] G. Yun, “Compact oscillator-type active antennas for UHF RFID reader”, Electronics Letters, vol. 43, no. 6, pp. 3-4, 15th March 2007.

LIST OF AUTHOR PUBLICATIONS

JOURNAL ARTICLES:

[1] A. Ghorbani, R. A. Abd-Alhameed, N. J. McEwan and **D. Zhou**, "An approach for calculating the limiting bandwidth-reflection coefficient product for microstrip patch antennas", IEEE Transactions on Antennas and Propagation, Vol. 54, No. 4, pp. 1328-1331, April, 2006.

[2] R.A. Abd-Alhameed, **D. Zhou**, N.J. McEwan, P.S. Excell and A. Ghorbani, "A CAD-oriented Approach to Design of Load Impedance and Input Matching in Active Transmitting Antennas", Microwave Journal, pp. 98-112, March, 2005.

CONFERENCES and WORKSHOPS

[1] **D. Zhou**, R.A. Abd-Alhameed and P.S. Excell, "Bandwidth enhancement of balanced folded loop antenna design for mobile handsets using genetic algorithms", National URSI symposium, University of Portsmouth, Portsmouth, UK, 2–3 July 2007.

[2] **D. Zhou**, R.A. Abd-Alhameed and P.S. Excell, "New and wide harmonic rejection antenna design using shorting wall by genetic algorithm", National URSI symposium, University of Portsmouth, Portsmouth, UK, 2–3 July 2007.

[3] K. Khalil, **D. Zhou**, R.A. Abd-Alhameed and P.S. Excell, "Adaptive meshing program for microstrip patch antenna designs using a genetic algorithm", National URSI symposium, University of Portsmouth, Portsmouth, UK, 2–3 July 2007.

[4] M.M. Abusitta**, D. Zhou**, R.A. Abd-Alhameed and P.S. Excell, "Simulation and measurement of controlled RF switch for beam steering antenna array", National URSI symposium, University of Portsmouth, Portsmouth, UK, 2–3 July 2007.

[5] M.M. Abusitta**, D. Zhou**, R.A. Abd-Alhameed and P.S. Excell, "RF switch design for beam-steering antenna-array mobile communication base stations", The eighth informatics workshop for research students, pp. 12-15, University of Bradford, Bradford, UK, 28 June 2007.

[6] **D. Zhou**, R.A. Abd-Alhameed, C.H. See, P.S. Excell, and E.A. Amushan, "Design of quadrifilar helical and spiral antennas in the presence of mobile handsets using genetic algorithms", The first European Conference on Antennas and Propagation (EuCAP2006), Session 3PA1, Paper no.122, Nice, France, 6-10 November 2006.

[7] C.H. See, R.A. Abd-Alhameed, **D. Zhou**, P.S. Excell and Y.F. Hu, "A new design of circularly-polarised conical-beam microstrip patch antennas using a genetic algorithm", The first European Conference on Antennas and Propagation (EuCAP2006), Session 4PA1, Paper no.100, Nice, France, 6-10 November 2006.

[8] A. Ghorbani, M.A. Ansarizadeh, N.J. McEwan, R.A. Abd-Alhameed, and **D. Zhou**, "The Bode-Fano integrals as an objective measure of antenna bandwidth reflection coefficient product limit", In proceeding of International RF and Microwave Conference, pp. 210-215, Putrajaya, Malaysia, 12-14 September 2006.

[9] **D. Zhou**, R.A. Abd-Alhameed, S.J.P. Heng and P.S. Excell, "Design of amplitude modulator using active integrated antennas", National URSI symposium, Abingdon, UK, 3-4 July 2006.

[10] **D. Zhou**, R.A. Abd-Alhameed, C.H. See, K. Khalil and P.S. Excell, "Adaptive meshing for numerical antenna designs using genetic algorithms", National URSI symposium, Abingdon, UK, 3-4 July 2006.

[11] **D. Zhou**, R.A. Abd-Alhameed and P.S. Excell, "Design of harmonic rejection antennas with a shorting wall using a genetic algorithm", National URSI symposium, Abingdon, UK, 3-4 July 2006.

[12] K. Khalil, **D. Zhou**, R.A. Abd-Alhameed and P.S. Excell, "Design of quadrifilar helical and spiral antennas using genetic algorithms", In proceeding of the seventh informatics workshop for research students, pp. 119-120, Bradford, UK, 29 March 2006.

[13] **D. Zhou**, R.A. Abd-Alhameed, S.J.P. Heng and P.S. Excell, "AM and ASK modulation using integrated oscillator antennas", In proceeding of the seventh informatics workshop for research students, pp. 196-199, Bradford, UK, 29 March 2006.

[14] **D. Zhou**, R.A. Abd-Alhameed, N.J. McEwan and P.S. Excell, "Investigations on second harmonic measurements using a sensor patch for active patch antennas", In proceeding of the seventh informatics workshop for research students, pp. 200-201, Bradford, UK, 29 March 2006.

[15] **D. Zhou**, R.A. Abd-Alhameed and P.S. Excell, "Design of active oscillator microstrip patch antenna for 2.4 GHz", In proceeding of the sixth informatics workshop for research students, pp. 216-219, Bradford, UK, 23 March, 2005.

[16] **D. Zhou**, R.A. Abd-Alhameed and P.S. Excell, "Investigation on modeling aspects of active antennas of class F power amplifiers", In proceeding of the sixth informatics workshop for research students, pp. 212-215, Bradford, UK, 23 March, 2005.

[17] **D. Zhou**, R.A. Abd-Alhameed, R.W. Clarke, G. Qasim and P.S. Excell, "Simulation and measurement of dielectric resonator oscillator around 5.5GHz", In proceeding of the sixth informatics workshop for research students, pp. 208-211, Bradford, UK, 23 March, 2005.

PENDING PUBLICATIONS:

[1] **D. Zhou**, R.A. Abd-Alhameed and P.S. Excell, "Wideband balanced folded dipole antenna for mobile handsets", The 2nd European Conference on Antennas and Propagation (EuCAP2007), 2007 (Accepted).

[2] R.A. Abd-Alhameed, N.J. McEwan, A. Ghorbani and **D. Zhou**, "The Bode-Fano integral as an objective measure of antenna bandwidth", International Journal of Microwave Science and Technology.